University of Alabama at Birmingham
UAB Digital Commons

All ETDs from UAB | UAB Theses & Dissertations

2005

Analysis and mitigation of high frequency harmonic interference in high voltage power line carrier coupling systems.

Gregory A. Franklin
University of Alabama at Birmingham

Follow this and additional works at: https://digitalcommons.library.uab.edu/etd-collection

Recommended Citation

Franklin, Gregory A., "Analysis and mitigation of high frequency harmonic interference in high voltage power line carrier coupling systems." (2005). *All ETDs from UAB*. 5447.
https://digitalcommons.library.uab.edu/etd-collection/5447

This content has been accepted for inclusion by an authorized administrator of the UAB Digital Commons, and is provided as a free open access item. All inquiries regarding this item or the UAB Digital Commons should be directed to the UAB Libraries Office of Scholarly Communication.

NOTE TO USERS

This reproduction is the best copy available.

UMI®

Reproduced with permission of the copyright owner. Further reproduction prohibited without permission.

Reproduced with permission of the copyright owner. Further reproduction prohibited without permission.

ANALYSIS AND MITIGATION OF HIGH FREQUENCY HARMONIC INTERFERENCE IN HIGH VOLTAGE POWER LINE CARRIER COUPLING SYSTEMS

by

GREGORY A. FRANKLIN

A DISSERTATION

Submitted to the graduate faculty of The University of Alabama at Birmingham and The University of Alabama in Huntsville, in partial fulfillment of the requirements for the degree of Doctor of Philosophy

BIRMINGHAM, ALABAMA

2005

Reproduced with permission of the copyright owner. Further reproduction prohibited without permission.

UMI Number: 3201154

Copyright 2005 by
Franklin, Gregory A.

All rights reserved.

INFORMATION TO USERS

The quality of this reproduction is dependent upon the quality of the copy submitted. Broken or indistinct print, colored or poor quality illustrations and photographs, print bleed-through, substandard margins, and improper alignment can adversely affect reproduction.

In the unlikely event that the author did not send a complete manuscript and there are missing pages, these will be noted. Also, if unauthorized copyright material had to be removed, a note will indicate the deletion.

UMI®

UMI Microform 3201154
Copyright 2006 by ProQuest Information and Learning Company.
All rights reserved. This microform edition is protected against unauthorized copying under Title 17, United States Code.

ProQuest Information and Learning Company
300 North Zeeb Road
P.O. Box 1346
Ann Arbor, MI 48106-1346

Reproduced with permission of the copyright owner. Further reproduction prohibited without permission.

Copyright by
Gregory Allen Franklin
2005

Reproduced with permission of the copyright owner. Further reproduction prohibited without permission.

ABSTRACT OF DISSERTATION
GRADUATE SCHOOL, UNIVERSITY OF ALABAMA AT BIRMINGHAM

Degree PhD Program Computer Engineering

Name of Candidate Gregory A. Franklin

Committee Chair Gregg L. Vaughn

Title Analysis and Mitigation of High Frequency Harmonic Interference in High Voltage Power Line Carrier Coupling Systems

Interference resulting from high-frequency power system harmonics in the band below 10 kHz has been previously reported to adversely affect high-voltage power line carrier coupling systems. Problems such as equipment failures and carrier signal interference have been experienced. Previous work by others has characterized the nature and origin of power line carrier coupling system problems caused by harmonic frequency interference. However, computer-based modeling of coupling systems suitable for frequency response analysis was not made available. Also not made available by previous work was an analysis of simple and inexpensive methods for mitigating harmonic frequency interference.

The results of the study presented expand previous work by providing an additional resource on high-frequency harmonic interference. Frequency response measurements of three common types of coupling systems using typical coupling capacitance and drain coil inductance values are provided. Also presented are state-space models of the coupling systems suitable for estimating the frequency responses of the coupling systems in the harmonic frequency band. Finally, coupling system components that can be altered for problem mitigation are identified, along with an example of interference mitigation on a 230-kV coupling system that was severely affected by harmonic frequency interference.

Reproduced with permission of the copyright owner. Further reproduction prohibited without permission.

DEDICATION

This work is dedicated to my wife, Christy, and my son, Ethan. Their patience and support during this endeavor were greatly appreciated.

Reproduced with permission of the copyright owner. Further reproduction prohibited without permission.

TABLE OF CONTENTS

Page

ABSTRACT iii

DEDICATION iv

LIST OF TABLES viii

LIST OF FIGURES ix

CHAPTER

1 INTRODUCTION 1

General Description of High-Voltage PLC Systems 2
The Impact of High-Frequency Harmonics on PLC Coupling Systems 3
Problems Encountered on a 230-kV Coupling System 5
Purpose of Study 14

2 PLC COUPLING SYSTEM TESTS AND MEASUREMENTS 17

Descriptions of PLC Coupling Systems Tested 17
Phase-to-Ground Coupled Narrowband Resonant Systems 17
Phase-to-Ground Coupled Second-Order Wideband Band-Pass Systems 19
Drain Coil Inductance and Resistance Measurements 19
IMT Tests 21
Winding Inductance and Resistance Measurements 23
Coefficient-of-Coupling Measurements 24
Short-Circuit and Open-Circuit Tests at Harmonic Frequencies 26
Saturation Tests at Harmonic Frequencies 28
Equivalent Series Inductance at Carrier Frequencies 28
Effect of Harmonic-Frequency Interference on Impedance Matching at Carrier Frequencies 33
PLC Coupling System Measurements 44
Peak Voltage Gain Measurements 44
Frequency Response Measurements 49

Reproduced with permission of the copyright owner. Further reproduction prohibited without permission.

TABLE OF CONTENTS (Continued)

Page

CHAPTER

3 PLC COUPLING SYSTEM MODELING 59

Effect of Coupling Capacitor Voltage Transformer Voltage Transformation Circuitry on Coupling System Frequency Response in the Harmonic Frequency Band 59
PSpice Modeling 62
Acquisition of Coupling System Component Data for Use With Models ... 64
Detailed PSpice Models 66
Simplified PSpice Models 70
Comparison of Detailed and Simplified PSpice Models to Measured Data 74
State-Space Modeling 74
General Narrowband Resonant Coupling System State-Space Model 76
Second-Order Wideband Coupling System State-Space Model 81
Comparison of Measured Frequency Response to Simulated Frequency Response 84
Limitations of Models 90

4 MITIGATION OF HARMONIC FREQUENCY INTERFERENCE 96

Identifying and Altering Coupling System Components for Mitigation of Harmonic Frequency Interference 96
Effect of Altering Drain Coil Inductance and Line Tuner Capacitance on Voltage Gain at the Drain Coil 100
Carrier Frequency Considerations When System Components Are Being Altered for Mitigation of Harmonic Frequency Interference 103
Considerations When Increasing Line Tuner Series Capacitance 104
Considerations When Decreasing Drain Coil Inductance 106
Example of Altering Coupling System Components to Mitigate Harmonic Frequency Interference 113

5 CONCLUSION 117

Summary of Research Goals and Results 117
Relating Harmonic Frequency Interference to Standard Harmonic Voltage Distortion Limits 120
Recommendations for Future Research in the Area of Harmonic Frequency Interference 121

LIST OF REFERENCES 123

Reproduced with permission of the copyright owner. Further reproduction prohibited without permission.

TABLE OF CONTENTS (Continued)

Page

APPENDIX

A COUPLING SYSTEM TEST DATA 125

B COUPLING SYSTEM MODELING AND SIMULATION DATA 143

Reproduced with permission of the copyright owner. Further reproduction prohibited without permission.

LIST OF TABLES

Table *Page*

1 Impedance-Matching Transformer (IMT) Winding Inductance and Resistance 23

2 Impedance-Matching Transformer (IMT) Coefficient of Coupling 25

3 Impedance-Matching Transformer (IMT) Leakage Inductance at Harmonic Frequencies 27

4 Impedance-Matching Transformer (IMT) Equivalent Series Inductance at Carrier Frequencies 32

5 Results of Test to Determine the Effect of Harmonic Frequency Interference on Impedance Matching at Carrier Frequencies 37

6 Results of Peak Voltage Gain Measurements 47

7 Percentage-of-Error Comparison Between PSpice Model Simulations and Measurements 75

Reproduced with permission of the copyright owner. Further reproduction prohibited without permission.

LIST OF FIGURES

Figure *Page*

1 Schematic of a phase-to-ground coupled single-frequency resonant power line carrier system 3

2 Waveform and frequency spectrum of drain coil voltage on a 230-kV coupling system during arc furnace melting cycle 6

3 Waveform and frequency spectrum of voltage at drain coil of a coupling system not adversely affected by harmonic noise 7

4 Waveform and frequency spectrum illustrating impedance-matching transformer (IMT) saturation 9

5 Waveform and frequency spectrum of arc transient 10

6 PSpice model of a 230-kV coupling system 12

7 Comparison of simulated and measured frequency responses for a 230-kV coupling system 13

8 Schematic of a phase-to-ground two-frequency resonant coupling system 18

9 Schematic of a phase-to-ground second-order wideband coupling system 20

10 Variation in drain coil resistance versus frequency 22

11 Saturation curves for impedance-matching transformer with toroidal core 29

12 Saturation curves for impedance-matching transformer with pot core 30

13 Test circuit for measuring the equivalent series inductance of an impedance-matching transformer (IMT) at carrier frequencies 31

14 Test circuit for measuring the effect of harmonic frequency interference on impedance matching 34

15 Curves of impedance-matching transformer (IMT) saturation and percentage of reflected power for a toroidal core IMT at 600 Hz 38

Reproduced with permission of the copyright owner. Further reproduction prohibited without permission.

LIST OF FIGURES (Continued)

Figure *Page*

16 Curves of impedance-matching transformer (IMT) saturation and percentage of reflected power for a toroidal core IMT at 1,000 Hz 39

17 Curves of impedance-matching transformer (IMT) saturation and percentage of reflected power for a toroidal core IMT at 3,000 Hz 40

18 Curves of impedance-matching transformer (IMT) saturation and percentage of reflected power for a pot core IMT at 600 Hz 41

19 Curves of impedance-matching transformer (IMT) saturation and percentage of reflected power for a pot core IMT at 1,000 Hz 42

20 Test configuration for measuring peak voltage gain 45

21 Test configuration for frequency response measurements 50

22 Comparison of frequency responses measured at the drain coil of a single-frequency resonant coupling system with large and small values of line tuner series capacitance and impedance-matching transformer (IMT) terminating resistance 51

23 Comparison of frequency responses measured at the impedance-matching transformer (IMT) of a single-frequency resonant coupling system with large and small values of line tuner series capacitance and IMT terminating resistance 52

24 Comparison of frequency responses measured at the drain coil and impedance-matching transformer (IMT) of a single-frequency resonant coupling system with a large-valued line tuner series capacitance 53

25 Comparison of frequency responses measured at the drain coil and impedance-matching transformers (IMTs) of a two-frequency resonant coupling system with a small-valued line tuner series capacitance in each tuning leg 55

26 Comparison of frequency responses measured at the drain coil and impedance-matching transformers (IMTs) of a two-frequency resonant coupling system with a small-valued line tuner series capacitance in one tuning leg and a large-valued line tuner series capacitance in the other tuning leg 56

Reproduced with permission of the copyright owner. Further reproduction prohibited without permission.

LIST OF FIGURES (Continued)

Figure *Page*

27 Comparison of frequency responses measured at the drain coil and impedance-matching transformer (IMT) of a second-order wideband coupling system with large and small values of IMT terminating resistance 58

28 PSpice model of simplified circuit for a Westinghouse type PCA-5 coupling capacitor voltage transformer 60

29 Frequency response comparison illustrating the effect of coupling capacitor voltage transformation circuitry on frequency response at the drain coil 63

30 Detailed PSpice model of a single-frequency resonant coupling system 66

31 Detailed PSpice model of a two-frequency resonant coupling system 68

32 Detailed PSpice model of a second-order wideband coupling system 69

33 Simplified PSpice model of a single-frequency resonant coupling system 70

34 Simplified PSpice model of a two-frequency resonant coupling system 72

35 Simplified PSpice model of a second-order wideband coupling system 73

36 Schematic of narrowband resonant coupling system used for developing state-space model 77

37 Schematic of second-order wideband coupling system used for developing state-space model 82

38 Calculated and measured frequency responses at the drain coil and impedance-matching transformer (IMT) of a single-frequency coupling system with the IMT terminated into 2,000 Ω 85

39 Calculated and measured frequency responses at the drain coil and impedance-matching transformer (IMT) of a single-frequency coupling system with the IMT terminated into 50 Ω 86

40 Calculated and measured frequency responses at the drain coil and each impedance-matching transformer (IMT) of a two-frequency coupling system with each IMT terminated into a high resistance 87

Reproduced with permission of the copyright owner. Further reproduction prohibited without permission.

LIST OF FIGURES (Continued)

Figure *Page*

41 Calculated and measured frequency responses at the drain coil and impedance-matching transformer (IMT) of a second-order wideband coupling system with the IMT terminated into 2,000 Ω 88

42 Calculated and measured frequency responses at the drain coil and impedance-matching transformer (IMT) of a second-order wideband coupling system with the IMT terminated into 50 Ω 89

43 Calculated and measured frequency responses at the drain coil and impedance-matching transformer (IMT) of a single-frequency coupling system when the IMT magnetizing reactance is dominant 92

44 Waveform and frequency spectrum of impedance-matching transformer (IMT) primary voltage with source voltage frequency of 3 kHz 94

45 Waveform and frequency spectrum of impedance-matching transformer (IMT) primary voltage with source voltage frequency of 4 kHz 95

46 Generalized equivalent circuits for a coupling system 97

47 Single-frequency coupling system model for illustrating the effects of various combinations of drain coil inductance and line tuner series capacitance on voltage gain at the drain coil 100

48 Comparison of voltage gain at drain coil of a single-frequency coupling system for various combinations of drain coil inductance and line tuner series capacitance 102

49 Plots showing additional line tuner series capacitance required to resonate with an inductance of 200 μH for coupling capacitance values of 0.003 μF and 0.006 μF 105

50 Equivalent circuit of coupling system at carrier frequencies 107

51 Plots of equivalent load resistance versus frequency for various values of drain coil inductance 110

52 Plots of equivalent load reactance versus frequency for various values of drain coil inductance 112

Reproduced with permission of the copyright owner. Further reproduction prohibited without permission.

LIST OF FIGURES (Continued)

Figure *Page*

53 Comparison of calculated voltage gain at drain coil before and after disabling one of the high-frequency tuning capacitors in a 230-kV two-frequency coupling system 115

54 Waveforms of drain coil voltage on a 230-kV coupling system taken before and after alteration of line tuner series capacitance 116

Reproduced with permission of the copyright owner. Further reproduction prohibited without permission.

CHAPTER 1

INTRODUCTION

Interference resulting from high-frequency power system harmonics in the band below 10 kHz has been previously reported to adversely affect high-voltage power line carrier (PLC) coupling systems. Problems such as equipment failures and carrier signal interference have been experienced. Previous work by others has characterized the nature and origin of PLC coupling system problems caused by harmonic frequency interference. However, computer-based modeling of coupling systems suitable for frequency response analysis was not made available. Also not made available by previous work was an analysis of simple and inexpensive methods for mitigating harmonic frequency interference.

The purpose of the study presented herein is to expand previous work by providing an additional resource on high-frequency harmonic interference. Frequency response measurements of three common types of coupling systems using typical coupling capacitance and drain coil inductance values are provided. Also presented are state-space models of the coupling systems suitable for estimating the frequency responses of the coupling systems in the harmonic frequency band. Finally, coupling system components that can be altered for problem mitigation are identified, along with an example of interference mitigation on a 230-kV coupling system that was severely affected by harmonic frequency interference.

Reproduced with permission of the copyright owner. Further reproduction prohibited without permission.

General Description of High-Voltage PLC Systems

PLC systems are commonly used by electric utilities for high-speed protection of transmission lines, transformer banks, and breaker failure protection. As the name implies, the communication medium is the high-voltage transmission line. Information transmitted by carrier signals is binary, basically telling a protective device to operate or not to operate. PLC systems utilize radio frequency signals in the range of 30 kHz to 500 kHz, with typical power levels of 1 W or 10 W into 50 Ω.

A schematic of a phase-to-ground coupled single-frequency resonant PLC system is shown in Figure 1. There would be an identical system on the opposite end of the transmission line. The PLC system is composed of a line trap, coupling system, and communication equipment. The line trap for a single-frequency system is a parallel resonant circuit that is tuned to the carrier frequency and thus presents high impedance to the carrier signal, helping to confine the signal to the transmission line. The coupling system couples the low-level carrier signal to the transmission line and consists of the coupling capacitor, drain coil with arc gap, and line-tuning equipment. The line-tuning equipment is composed of the line tuner and the impedance-matching transformer (IMT). The line tuner is tuned to form a series-resonant circuit with the coupling capacitor at the carrier frequency and thus provides a low-impedance path for the carrier signal to the transmission line. The line tuner consists of either a variable inductance coil alone or a variable inductance coil in series with a variable capacitance when higher frequency tuning is required. Another much higher value capacitor is also in series with the IMT for preventing power frequency (60 Hz) signals from saturating the IMT when the high-frequency tuning capacitor is not used. The IMT provides impedance matching between the transmission line

Reproduced with permission of the copyright owner. Further reproduction prohibited without permission.

and the communication equipment. The drain coil provides low impedance (20-30 Ω) at power system frequency and at the same time provides high impedance (typically >30,000 Ω) at the PLC frequency. Under normal conditions, the drain coil impedance at power system frequency produces a voltage of less than 30 Vrms across the drain coil and tuning equipment. The arc gap across the drain coil provides transient protection.

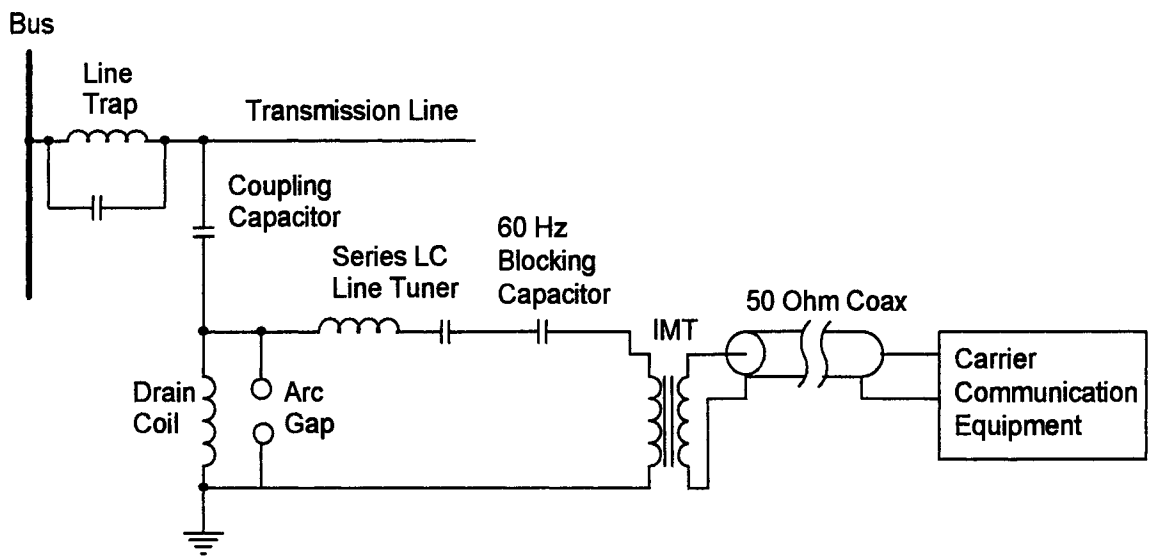

Figure 1. Schematic of a phase-to-ground coupled single-frequency resonant power line carrier system. LC = inductance and capacitance; Coax = coaxial cable; IMT = impedance-matching transformer.

The Impact of High-Frequency Harmonics on PLC Coupling Systems

With the installation of loads utilizing large-scale power electronic devices, some electric utilities have experienced problems with PLC systems resulting from high-frequency harmonics produced by these devices. High-frequency harmonics are considered herein to be those in the frequency band of 600 Hz to 10 kHz. Examples of loads

Reproduced with permission of the copyright owner. Further reproduction prohibited without permission.

utilizing large-scale power electronic devices are DC electric arc furnaces, static var compensators, and motor speed controllers.

From a previous work on this subject (Tatro, Adamson, Eitzmann, & Smead, 1993), high-frequency harmonics produced by a high-voltage DC (HVDC) converter were documented to cause problems such as failures of line-tuning components, as well as IMT and drain coil saturation. Both IMT and drain coil saturation can cause PLC signal interference by effectively shorting the carrier signal to ground (Sanders & Ray, n.d.). Crowley and Parker (1993) also describe PLC signal interference that occurred as a result of IMT saturation caused by harmonics produced by a motor speed controller. In addition to the aforementioned PLC signal interference problems, other problems can be encountered at lower levels of harmonic frequency interference. Harmonic frequency interference can cause problems during routine system maintenance by adversely affecting PLC test equipment such as signal generators and reflectometers. When harmonic voltage levels approach the levels of the PLC signals, simple line tuning can become difficult for field personnel.

Tatro et al. (1993) found that the PLC problems generally result from excessive voltage levels impressed on the PLC coupling system components; the excessive voltage levels are a consequence of the excitation of an undesirable series resonance that exists between the coupling capacitor and the parallel combination of the drain coil and line-tuning equipment. When excited, this resonance can produce a large node voltage across the drain coil and tuning equipment, resulting in coupling system component saturation and failure problems. The coupling systems studied by Tatro et al. typically exhibited this undesirable resonance in the 3 kHz to 10 kHz band. However, even in cases where reso-

Reproduced with permission of the copyright owner. Further reproduction prohibited without permission.

nance between the coupling capacitor and the parallel combination of the drain coil and line-tuning equipment does not occur, abnormally high voltage levels can still exist at the drain coil and line-tuning equipment, depending on the magnitude of the harmonic frequency interference at the coupling system's location and the voltage gain response of the coupling system.

Problems Encountered on a 230-kV Coupling System

An illustration of problems associated with harmonic frequency interference can be seen in Figure 2, which shows a voltage measurement taken across the drain coil and line tuner of a PLC coupling system on a 230-kV transmission line. Figure 2 also shows the frequency spectrum of the drain coil voltage. A 66-MW DC electric arc furnace served by the 230-kV line was operating at the time of the measurement. The furnace utilized a 48-pulse converter for AC-to-DC conversion. The 48-pulse converter produced 47th (2,820 Hz) and 49th (2,940 Hz) harmonics, which are the dominant frequencies shown in the frequency spectrum of Figure 2. For comparison to the drain coil voltage of Figure 2, Figure 3 is provided to show the voltage across the drain coil and tuning equipment of a coupling system not adversely affected by harmonic noise. Figure 3 also shows the frequency spectrum of this voltage. As shown in the frequency spectrum, high-frequency harmonics are present, but their magnitudes are very small compared to the 60-Hz component. Section 5.7.1.2 of an industry standard for coupling capacitors used in PLC applications (*Requirements for Power-Line Carrier Coupling Capacitors and Coupling Capacitor Voltage Transformers (CCVT)*, 1999) specifies that the voltage drop across the carrier drain coil shall not exceed 30 Vrms at power frequency with maximum

Reproduced with permission of the copyright owner. Further reproduction prohibited without permission.

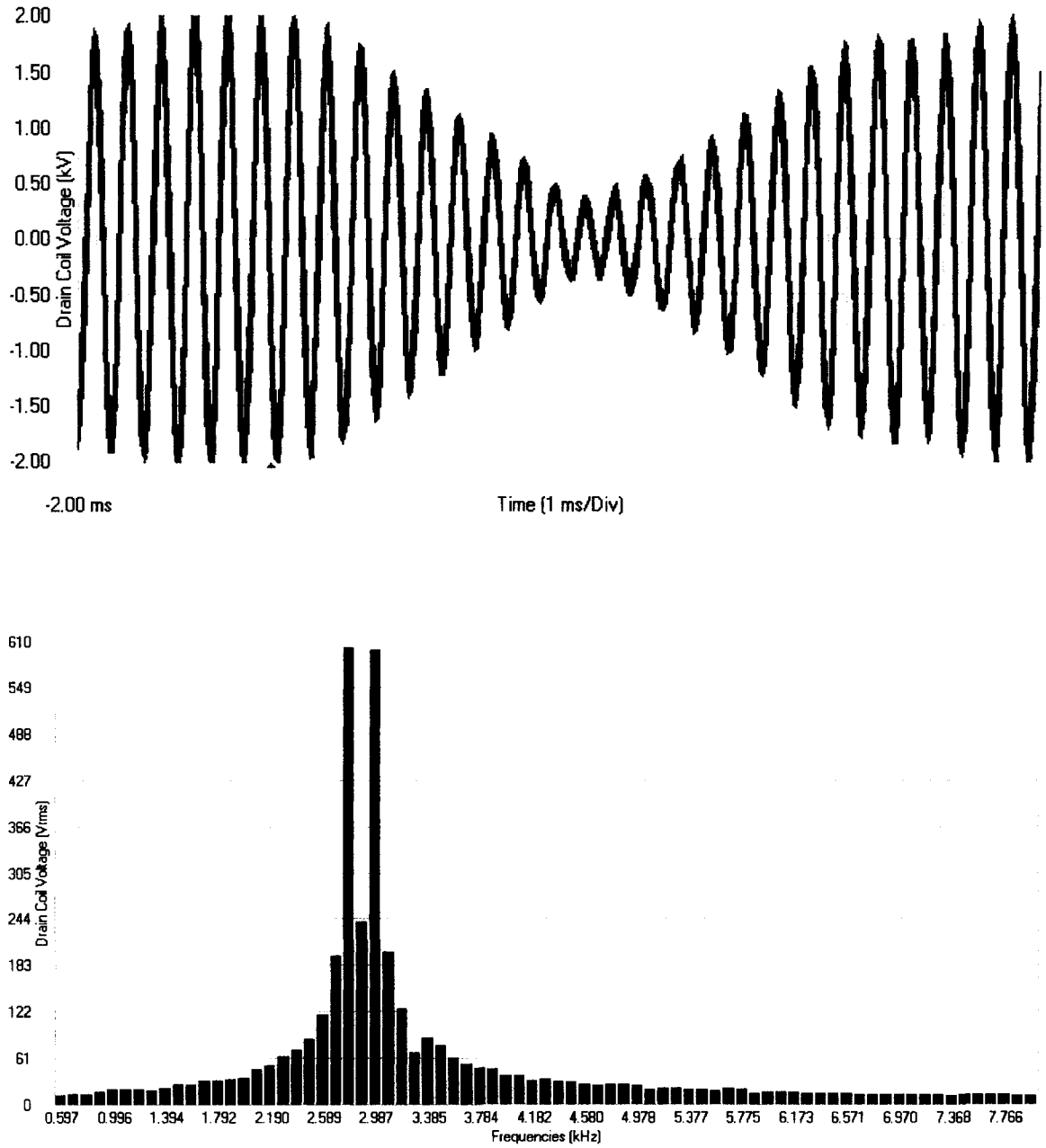

Figure 2. Waveform and frequency spectrum of drain coil voltage on a 230-kV coupling system during arc furnace melting cycle.

Reproduced with permission of the copyright owner. Further reproduction prohibited without permission.

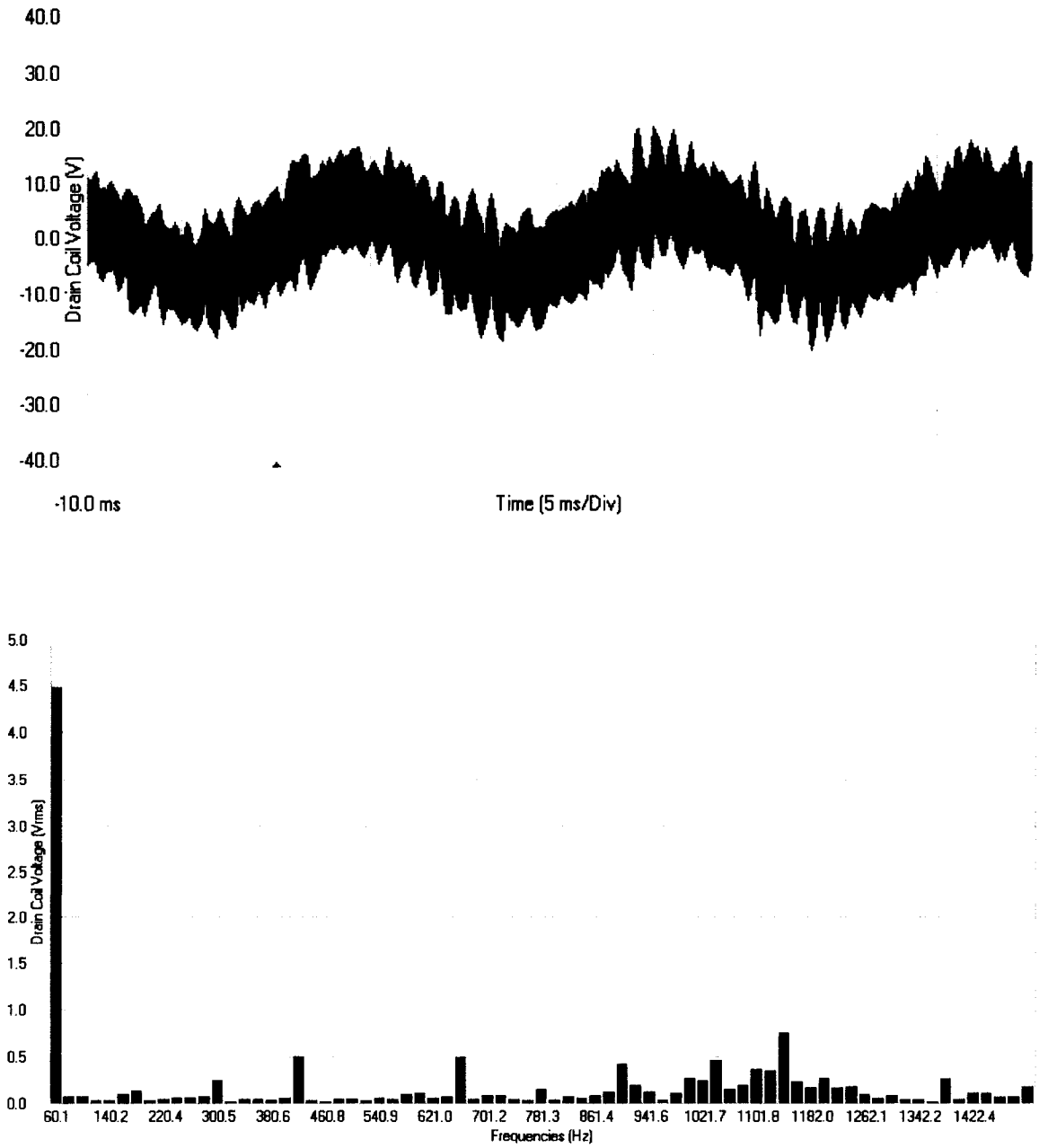

Figure 3. Waveform and frequency spectrum of voltage at drain coil of a coupling system not adversely affected by harmonic noise.

Reproduced with permission of the copyright owner. Further reproduction prohibited without permission.

rated voltage applied to the high-voltage terminal of the capacitor. However, no specification is given for frequencies above power frequency.

As noted previously, harmonic frequency interference can cause IMT saturation. Figure 4 shows the effects of IMT saturation. In the figure, the smaller magnitude, distorted waveform is the voltage on the transmission line side of the IMT (hereafter referred to as the primary of the IMT), and the other waveform is the voltage at the drain coil. Figure 4 also shows the frequency spectrum of the IMT primary voltage. Tatro et al. (1993) describe the possibility of false signal reception by on/off-keyed (OOK) carrier receivers resulting from harmonic sidebands created by IMT saturation. As shown in Figure 4, the sidebands are harmonics of the dominant frequency causing saturation and can extend well into the PLC frequency band, possibly hitting the receive frequency of an OOK carrier receiver.

Another problem not described by Crowley and Parker (1993) or Tatro et al. (1993) is that of voltage levels high enough to breakover the protective arc gap that is in parallel with the drain coil and line-tuning components. The arc gap, which is basically a spark plug located in the line tuner cabinet, is typically set to breakover at approximately 1,500 Vrms. The arcing creates transient voltages that are transmitted to the carrier communication equipment. These transients contain significant energy in the PLC frequency band and can also cause false signal reception by OOK carrier receivers. Figure 5 shows a simultaneous measurement of an arc transient at the primary of the IMT and the communication equipment side of the IMT (hereafter referred to as the secondary of the IMT). Figure 5 also shows the frequency spectrum of the IMT secondary voltage. The frequency spectrum of Figure 5 shows that the majority of the frequency content of the

Reproduced with permission of the copyright owner. Further reproduction prohibited without permission.

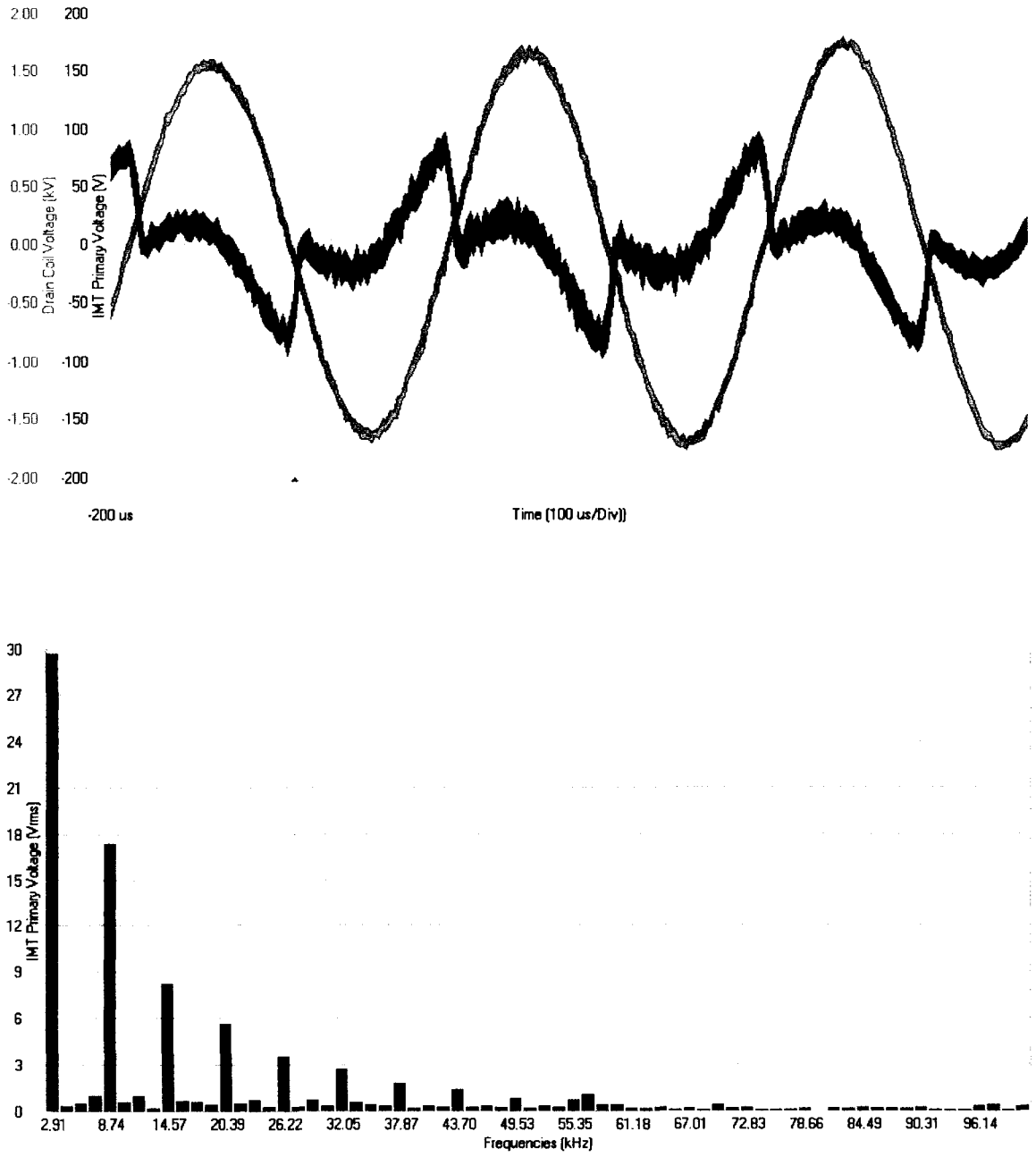

Figure 4. Waveform and frequency spectrum illustrating impedance-matching transformer (IMT) saturation.

Reproduced with permission of the copyright owner. Further reproduction prohibited without permission.

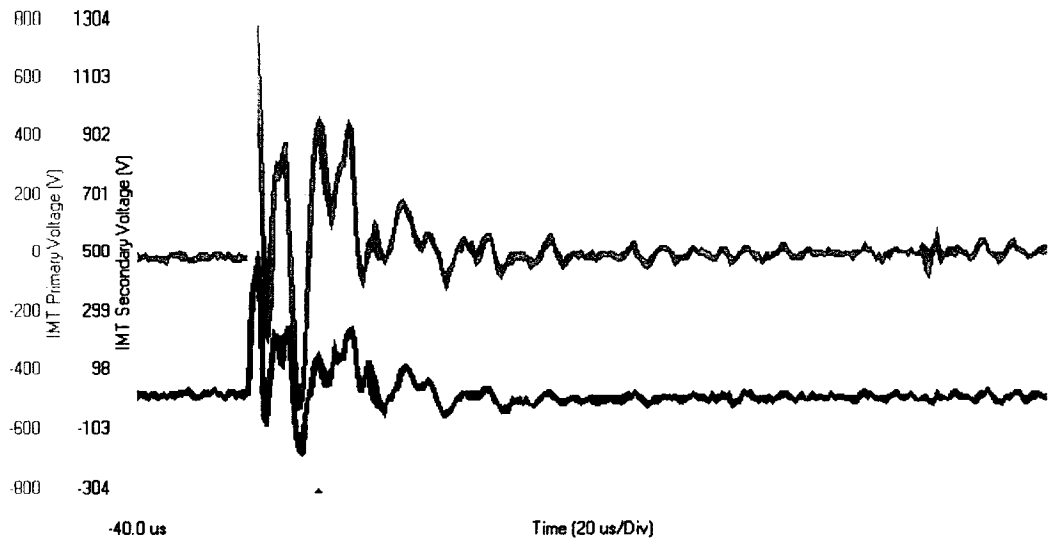

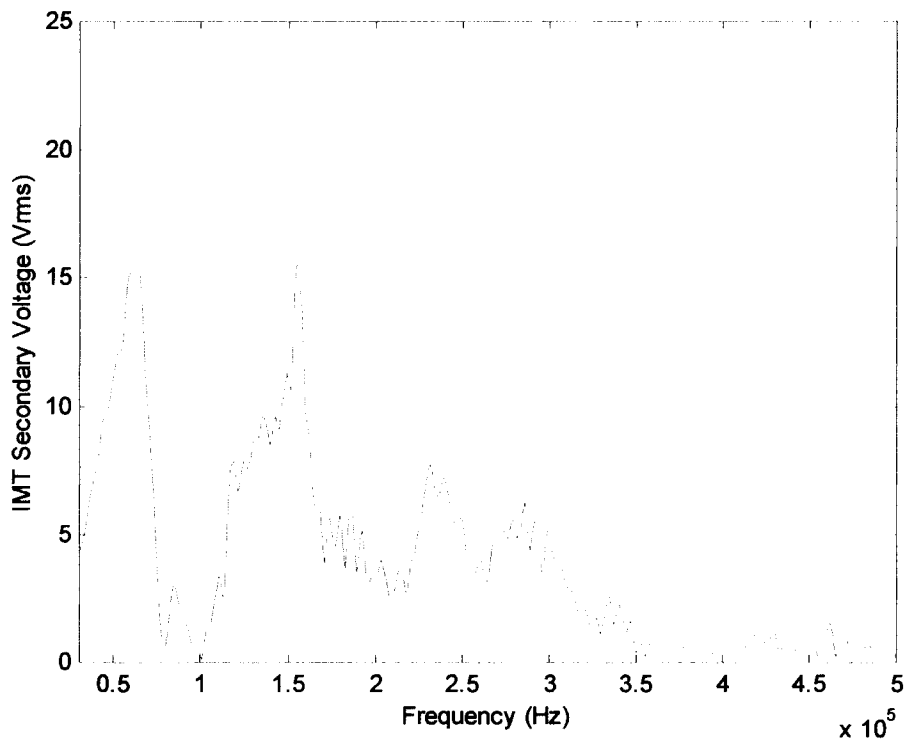

Figure 5. Waveform and frequency spectrum of arc transient. Arc transient measured simultaneously at the primary and secondary of the impedance-matching transformer (IMT) with the secondary of the IMT terminated into the carrier communication equipment. The frequency spectrum is that of the arc transient measured at the secondary of the IMT.

Reproduced with permission of the copyright owner. Further reproduction prohibited without permission.

arc transient lies in the frequency band below 300 kHz, which is a large portion of the PLC frequency band of 30 kHz to 500 kHz. Depending on the input sensitivity setting of a particular carrier receiver, the magnitude and frequency content of an arc transient could activate an OOK carrier receiver, producing a false signal reception. As is shown by the waveform of Figure 5, the majority of the arc transient's energy is dissipated over a time span of approximately 60 μs. Whether a single transient in this amount of time could activate a particular carrier receiver was not determined. However, the OOK carrier receiver at which the arc transient of Figure 5 was measured had a receive frequency of 180 kHz and was observed to activate intermittently during arcing of the arc gap. The false signal receptions by this receiver caused the supervisory control and data acquisition (SCADA) remote terminal unit (RTU) at the power substation to malfunction as a result of excessive state transitions of the status point monitoring carrier signal reception.

To determine if the high voltage levels measured on the 230-kV coupling system were caused by the excitation of a series resonance, the coupling system was modeled using PSpice. Frequency response analysis of the coupling system revealed that the system exhibited high voltage gain at the drain coil at about 2.95 kHz, which coincided with the dominant harmonic frequencies measured. The circuit used for PSpice analysis is shown in Figure 6. The voltage gain calculated at the drain coil is shown in the frequency response plot of Figure 7. The voltage gain is given in dB referenced to the source voltage. For further validation, a physical model of the coupling system was built, and the frequency response of the model was measured. The model consisted of an identical line tuner with the same settings as those on the line tuner of the actual 230-kV coupling system. The drain coil used with the model was also identical to that of the actual coupling

Reproduced with permission of the copyright owner. Further reproduction prohibited without permission.

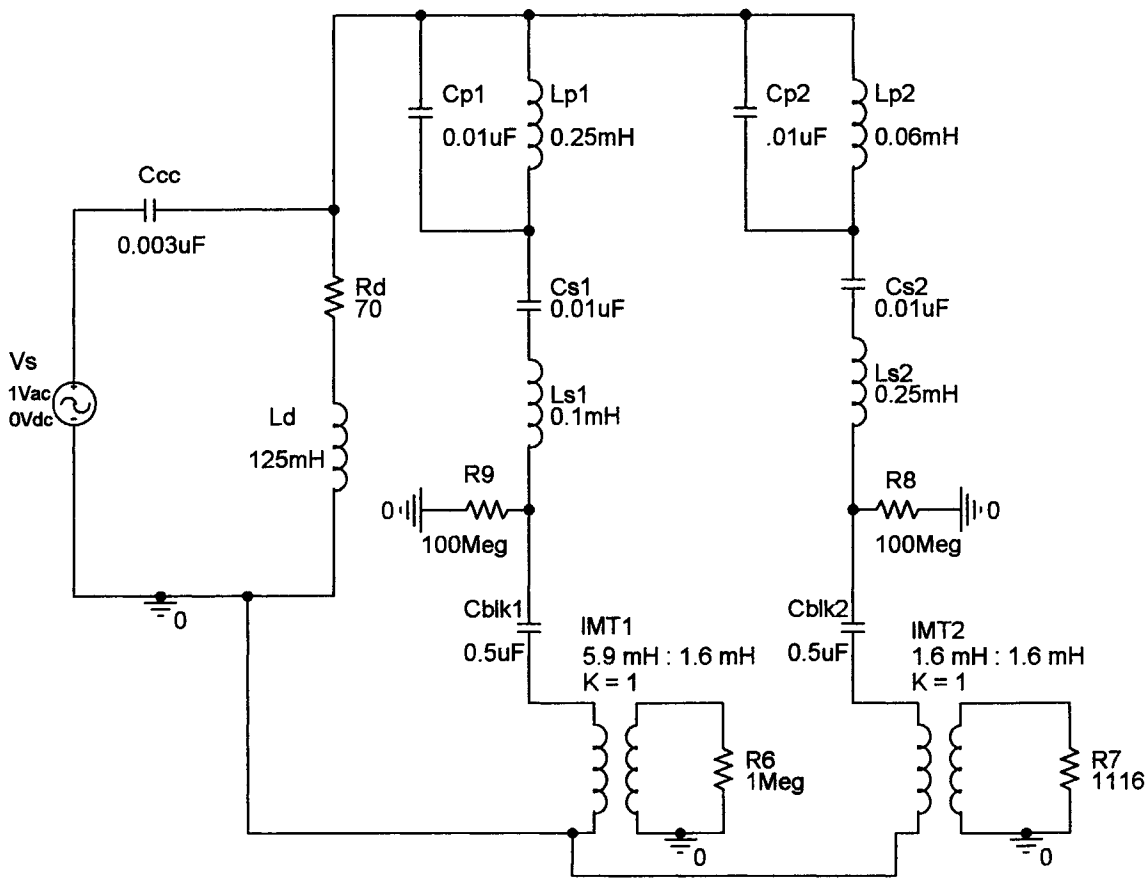

Figure 6. PSpice model of a 230-kV coupling system.

Reproduced with permission of the copyright owner. Further reproduction prohibited without permission.

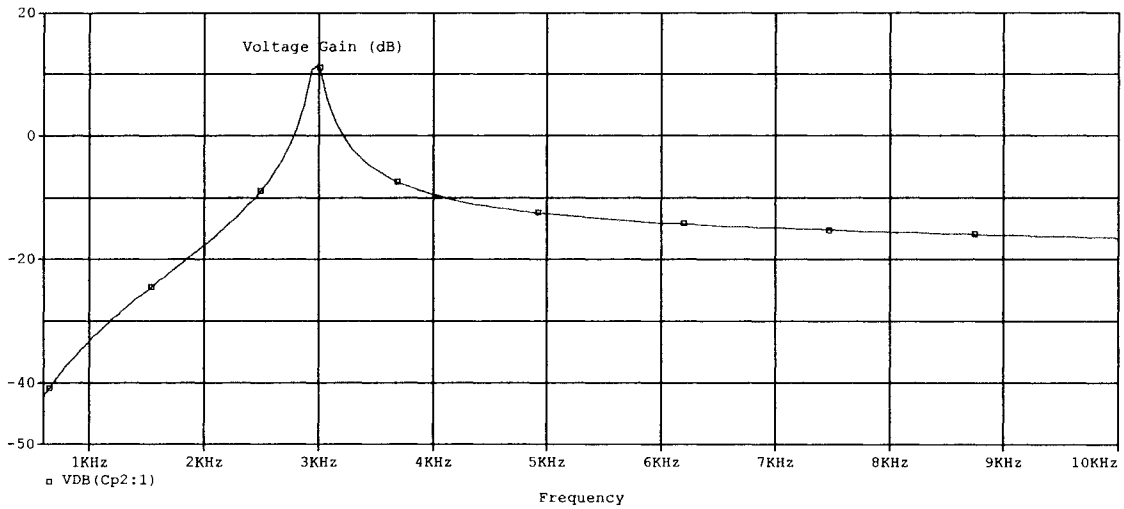

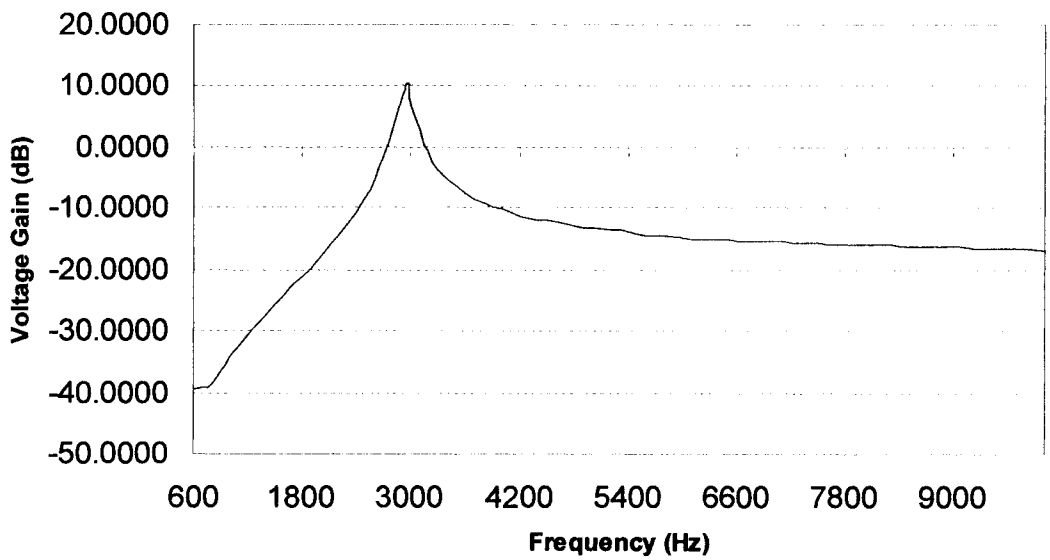

Figure 7. Comparison of simulated and measured frequency responses for a 230-kV coupling system. The top figure is the PSpice simulated frequency response of a 230-kV coupling system, and the lower figure is the measured frequency response of the same 230-kV coupling system. For both cases, voltage gain is calculated in dB at the drain coil referenced to the source voltage.

Reproduced with permission of the copyright owner. Further reproduction prohibited without permission.

system. A small capacitor with the same capacitance as the 230-kV coupling capacitor was used with the model. The measured frequency response of the model, also shown in Figure 7, confirmed the PSpice analysis. The frequency response and coupling system data are those of the two-frequency system provided in Appendix A.

Purpose of Study

The work by Crowley and Parker (1993) and Tatro et al. (1993) characterized the nature and origin of PLC coupling system problems caused by high-frequency harmonics. However, neither of the works presented coupling system modeling or provided detailed analysis of the effects of the various coupling system components on the frequency response of the systems. Tatro et al. stated that line tuner configuration and settings affect frequency response, but did not describe how they affect frequency response other than stating that the presence of the line tuner causes the undesirable series resonant frequency to be lower than that of the lone combination of the coupling capacitor and drain coil. Tatro et al. also suggested that altering the drain coil inductance in an effort to shift the undesirable resonant frequency to a point absent from harmonic noise could mitigate the problems. However, no guidance on determining suitable values for drain coil inductance was provided. Crowley and Parker presented a method for mitigation of IMT saturation problems. They added an additional parallel inductor and capacitor (LC) trap circuit in parallel with the existing line tuner. The parallel LC trap was tuned to the carrier frequency, thus presenting low impedance to harmonic frequencies. However, no explanation was given regarding how the trap circuit affected performance of the line tuner at carrier frequencies, particularly when two or more carrier frequencies are being transmit-

Reproduced with permission of the copyright owner. Further reproduction prohibited without permission.

ted through the tuner. Concerns may be raised over line tuner insertion loss with multiple carrier frequencies present since the parallel LC trap will only present high impedance to the one carrier frequency to which it is tuned to resonate.

Some other resources on high-voltage PLC systems (e.g., General Electric [GE], n.d.a, n.d.b, n.d.c, n.d.d; Podszeck, 1972; *IEEE Guide for Power-Line Carrier Applications*, 1980; Sanders & Ray, n.d.; Trench, n.d.) either do not mention harmonic frequency interference at all or mention it only in passing. For example, an industry standard for PLC systems (*IEEE Guide for Power-Line Carrier Applications*), Podszeck, and manufacturers' instruction books (GE, n.d.a, n.d.b, n.d.c, n.d.d; Trench) do not discuss the problem at all. Sanders and Ray do note that a series resonance between the coupling capacitor and drain coil can possibly be excited by HVDC converter harmonics. However, no discussion of the effect of the line-tuning components on the series resonance is provided. The fact that simply calculating the resonant frequency of the PLC system using only the drain coil inductance and coupling capacitance is not sufficient can be exemplified by the previously described PLC system on the 230-kV line. This system had a drain coil inductance of approximately 125 mH and a coupling capacitance of 0.003 μF. If the familiar equation $f = 1/(2\pi\sqrt{LC})$ for calculating the resonant frequency of a series LC circuit is used, the resonant frequency for the coupling capacitor and drain coil combination is approximately 8.22 kHz. This result is significantly different from the measured resonant frequency of approximately 2.95 kHz.

Therefore, the purpose of this study is to expand previous work (e.g., Crowley & Parker, 1993; Tatro et al., 1993) and provide an additional resource on high-frequency harmonic interference by providing the following information:

Reproduced with permission of the copyright owner. Further reproduction prohibited without permission.

1. Frequency response measurements of three common types of coupling systems using typical coupling capacitance and drain coil inductance values, where the three types of coupling systems are the single-frequency and two-frequency resonant types, and the second-order wideband band-pass type. This information will aid in gaining a general understanding of the susceptibility of the different coupling system configurations to harmonic frequency interference, as well as provide data for validation of coupling system models.
2. Computer models suitable for estimating the frequency response of these three common types of coupling systems in the harmonic frequency band. Having models of the coupling systems will be useful in predicting possible problems so that the problems can be anticipated and addressed proactively.
3. Identification of coupling system components that can be altered for problem mitigation purposes. The computer models, along with knowledge of how the system components affect frequency response, will provide a means for determining the suitability of a particular method of problem mitigation.

Reproduced with permission of the copyright owner. Further reproduction prohibited without permission.

CHAPTER 2

PLC COUPLING SYSTEM TESTS AND MEASUREMENTS

Various tests were performed on the coupling systems to obtain data for model validation and to gain a general understanding of the susceptibility of the systems to harmonic frequency interference. Tests and measurements were made on drain coils and IMTs, including a test to determine the effect of IMT saturation on impedance matching using various frequencies in the harmonic frequency band. Several other tests were also performed on the IMTs to acquire data for modeling purposes. In addition to the drain coil and IMT tests, frequency response measurements over the harmonic frequency band were taken on the three coupling systems under study. Also, using typical coupling capacitance and drain coil inductance values, measurements were made of the peak voltage gain at the drain coil and IMT for the three coupling systems.

Descriptions of PLC Coupling Systems Tested

Phase-to-Ground Coupled Narrowband Resonant Systems

There are two types of phase-to-ground coupled narrowband resonant systems commonly used; those are the single-frequency and the two-frequency resonant systems. The single-frequency system is described in chapter 1 and shown in Figure 1. The two-frequency system, shown in Figure 8, is basically two single-frequency systems with the addition of parallel LC trap circuits in series with each line tuner. Each trap circuit is tuned to block the alternate carrier signal, thus isolating the two carrier transmitters.

Reproduced with permission of the copyright owner. Further reproduction prohibited without permission.

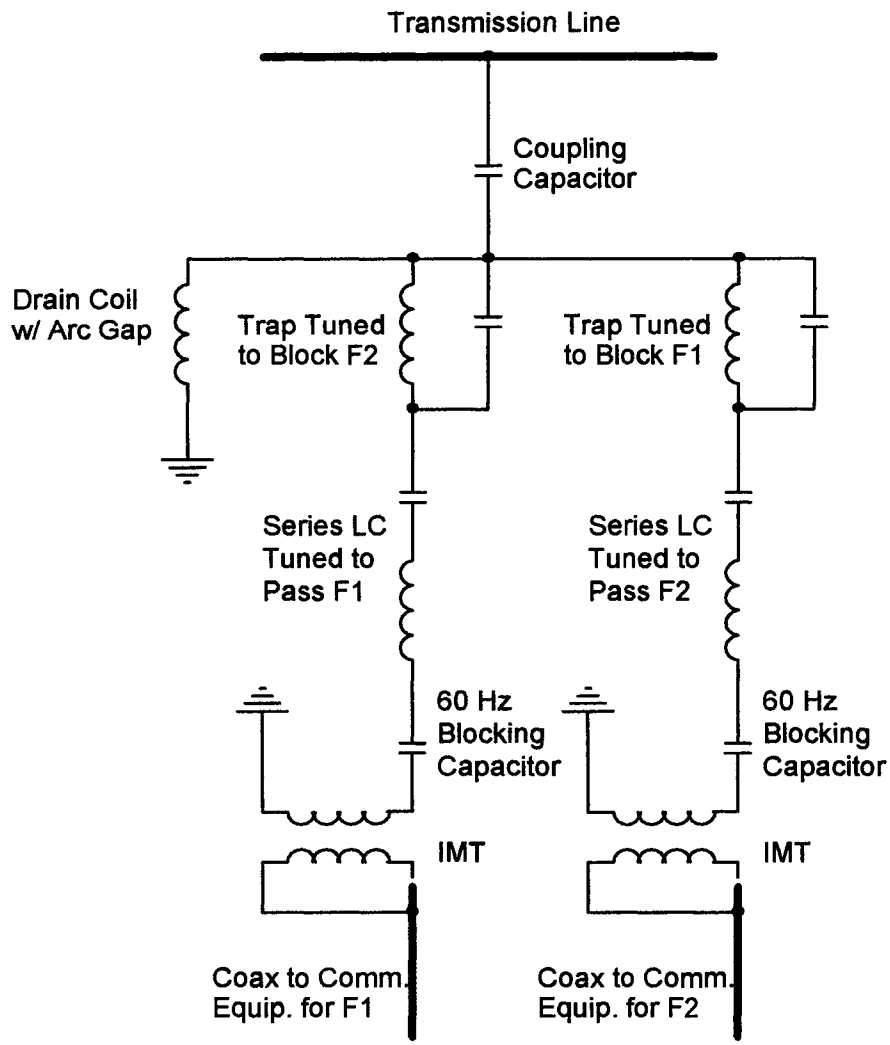

Figure 8. Schematic of a phase-to-ground two-frequency resonant coupling system. Comm. Equip. = communication equipment; LC = inductance and capacitance; L = inductance; IMT = impedance-matching transformer; Coax = coaxial cable; F1 = frequency No.1; F2 = frequency No.2.

Reproduced with permission of the copyright owner. Further reproduction prohibited without permission.

Phase-to-Ground Coupled Second-Order Wideband Band-Pass Systems

Wideband coupling systems are used when two or more carrier signals are coupled to the transmission line. Wideband coupling systems exhibit a broad band-pass response. There are also high-pass wideband coupling systems that produce a high-pass filter response. A commonly used wideband coupling system, known as a second-order wideband system, is shown in Figure 9. The order of the system determines the width of the passband. Higher order systems have more components and a wider passband.

Drain Coil Inductance and Resistance Measurements

To provide data for models, three drain coils with nameplate values of 10 mH, 25 mH, and 125 mH were tested for inductance and frequency-dependent resistance. An inductance, capacitance, and resistance (LCR) meter was used to measure inductance and resistance at 1 kHz. The inductance of each of the drain coils was measured to be within 1 or 2 mH of the nameplate value. The resistance of each drain coil at frequencies above the 1-kHz test frequency of the LCR meter was calculated from measurements of the 3-dB bandwidth of a series LC circuit composed of the drain coil and a capacitor. Each drain coil was resonated with different capacitor values to produce a range of frequencies corresponding to the harmonic frequency band. The resistance of each coil was calculated at each frequency as

$$R = 2\pi \cdot L \cdot BW, \tag{1}$$

where R is resistance, L is inductance, and BW is the 3-dB bandwidth.

Reproduced with permission of the copyright owner. Further reproduction prohibited without permission.

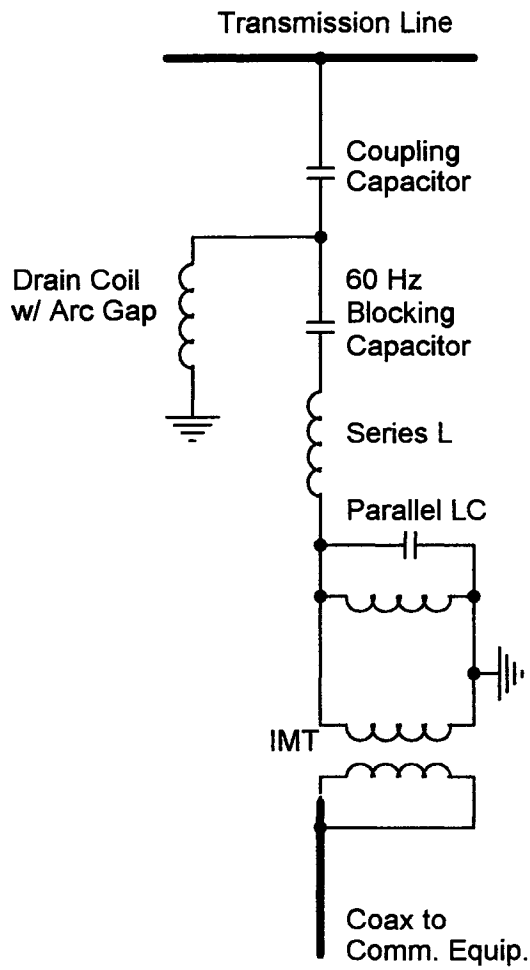

Figure 9. Schematic of a phase-to-ground second-order wideband coupling system. Comm. Equip. = communication equipment; LC = inductance and capacitance; L = inductance; IMT = impedance-matching transformer; Coax = coaxial cable.

Reproduced with permission of the copyright owner. Further reproduction prohibited without permission.

Equation 1 was derived from two equations for tuned circuits given by Temes (1979) as

$$Q = \frac{2\pi f_0 L}{R} \tag{2}$$

and

$$Q = \frac{f_0}{BW}. \tag{3}$$

In Equations 2 and 3,

Q is the quality factor of the inductor,

f_0 is the resonant frequency of the series LC circuit,

R is resistance,

L is inductance, and

BW is the 3-dB bandwidth of the series LC circuit.

Figure 10 shows a plot of frequency versus resistance for the drain coils. The data from the drain coil tests are provided in Appendix A.

IMT Tests

Two types of IMTs were tested to obtain data for modeling purposes. One type was an older generation IMT that utilizes a toroidal core design, and the other type was a newer generation IMT that utilizes a pot core design. For modeling purposes, measurements were made of the winding inductance and resistance, and the coefficient of coupling was also derived. Short-circuit tests were also performed using frequencies in the harmonic frequency band to determine the significance of IMT leakage reactance at

Reproduced with permission of the copyright owner. Further reproduction prohibited without permission.

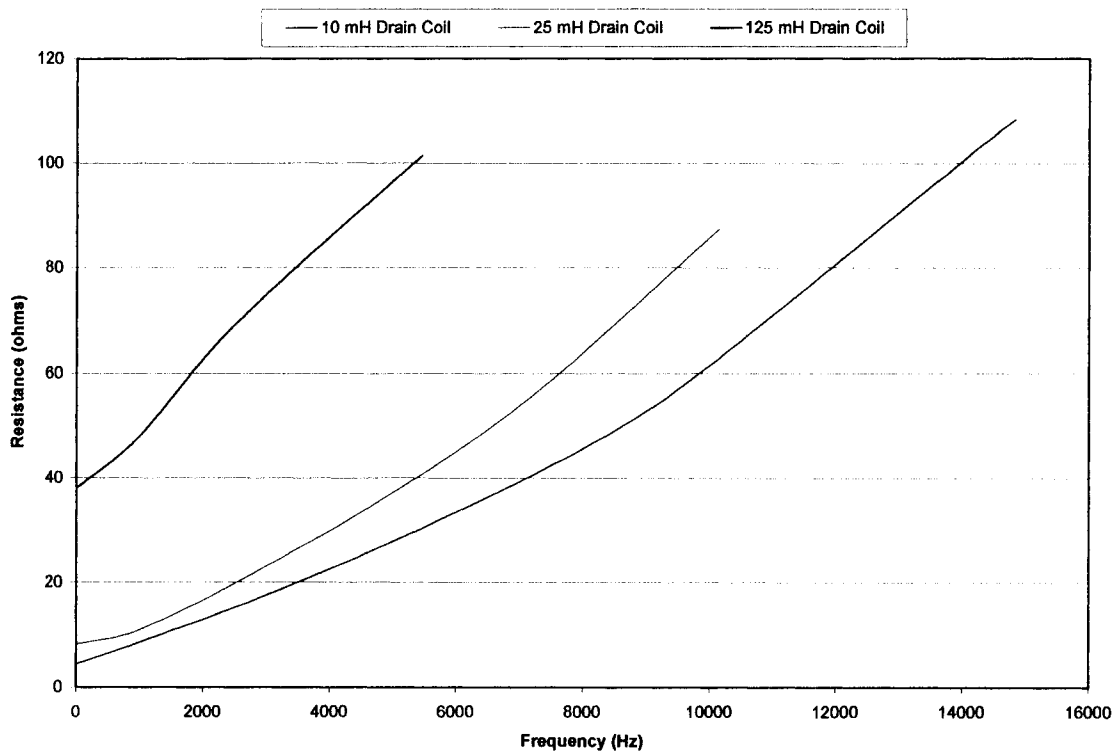

Figure 10. Variation in drain coil resistance versus frequency.

Reproduced with permission of the copyright owner. Further reproduction prohibited without permission.

harmonic frequencies. In addition, other tests such as saturation at harmonic frequencies and equivalent series inductance at PLC frequencies were performed.

Winding Inductance and Resistance Measurements

Using an LCR meter with a 1-kHz test frequency, measurements were taken of the IMT open-circuit winding inductance and resistance at different taps. The impedance transformation ratio using the winding inductance measurements was then calculated and compared to the IMT nameplate impedance transformation ratio to validate the measurements. The results of the measurements are shown in Table 1.

Table 1

Impedance-Matching Transformer (IMT) Winding Inductance and Resistance

IMT core type	Nameplate impedance transformation ratio	Calculated impedance transformation ratio	Winding inductance (mH)	Winding resistance (Ω)
Toroidal	1.0 : 1	1.1 : 1	1.795	0.83
Toroidal	1.6 : 1	1.7 : 1	2.820	1.19
Toroidal	2.8 : 1	3.1 : 1	5.094	1.89
Toroidal	4.6 : 1	5.2 : 1	8.426	2.87
Toroidal	7.8 : 1	8.7 : 1	14.290	4.75
Toroidal	*	*	1.636	0.76
Pot	3 .0: 1	3.0 : 1	13.840	0.75
Pot	3.6 : 1	3.6 : 1	16.660	0.96
Pot	4.3 : 1	4.4 : 1	20.260	1.24
Pot	5.2 : 1	5.3 : 1	24.240	1.52
Pot	6.2 : 1	6.4 : 1	29.180	1.85
Pot	7.5 : 1	7.7 : 1	35.270	2.28
Pot	9.0 : 1	9.1 : 1	41.700	2.50
Pot	*	*	4.592	0.34

* Indicates the secondary winding of the impedance-matching transformer, which does not have multiple taps. The other measurements are for the primary winding at each tap.

Reproduced with permission of the copyright owner. Further reproduction prohibited without permission.

Coefficient-of-Coupling Measurements

The coefficient of coupling of each IMT was calculated according to an industry standard for testing electronics transformers (*IEEE Recommended Practice for Testing Electronics Transformers and Inductors*, 1996). As defined in the standard, the coefficient of coupling is the ratio of the impedance of the coupling to the square root of the product of the total impedances of similar elements in the two meshes. In the case of transformers, coupling refers to inductive coupling. The standard indicates that the coefficient of coupling can be calculated as

$$K = \frac{L_{sa} - L_{so}}{4\sqrt{L_{1o} \cdot L_{2o}}}. \tag{4}$$

In Equation 4,

K is the coefficient of coupling,

L_{sa} is the inductance of the two windings connected series-aiding,

L_{so} is the inductance of the two windings connected series-opposing,

L_{1o} is the open circuit or self-inductance of Winding 1, and

L_{2o} is the open circuit or self-inductance of Winding 2.

The inductance of the windings connected series-aiding and series-opposing was measured using an LCR meter with a 1-kHz test frequency, and the results are shown in Table 2. The open-circuit inductance measurements of each winding were presented previously in Table 1. Using the measured inductance values, the coefficient of coupling was calculated for each IMT tap using Equation 4 and is presented in Table 2. As shown in

Reproduced with permission of the copyright owner. Further reproduction prohibited without permission.

Table 2

Impedance-Matching Transformer (IMT) Coefficient of Coupling

IMT Core type	Name-plate impedance transformation ratio	L_{sa} (mH)	L_{so} (mH)	Coefficient of coupling	L_{so} + Error (mH)	Coefficient of coupling with meter error
Toroidal	1.0 : 1	6.97	0.56	0.94	0.62	0.93
Toroidal	1.6 : 1	8.89	0.44	0.98	0.49	0.98
Toroidal	2.8 : 1	12.68	1.07	1.01	1.19	0.99
Toroidal	4.6 : 1	17.68	2.66	1.01	2.97	0.99
Toroidal	7.8 : 1	25.83	6.21	1.01	6.91	0.98
Pot	3.0 : 1	34.65	2.42	1.01	2.70	1.00
Pot	3.6 : 1	39.00	3.67	1.01	4.09	1.00
Pot	4.3 : 1	44.36	5.45	1.01	6.07	0.99
Pot	5.2 : 1	50.11	7.60	1.01	8.46	0.99
Pot	6.2 : 1	57.05	10.49	1.01	11.67	0.98
Pot	7.5 : 1	65.38	14.27	1.00	15.87	0.97
Pot	9.0 : 1	74.28	18.66	1.00	20.75	0.97

Note: L_{sa} = inductance of the windings connected series-aiding; L_{so} = inductance of the windings connected series-opposing.

Table 2, the calculation of the coefficient of coupling for several of the IMT taps resulted in values greater than unity. Therefore, the measurement error of the LCR meter was taken into account to determine if measurement error could have caused the coefficient-of-coupling calculations to result in values greater than unity. The meter manufacturer's instruction book (Extech Instruments, 2003) indicates that the measurement error for the meter can be calculated using Equation 5, which is the equation for error when the meter's range is set to 19.999 mH. Equation 5 is

$$Error = \pm(0.012 \cdot rdg + \frac{rdg}{10} + 0.005)\ \text{mH}, \tag{5}$$

Reproduced with permission of the copyright owner. Further reproduction prohibited without permission.

where

Error is the measurement error in units of milli-henries, and

rdg is the meter reading.

Using Equation 5, the error of the L_{so} measurements was calculated and added to the L_{so} measurements, and the coefficient of coupling was recalculated using the values for L_{so} plus the measurement error. The results are given in Table 2. As shown in Table 2, taking the meter error into account resulted in coefficient-of-coupling values less than or equal to unity. Since the coefficient of coupling was very close to unity and could only be considered accurate to within a couple of hundredths, the coefficient of coupling was set to unity for IMT modeling in PSpice.

Short-Circuit and Open-Circuit Tests at Harmonic Frequencies

According to Fitzgerald, Kingsley, and Umans (1990), the magnetizing inductance of a broadband transformer such as an IMT at low frequencies is approximately the self-inductance of the primary winding. The frequencies in the harmonic frequency band are low relative to carrier frequencies for which the IMT was designed. Therefore, in lieu of open-circuit tests, the winding self-inductance measurements presented in Table 1 are used for modeling the IMT magnetizing inductance.

Fitzgerald et al. (1990) also stated that, at low frequencies, the IMT leakage inductance is negligible. Nevertheless, short-circuit tests were performed to verify that the IMT leakage inductance is insignificant in the harmonic frequency band. The short-circuit tests were performed in the traditional manner with the secondary, or low-impedance side, of the IMT shorted. Voltage was applied to the primary terminals; the

Reproduced with permission of the copyright owner. Further reproduction prohibited without permission.

current, including phase angle, was then measured. The phase angle of the current was referenced to the input voltage. From the voltage, current, and phase angle measurements, the real and reactive parts of the IMT impedance were calculated. The leakage inductance was then calculated from the reactive part of the IMT impedance. The results of the tests are shown in Table 3. The tests were performed on only one tap of each IMT, but the tap chosen was in the middle of the IMT tap range. For both IMTs, the leakage inductance is very small in comparison to the self-inductance of each IMT winding, which confirms Fitzgerald et al.'s statement that a broad bandwidth transformer requires a high ratio of self-inductance to leakage inductance. The test results also confirm the insignificance of the IMT leakage inductance in the harmonic frequency band.

Table 3

Impedance-Matching Transformer (IMT) Leakage Inductance at Harmonic Frequencies

IMT Core type	Name-plate impedance transformation ratio	Frequency (Hz)	Input voltage (Vrms)	Current (Arms)	Phase angle of current (degrees)	IMT leakage inductance (μH)
Toroidal	4.6 : 1	1,000	2.084	0.425	-21	279.68
Toroidal	4.6 : 1	3,000	3.010	0.451	-45	250.37
Toroidal	4.6 : 1	5,000	4.000	0.458	-62	245.46
Toroidal	4.6 : 1	7,000	4.920	0.448	-69	233.11
Toroidal	4.6 : 1	9,000	6.550	0.489	-71	223.96
Pot	5.2 : 1	1,000	0.662	0.511	-13	46.38
Pot	5.2 : 1	3,000	0.750	0.521	-30	38.18
Pot	5.2 : 1	5,000	0.859	0.514	-44	36.95
Pot	5.2 : 1	7,000	0.800	0.409	-56	36.87
Pot	5.2 : 1	9,000	0.886	0.386	-66	37.08

Note: Vrms = root-mean-square volts; Arms = root-mean-square amperes.

Reproduced with permission of the copyright owner. Further reproduction prohibited without permission.

Saturation Tests at Harmonic Frequencies

IMT saturation has been reported by others (e.g., Crowley & Parker, 1993; Tatro et. al., 1993) to cause PLC signal interference, but no data were presented regarding voltage levels required to induce saturation. Therefore, saturation tests were performed on the IMTs at several different frequencies in the harmonic frequency band. Saturation curves for the toroidal core IMT are shown in Figure 11, and those for the pot core IMT are shown in Figure 12. The saturation curves were obtained by applying voltage to the secondary, or low-impedance terminals, of the IMT and measuring the current into the IMT. The corresponding primary voltage required to induce saturation can be found by multiplying the voltage levels shown in Figures 11 and 12 by the IMT voltage transformation ratio, which is the square root of the impedance transformation ratio given by the IMT tap setting. On the basis of the saturation curves, the newer IMT with the pot core design is much less susceptible to saturation problems at harmonic frequencies than the older IMT with the toroidal core design is found to be. Also, as expected, voltage levels inducing saturation increase with frequency for both types of IMTs. Thus, IMT saturation becomes less of a problem as interfering signals increase in frequency.

Equivalent Series Inductance at Carrier Frequencies

The equivalent series inductance presented to a carrier transmitter by an IMT at carrier frequencies can be relevant when assessing harmonic interference mitigation methods since this inductance affects line tuning for resonant type coupling systems and thus may constrain alteration of the line tuner series capacitance. Therefore, this inductance was measured for both types of IMTs at two carrier frequencies separated by more

Reproduced with permission of the copyright owner. Further reproduction prohibited without permission.

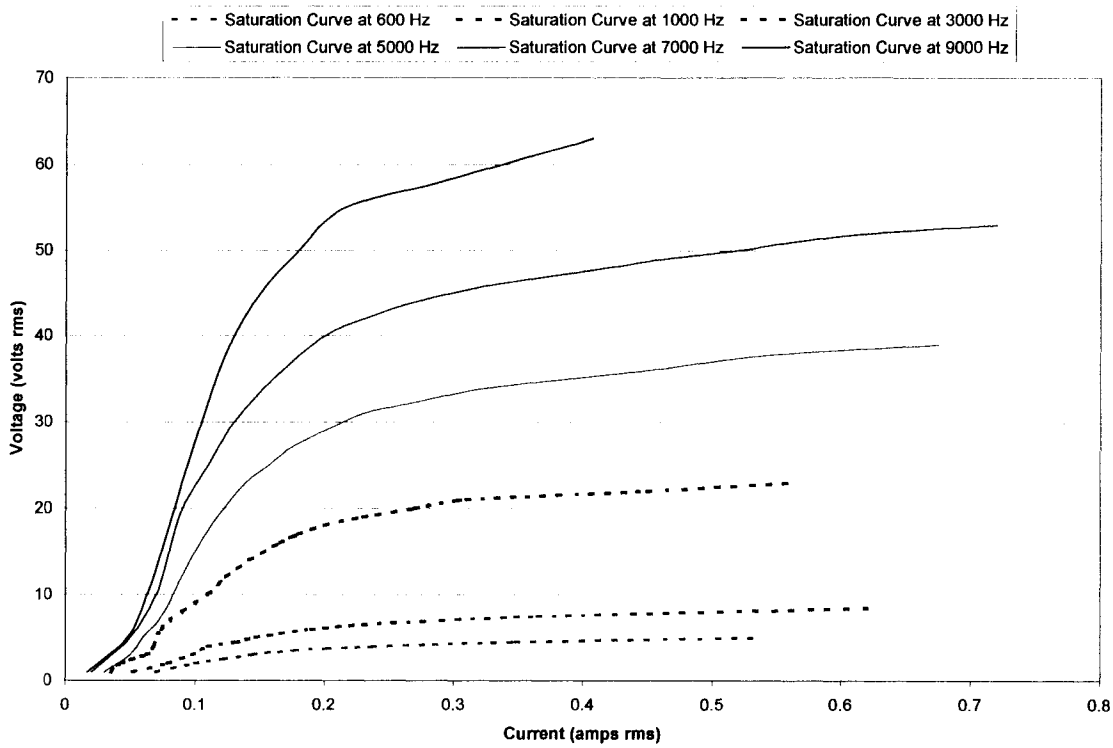

Figure 11. Saturation curves for impedance-matching transformer with toroidal core. Voltage applied to secondary side of impedance-matching transformer, which is the low-impedance side.

Reproduced with permission of the copyright owner. Further reproduction prohibited without permission.

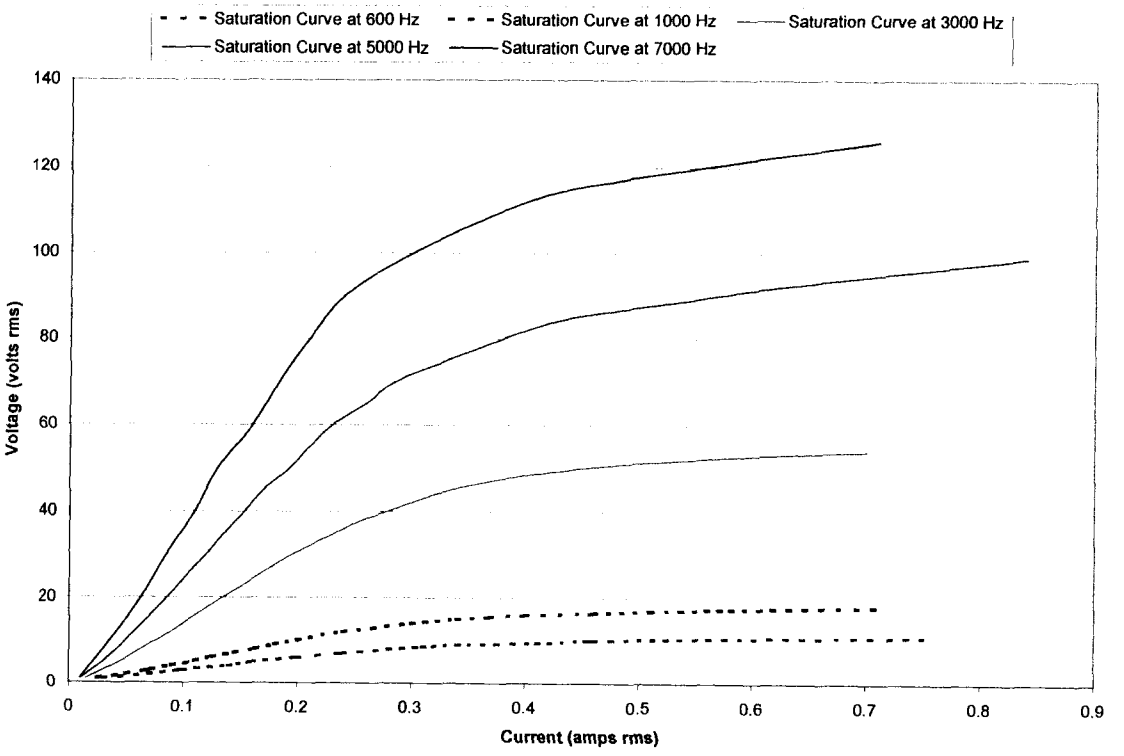

Figure 12. Saturation curves for impedance-matching transformer with pot core. Voltage applied to secondary side of impedance-matching transformer, which is the low-impedance side.

Reproduced with permission of the copyright owner. Further reproduction prohibited without permission.

than 100 kHz. Two widely separate carrier frequencies were used to determine if the inductance varied significantly with frequency. Also, the inductance was measured at three IMT tap settings for each IMT; the IMT taps chosen were those typically used for overhead transmission lines.

The test circuit used to measure the inductance is shown in Figure 13. Basically, the equivalent series inductance of the IMT and the terminating capacitor form a series LC circuit. Thus, at some frequency, the equivalent series inductance presented by the IMT will be series resonant with the terminating capacitor. With the capacitance and the resonant frequency known, the equivalent series inductance of the IMT can be calculated using the well-known equation for LC resonant circuits of $L = 1/(\omega^2 C)$, where $\omega = 2\pi f$ and where f is the frequency. The test consisted of varying the frequency of the carrier

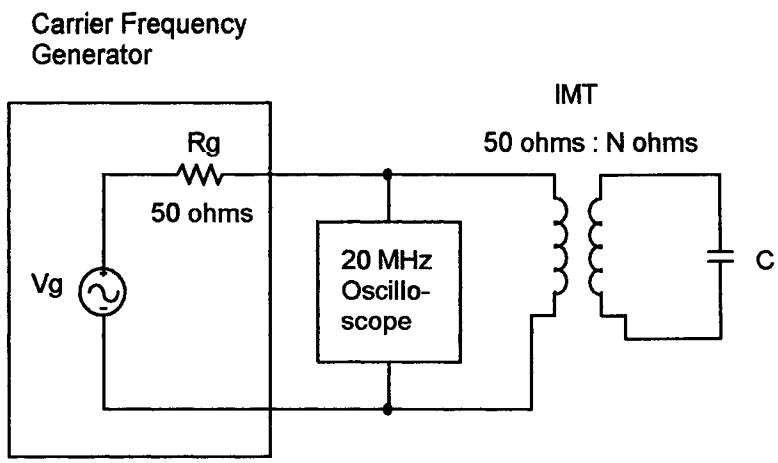

Figure 13. Test circuit for measuring the equivalent series inductance of an impedance-matching transformer (IMT) at carrier frequencies. Frequency swept until null voltage appeared on the oscilloscope, which indicated the IMT equivalent series inductance and the terminating capacitance were series resonant. C = capacitor; Rg = generator resistance.

Reproduced with permission of the copyright owner. Further reproduction prohibited without permission.

frequency generator until a null voltage appeared at the generator terminals, which meant that the IMT inductance was series resonant with the terminating capacitance. The test results are presented in Table 4.

Table 4

Impedance-Matching Transformer (IMT) Equivalent Series Inductance at Carrier Frequencies

IMT Core type	Nameplate impedance transformation ratio	Capacitance (μF)	Resonant frequency (kHz)	Equivalent series inductance (μH)
Toroidal	2.8 : 1	0.010246	145.4	116.94
Toroidal	2.8 : 1	0.003457	247.3	119.81
Toroidal	4.6 : 1	0.010246	122.2	165.56
Toroidal	4.6 : 1	0.003457	208.2	169.04
Toroidal	7.8 : 1	0.010246	103.7	229.89
Toroidal	7.8 : 1	0.003457	179.4	227.66
Pot	5.2 : 1	0.033920	182.3	22.47
Pot	5.2 : 1	0.010246	332.3	22.39
Pot	6.2 : 1	0.033920	166.0	27.10
Pot	6.2 : 1	0.010246	304.0	26.75
Pot	7.5 : 1	0.033920	137.4	39.56
Pot	7.5 : 1	0.010246	250.6	39.37

The test results show that the equivalent series inductance of an IMT does not vary significantly with carrier frequency. However, the inductance does vary somewhat with changes in IMT taps, especially for the older toroidal core IMT. Also, the equivalent series inductance of the toroidal core IMT is significantly larger than the newer IMT with the pot core design is found to be. The smaller series inductance presented by the pot core IMT explains why newer generation resonant type coupling systems do not require a high-frequency tuning capacitor; that is, at higher carrier frequencies and/or larger values of coupling capacitance, the larger equivalent series inductance of the older toroidal core

Reproduced with permission of the copyright owner. Further reproduction prohibited without permission.

IMT requires more canceling capacitive reactance to achieve resonance. This additional capacitive reactance is provided by the high-frequency tuning capacitor found in the older generation resonant type coupling systems.

Effect of Harmonic-Frequency Interference on Impedance Matching at Carrier Frequencies

To quantify the effects of harmonic frequency interference and IMT saturation on impedance matching at carrier frequencies, a test was devised to measure reflected power at carrier frequencies in the presence of harmonic frequency interference. Harmonic frequency interference was applied at voltage levels corresponding to those used to produce the IMT saturation curves of Figures 11 and 12. The percentage of reflected power was chosen as the quantifying measure because electric utilities generally use the percentage of reflected power as a measure of PLC line-tuning quality, according to a report by an Institute of Electrical and Electronics Engineers working group (Power Line Carrier Practices Working Group, 1995). From this report, most utilities accept an impedance mismatch that produces between 8% and 15% reflected power as seen by the carrier transmitter. Therefore, the primary goal of the test was to determine if harmonic frequency noise applied at voltage levels corresponding to the IMT saturation curves could produce a change in reflected power within this 8% to 15% range.

As shown in Figure 14, the test circuit was designed to impose both a carrier frequency signal and a harmonic frequency signal on the IMT simultaneously while isolating the carrier frequency and harmonic frequency sources from each other. The source isolation was accomplished by series and parallel LC circuits that were each tuned to resonate at the carrier test frequency of 200 kHz. The series LC circuit presents low

Reproduced with permission of the copyright owner. Further reproduction prohibited without permission.

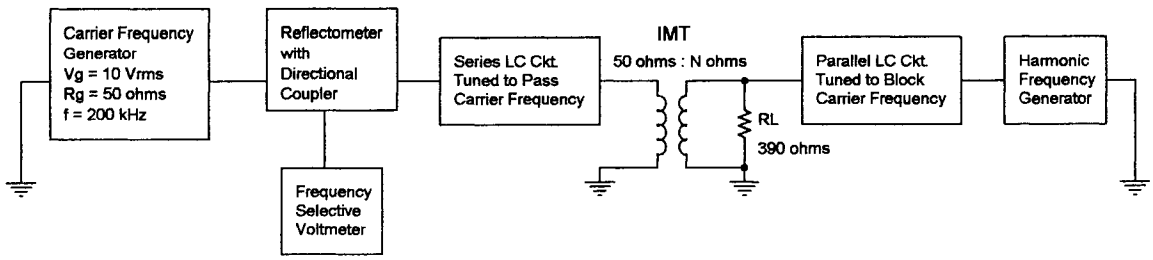

Figure 14. Test circuit for measuring the effect of harmonic frequency interference on impedance matching. IMT = impedance-matching transformer; LC = inductance and capacitance; RL = load resistance.

impedance to the carrier signal but high impedance to the harmonic frequency signal. In contrast, the parallel LC circuit presents high impedance to the carrier signal but low impedance to the harmonic frequency signal. In addition to isolating the sources, the circuit configuration also isolated the reflectometer from the harmonic frequency signal, which helped minimize error in the reflected power readings during the tests. The reflectometer interprets incoming signals from the IMT as reflected power, according to the manufacturer (Signalcrafters Tech, n.d.).

The percentage of reflected power was measured directly with the reflectometer and indirectly with a directional coupler integral to the reflectometer. The directional coupler was used to calculate the percentage of reflected power from measurements of incident and reflected voltages taken with a frequency-selective voltmeter (FSVM) with a 25-Hz notch filter. The percentage of reflected power was calculated from these voltage measurements by first calculating the reflection coefficient using Equation 6 from Hayt (1967) and then calculating the percentage of reflected power using Equation 7 from RFL Electronics (2003). Equations 6 and 7 are, respectively,

Reproduced with permission of the copyright owner. Further reproduction prohibited without permission.

$$\rho = \frac{V_{\text{Ref}}}{V_{\text{Inc}}} \tag{6}$$

and

$$\%RP = 100 \cdot \rho^2. \tag{7}$$

In Equations 6 and 7,

ρ is the reflection coefficient,

V_{Ref} is the reflected voltage,

V_{Inc} is the incident voltage, and

$\%RP$ is the percentage of reflected power.

The percentage of reflected power was measured using two different methods so that a comparison could be made between the direct reading from the reflectometer and the measurement obtained from the reflectometer's built-in directional coupler.

The tests consisted of the following steps:

1. The parallel LC blocking circuit was tuned to resonate at the carrier frequency.
2. With the harmonic source power on but output set to zero, the carrier signal was applied, and the series LC circuit and IMT were adjusted to produce minimum reflected power by adjusting for minimum reflected voltage as measured with the FSVM and directional coupler. The reflectometer was also read to verify the minimum percentage of reflected power. For the toroidal core IMT, the percentage of reflected power in the absence of the harmonic frequency source was approximately 0.01% as calcu-

Reproduced with permission of the copyright owner. Further reproduction prohibited without permission.

lated from incident and reflected voltage measurements using the FSVM. For the pot core IMT, the percentage of reflected power in the absence of the harmonic frequency source was approximately 0.12%.

3. With the carrier frequency source disabled, the harmonic frequency signal was applied; the voltage level was then adjusted to produce a voltage on the secondary, or 50-Ω side, of the IMT that corresponded to a point along the IMT saturation curve for the particular IMT under test.
4. With both sources on, measurements were taken of the incident and reflected voltages at the carrier frequency using the FSVM and directional coupler. The reflectometer reading was also recorded. To verify that both the harmonic and carrier frequency signals were applied to the IMT, voltage measurements using the FSVM were taken at both frequencies on the primary and secondary of the IMT. Similarly, to ensure the sources were isolated from each other, voltage measurements using the FSVM were taken at both frequencies at each source.

A summary of the test results is presented in Table 5, and complete test data are provided in Appendix A. Table 5 shows that a significant change in the percentage of reflected power was not encountered during the tests until the harmonic frequency interference was near or past the knee voltage on the IMT saturation curve for the particular interference frequency. For the pot core IMT, the change in the percentage of reflected power was minor even at interference levels past the saturation curve knee voltage. The correspondence between the IMT saturation curves and the percentage of reflected power is shown graphically in Figures 15 through 19. Figures 15 through 17 are for the toroidal core IMT, and Figures 18 and 19 are for the pot core IMT. Tests were not performed at

Reproduced with permission of the copyright owner. Further reproduction prohibited without permission.

Table 5

Results of Test to Determine the Effect of Harmonic Frequency Interference on Impedance Matching at Carrier Frequencies

IMT Core type	Harmonic frequency (Hz)	IMT secondary voltage at carrier frequency (Vrms)	IMT secondary voltage at harmonic frequency (Vrms)	Calculated % of reflected power using directional coupler	% of reflected power from reflectometer
Toroidal	600	11.63	1.97	0.02	0.0
Toroidal	600	11.16	3.03	0.26	0.1
Toroidal	600	11.16	4.45	0.67	1.5
Toroidal	600	11.55	5.14	13.19	45.0
Toroidal	1,000	11.12	4.95	0.28	0.0
Toroidal	1,000	11.22	6.88	0.58	0.5
Toroidal	1,000	11.38	7.75	1.30	4.0
Toroidal	1,000	11.83	8.41	5.26	33.0
Toroidal	3,000	11.09	13.66	0.30	0.0
Toroidal	3,000	11.12	15.58	0.28	0.1
Toroidal	3,000	11.14	19.37	0.40	0.5
Toroidal	3,000	11.24	25.30	11.11	21.0
Pot	600	9.23	6.85	0.12	0.0
Pot	600	9.31	7.88	0.13	0.0
Pot	600	9.25	10.72	0.32	1.0
Pot	600	8.99	11.64	1.54	9.0
Pot	1,000	9.31	11.82	0.10	0.0
Pot	1,000	9.36	13.62	0.10	0.0
Pot	1,000	9.29	17.54	0.17	0.5
Pot	1,000	9.02	19.37	1.50	8.0

Note: IMT = impedance-matching transformer; Vrms = root-mean-square volts.

Reproduced with permission of the copyright owner. Further reproduction prohibited without permission.

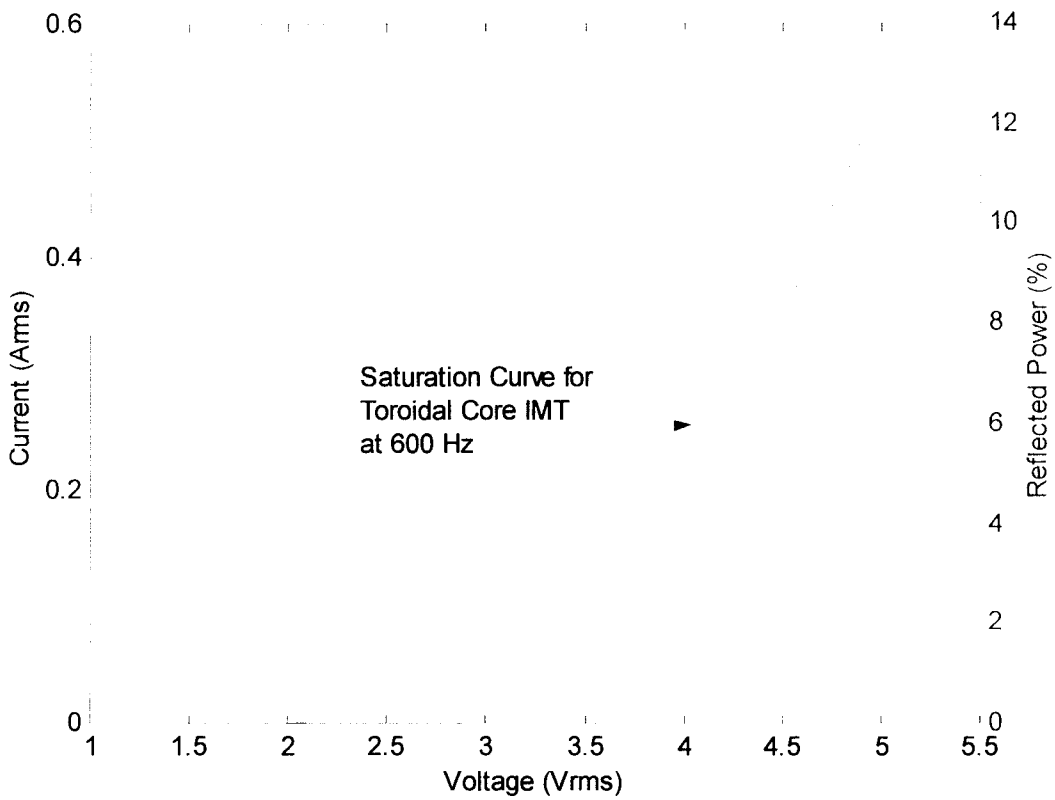

Figure 15. Curves of impedance-matching transformer (IMT) saturation and percentage of reflected power for a toroidal core IMT at 600 Hz. Voltage measured on the secondary, or low-impedance side, of the IMT.

Reproduced with permission of the copyright owner. Further reproduction prohibited without permission.

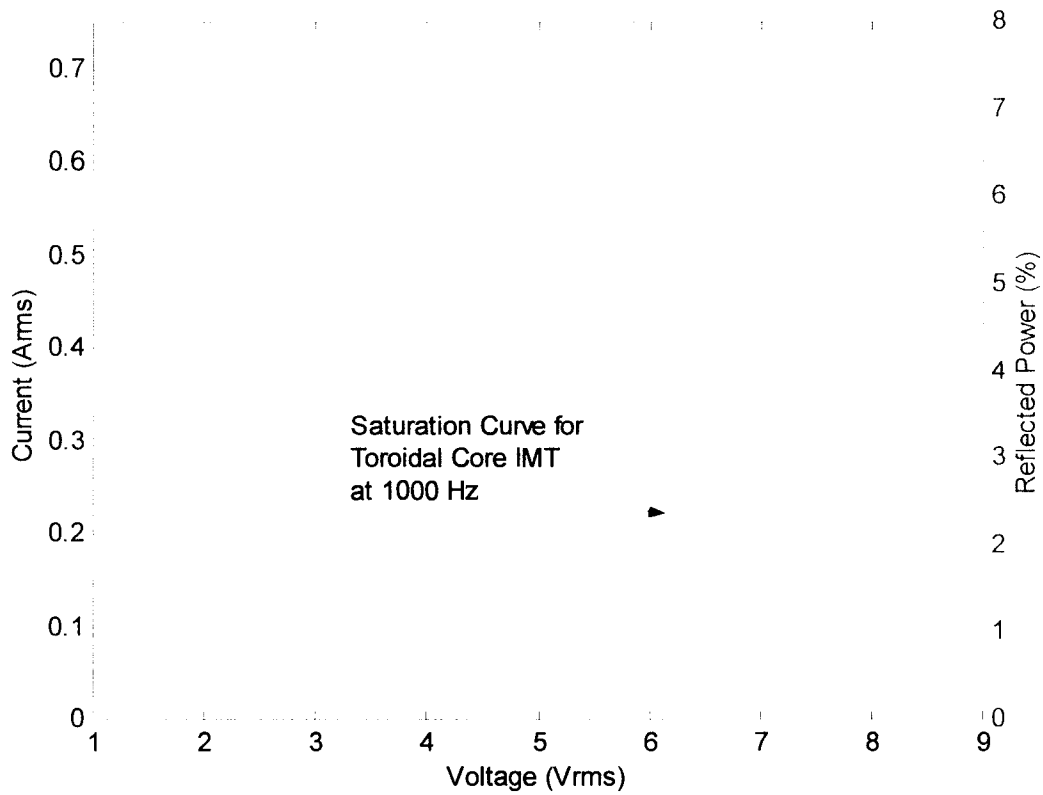

Figure 16. Curves of impedance-matching transformer (IMT) saturation and percentage of reflected power for a toroidal core IMT at 1,000 Hz. Voltage measured on the secondary, or low-impedance side, of the IMT.

Reproduced with permission of the copyright owner. Further reproduction prohibited without permission.

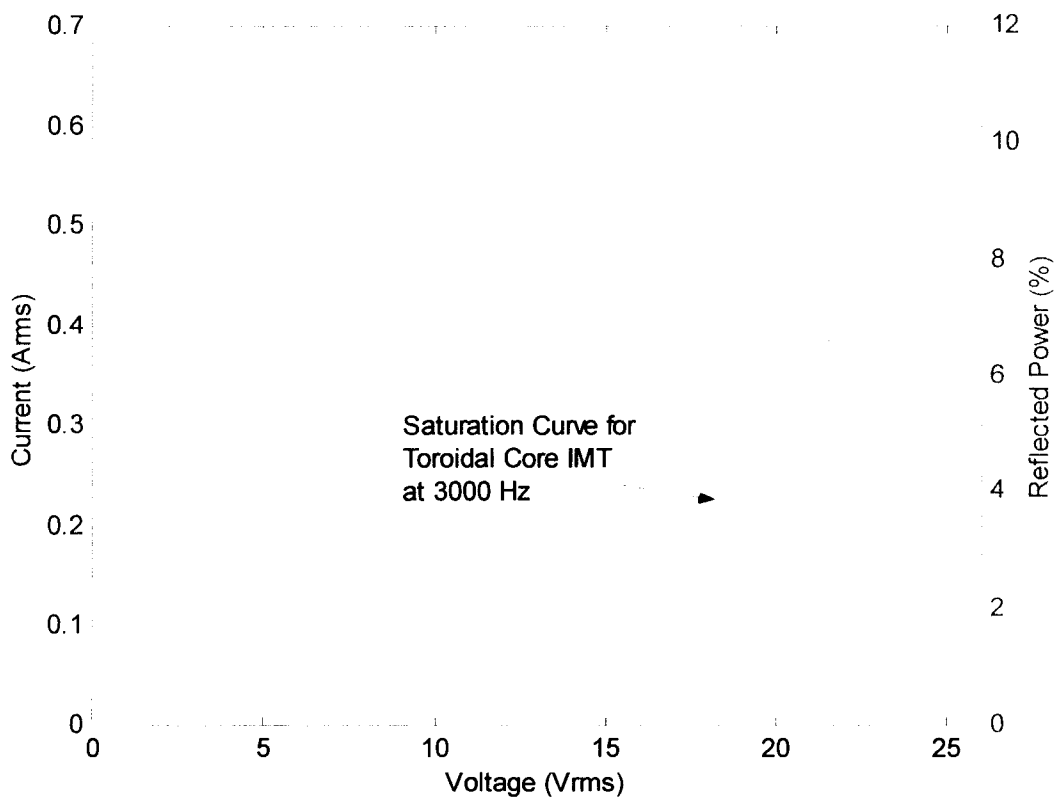

Figure 17. Curves of impedance-matching transformer (IMT) saturation and percentage of reflected power for a toroidal core IMT at 3,000 Hz. Voltage measured on the secondary, or low-impedance side, of the IMT.

Reproduced with permission of the copyright owner. Further reproduction prohibited without permission.

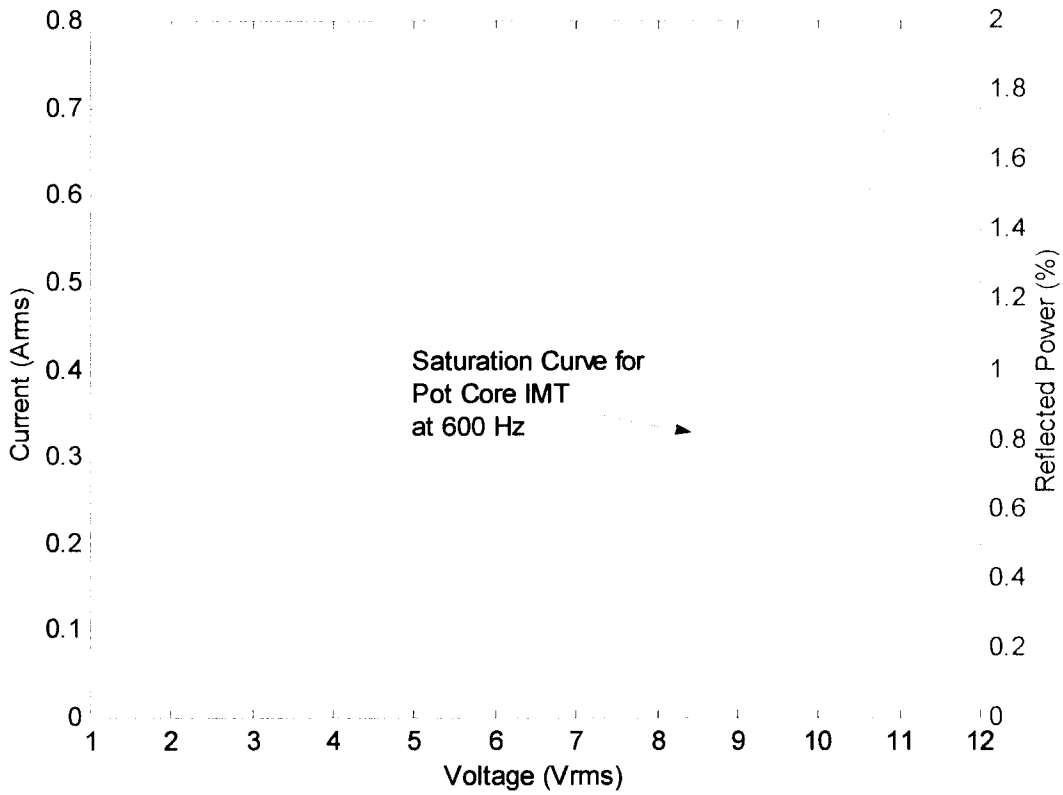

Figure 18. Curves of impedance-matching transformer (IMT) saturation and percentage of reflected power for a pot core IMT at 600 Hz. Voltage measured on the secondary, or low-impedance side, of the IMT.

Reproduced with permission of the copyright owner. Further reproduction prohibited without permission.

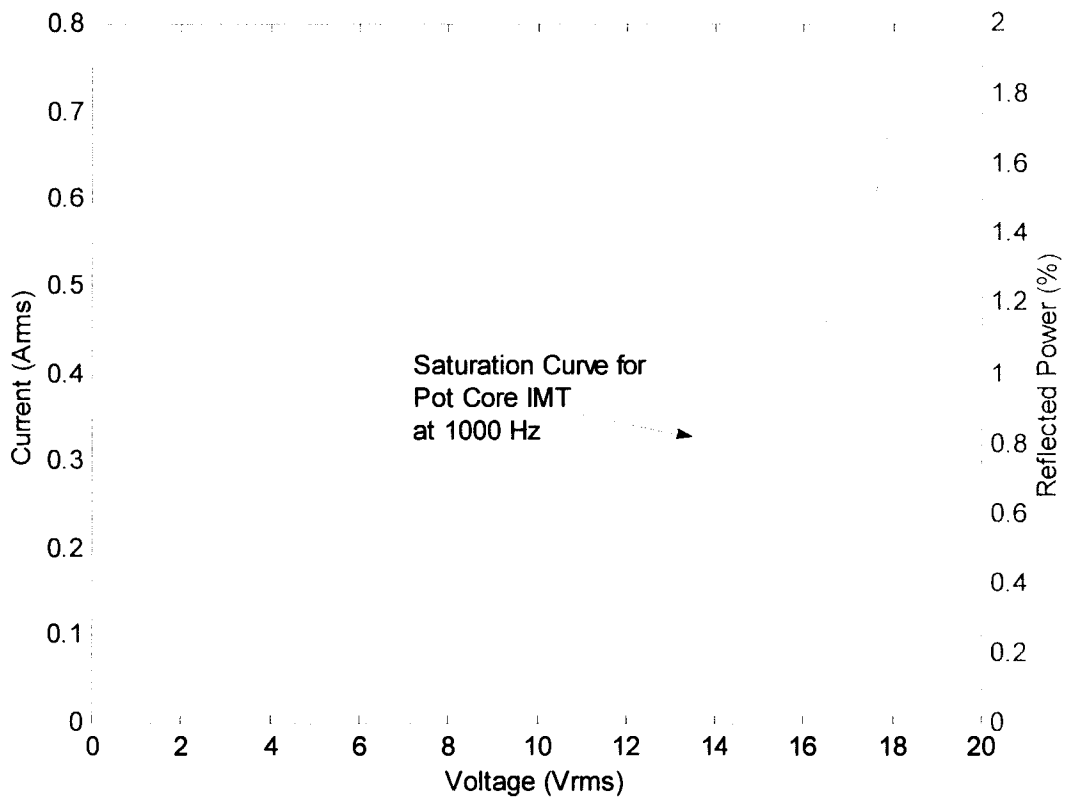

Figure 19. Curves of impedance-matching transformer (IMT) saturation and percentage of reflected power for a pot core IMT at 1,000 Hz. Voltage measured on the secondary, or low-impedance side, of the IMT.

Reproduced with permission of the copyright owner. Further reproduction prohibited without permission.

frequencies above 3 kHz for the toroidal core IMT or at frequencies above 1 kHz for the pot core IMT because of limitations of the harmonic frequency source used for the tests. Nevertheless, the results of the tests show that interference levels near the knee voltage of the IMT saturation curve can significantly affect impedance matching, especially for the older toroidal core IMT. Thus, IMT saturation curves can be used to help determine acceptable levels of harmonic frequency interference.

Also shown in Table 5 is a comparison between the percentage of reflected power read directly from the reflectometer and the percentage of reflected power calculated using the directional coupler and FSVM. The values obtained from the two measurement methods corresponded reasonably well until the IMT began to saturate. When the IMT began to saturate, the values diverged drastically for each IMT at each harmonic test frequency. The cause for the difference in the measurements could not be determined as the method used to compute the percentage of reflected power by the reflectometer was unknown. As mentioned previously, the reflectometer interprets incoming signals from the IMT as reflected power. Thus, the harmonic frequency signal could have been interpreted as reflected power. However, the level of the harmonic frequency signal passed through the series LC blocking circuit to the carrier frequency generator was approximately 10 mV or less in all cases, which was minuscule in comparison to the level of the carrier frequency signal and thus should not have impacted the reflectometer. Nevertheless, the close correspondence between the two methods of measurement at interference levels below the knee voltage of the IMT saturation curve, in conjunction with the low values of percentage of reflected power measured during the tests at those interference levels, indicates that harmonic frequency interference should not cause impedance-matching prob-

Reproduced with permission of the copyright owner. Further reproduction prohibited without permission.

lems until the IMT reaches saturation. Since mitigation of interference levels causing IMT saturation should be of primary concern, measurement of the percentage of reflected power in the presence of IMT saturation becomes an ancillary issue. However, discrepancies in the results obtained between the two measurement methods leave questions about which one is the better measurement method. Determining the best method for measuring the percentage of reflected power in the presence of harmonic frequency interference could be a topic for future work.

PLC Coupling System Measurements

Peak Voltage Gain Measurements

For each of the coupling systems, measurements were made of the peak voltage gain in the harmonic frequency band to acquire data for model validation and to determine the effect of variations in system parameters such as:

1. Type of coupling system (single frequency, two frequency, and wideband),
2. Coupling capacitance (related to the transmission line voltage),
3. Line tuner settings (related to carrier frequency), and
4. Drain coil inductance.

Each coupling system was tested with various drain coil and coupling capacitor values to provide a broad range of data. Three drain coils with nameplate values of 10 mH, 25 mH, and 125 mH were used; three values of capacitance corresponding to coupling capacitors found on the 115-kV, 230-kV, and 500-kV transmission systems were used.

The circuit configuration used for the tests is shown in Figure 20. The tests consisted of performing a frequency scan, starting at a low frequency, until a voltage peak at

Reproduced with permission of the copyright owner. Further reproduction prohibited without permission.

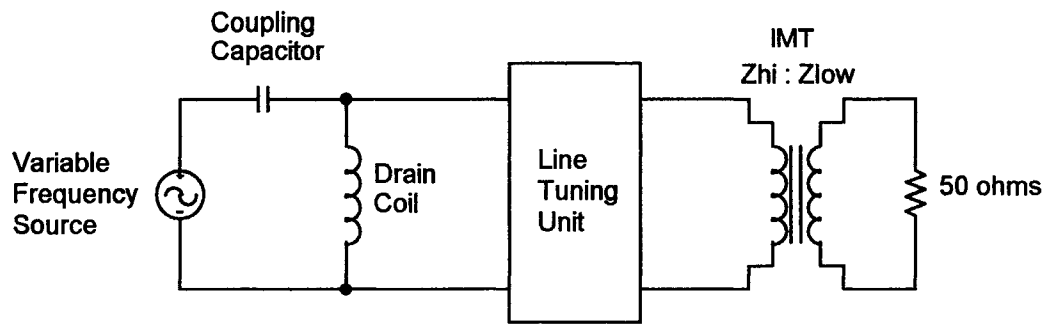

Figure 20. Test configuration for measuring peak voltage gain. The line-tuning unit is representative of any of the three types studied. Also, for all measurements, the impedance-matching transformer (IMT) was terminated into a 50-Ω resistor. The test consisted of varying the frequency of the source until a voltage peak at the drain coil was found.

the drain coil was found. At this voltage peak, voltage measurements were taken across the coupling capacitor, drain coil, and the primary and secondary of the IMT. For the cases where voltage gain at the drain coil did not exceed 0 dB in the harmonic frequency band, the voltage measurement recorded was that where the voltage peaked near the *low-order switching frequency* of the parallel combination of the drain coil and line tuner impedances. The low-order switching frequency is the lowest frequency at which the impedance formed by the parallel combination of the drain coil and line tuner impedances switches from inductive to capacitive. In other words, the low-order switching frequency is the lowest frequency at which the drain coil and line tuner impedances are parallel resonant. A voltage peak occurs at the drain coil prior to the low-order switching frequency because the inductive reactance of the drain coil and line tuner parallel combination peaks just prior to its resonance. Thus, the impedance ratio between the coupling capacitor and the combination of the drain coil and line tuner is at a minimum, which results in a voltage peak as measured at the drain coil.

Reproduced with permission of the copyright owner. Further reproduction prohibited without permission.

The results of the tests are summarized in Table 6. For brevity, only the results of the measurements using the 10-mH and 125-mH drain coils are presented in the table. Also, only the peak voltage gain at the drain coil, along with the corresponding IMT voltage gain, and the frequency at which the peak voltage gain occurred are presented in the table. The purpose of the table is to show, in general, the effects of system variations on voltage gain. The coupling system settings and complete measurement data for the tests, including the results for the 25-mH drain coil, are provided in Appendix A.

From the test data in Table 6, the following general conclusions can be drawn regarding how variations in coupling system parameters affect frequency response in the harmonic frequency band:

1. For all three coupling systems, the voltage gain at the drain coil varies directly with the inductance of the drain coil; that is, a larger inductance drain coil produces a higher voltage gain at the drain coil.
2. The coupling capacitance, which corresponds to the voltage level at which the coupling system is applied, primarily affects voltage gain, with higher voltage coupling capacitance corresponding to lower voltage gain. Stated another way, a larger valued coupling capacitance results in a higher voltage gain.
3. The line tuner setting to which frequency response was found to be most sensitive is the capacitance that is in series with the tuning inductor for single-frequency and two-frequency resonant systems. For these systems, utilization of the high-frequency tuning capacitor that is part of the series LC tuning unit drastically affects voltage gain compared to the 60-Hz blocking capacitor alone. This capacitance is identified in Table 6 as the line tuner series capacitance. The value of the high-frequency tuning

Reproduced with permission of the copyright owner. Further reproduction prohibited without permission.

Table 6

Results of Peak Voltage Gain Measurements

Coupling system	Coupling capacitance (μF)	Drain coil inductance (mH)	Series capacitance of line tuner (μF)	Frequency where voltage peak at drain coil occurred (Hz)	Voltage gain at drain coil (dB)	Voltage gain at primary of IMT (dB)
Wideband	0.006850	10	0.1	4,460	-2.52	-26.18
Wideband	0.003458	10	0.1	4,525	-8.26	-31.62
Wideband	0.001717	10	0.1	4,566	-14.17	-37.43
Wideband	0.006850	125	0.1	1,398	1.31	-42.79
Wideband	0.003458	125	0.1	1,421	-4.34	-47.90
Wideband	0.001717	125	0.1	1,435	-10.18	-53.66
Two-freq	0.006850	10	0.01, 0.01	8,696	4.39	-13.27
Two-freq	0.003458	10	0.01, 0.01	9,212	-1.57	-18.53
Two-freq	0.001717	10	0.01, 0.01	9,500	-7.68	-24.25
Two-freq	0.006850	125	0.01, 0.01	2,722	16.35	-16.40
Two-freq	0.003458	125	0.01, 0.01	2,903	11.41	-20.68
Two-freq	0.001717	125	0.01, 0.01	3,013	5.98	-25.73
Two-freq	0.006850	10	0.01, 0.5	1,566	-31.50	-35.92
Two-freq	0.003458	10	0.01, 0.5	1,562	-37.27	-41.78
Two-freq	0.001717	10	0.01, 0.5	1,563	-43.22	-47.64
Two-freq	0.006850	125	0.01, 0.5	610	-18.82	-42.56
Two-freq	0.003458	125	0.01, 0.5	611	-24.69	-48.18
Two-freq	0.001717	125	0.01, 0.5	612	-30.71	-53.76
Single-freq	0.006850	10	0.01	11,298	7.09	-8.17
Single-freq	0.003458	10	0.01	12,565	0.98	-13.15
Single-freq	0.001717	10	0.01	13,380	-5.30	-18.73
Single-freq	0.006850	125	0.01	3,456	19.51	-9.46
Single-freq	0.003458	125	0.01	3,852	14.55	-13.28
Single-freq	0.001717	125	0.01	4,114	8.92	-18.24
Single-freq	0.006850	10	0.5	1,617	-30.83	-35.19
Single-freq	0.003458	10	0.5	1,619	-36.57	-40.82
Single-freq	0.001717	10	0.5	1,625	-42.44	-46.56
Single-freq	0.006850	125	0.5	618	-18.34	-41.78
Single-freq	0.003458	125	0.5	620	-24.13	-47.23
Single-freq	0.001717	125	0.5	621	-30.05	-52.58

Note: For the second-order wideband system, the line tuner series capacitance refers to the 60-Hz blocking capacitor, which is not variable. For the two-frequency system, there are two values of line tuner series capacitance given since there are two tuning legs. The source voltage was the reference voltage for the gain calculations. IMT = impedance-matching transformer; freq = frequency.

Reproduced with permission of the copyright owner. Further reproduction prohibited without permission.

capacitor used for the tests was 0.01 μF, and the value for the 60-Hz blocking capacitor was 0.5 μF. For the single-frequency and two-frequency systems, removing the high-frequency tuning capacitor drastically lowers voltage gain.

4. For the single-frequency and two-frequency resonant systems, the voltage gain at the IMT does not change drastically for different values of drain coil inductance. However, the voltage gain at the IMT does vary significantly with coupling capacitance. Larger values of coupling capacitance result in higher voltage gain at the IMT. For the second-order wideband system, the voltage gain at the IMT varies significantly with both drain coil inductance and coupling capacitance.
5. For a given drain coil and coupling capacitor combination, the wideband system tends to be less susceptible to harmonic frequency interference than the resonant type coupling systems. This statement is based on the results of voltage gain measurements taken at the drain coil and IMT. Field measurements, as well as a lack of problems experienced with wideband systems, also indicate such systems are less susceptible to harmonic frequency interference. A primary reason for the insusceptibility of the wideband system to harmonic frequency interference is that the only series capacitance used in the second-order wideband line tuner is the 60-Hz blocking capacitor, which has a relatively large value.

The results of the measurements indicate that the coupling systems most likely to experience problems resulting from harmonic frequency interference are single-frequency and two-frequency resonant systems applied on the 115-kV and 230-kV transmission systems. These systems are most susceptible to harmonic frequency interference when they have the combination of a high-inductance drain coil and a small line tuner series capaci-

Reproduced with permission of the copyright owner. Further reproduction prohibited without permission.

tance (e.g., a single-frequency resonant type coupling system that has a drain coil inductance greater than 100 mH and utilizes a high-frequency tuning capacitor, which is typically less than 0.01 μF).

Frequency Response Measurements

The frequency response of each coupling system was measured from 600 Hz to 10 kHz at 200-Hz intervals. A frequency interval of 200 Hz was chosen to reduce the number of data points; also, the peak voltage gain had been measured in other tests described in the immediately preceding section. Since previous tests had identified larger values of coupling capacitance and drain coil inductance as being more problematic, the frequency response tests were performed with a coupling capacitance of 0.003458 μF and a drain coil inductance of approximately 125 mH. To determine the effect of the IMT termination on frequency response, two widely different IMT terminations were used for the single-frequency resonant system and the second-order wideband system. The IMT terminations used were a 50-Ω resistor and a carrier receiver having a 2,000-Ω resistance. For the two-frequency resonant system, the IMTs were terminated into carrier receivers identical to those on the 230-kV coupling system described in chapter 1. One of the IMTs was terminated into a carrier receiver having an input impedance of approximately 1 MΩ at frequencies in the harmonic frequency band, and the other IMT was terminated into two parallel receivers having an equivalent input resistance of approximately 1.16 kΩ.

The circuit used for the frequency response tests is shown in Figure 21. Frequency response was measured at the drain coil and at the primary, or high-impedance, side of the IMT for each coupling system. The voltage gain for both the drain coil and the IMT

Reproduced with permission of the copyright owner. Further reproduction prohibited without permission.

were referenced to the source voltage. The coupling system settings and measurement data for the frequency response tests are provided in Appendix A.

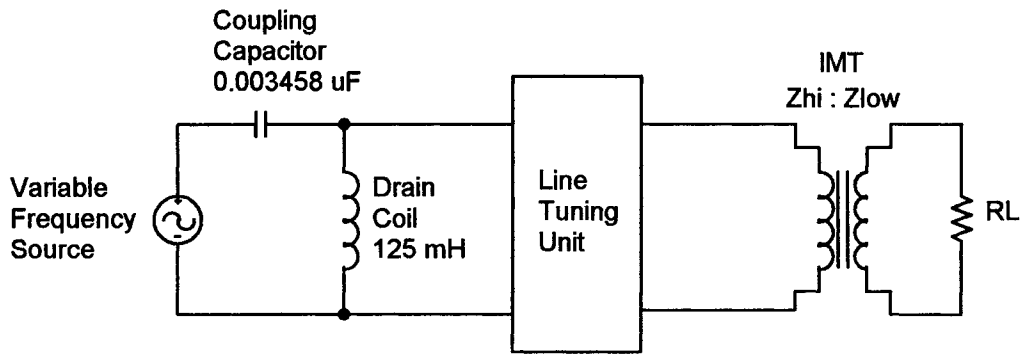

Figure 21. Test configuration for frequency response measurements. The line-tuning unit is representative of any of the three types studied. Also, for all measurements, the coupling capacitance was 0.003458 μF, and the drain coil inductance was approximately 125 mH. The frequency response was measured from 600 Hz to 10 kHz at 200-Hz intervals. The impedance-matching transformer (IMT) terminations, denoted as RL, were a 50-Ω resistor and a carrier receiver having a 2,000-Ω resistance.

The frequency response measurements for the single-frequency resonant system are shown in Figures 22 through 24. Figures 22 and 23 show the frequency responses measured at the drain coil and IMT, respectively, for combinations of large and small values of line tuner series capacitance and IMT terminating resistance. Figure 24 shows a comparison of the frequency responses measured at the drain coil and IMT for large and small values of IMT terminating resistance, and with a large-valued line tuner series capacitance. As can be seen in Figure 22, a large value of line tuner series capacitance resulted in very low gain at the drain coil. Thus, increasing the line tuner series capacitance is a possible solution for mitigating harmonic frequency interference. Figures 22 through

Reproduced with permission of the copyright owner. Further reproduction prohibited without permission.

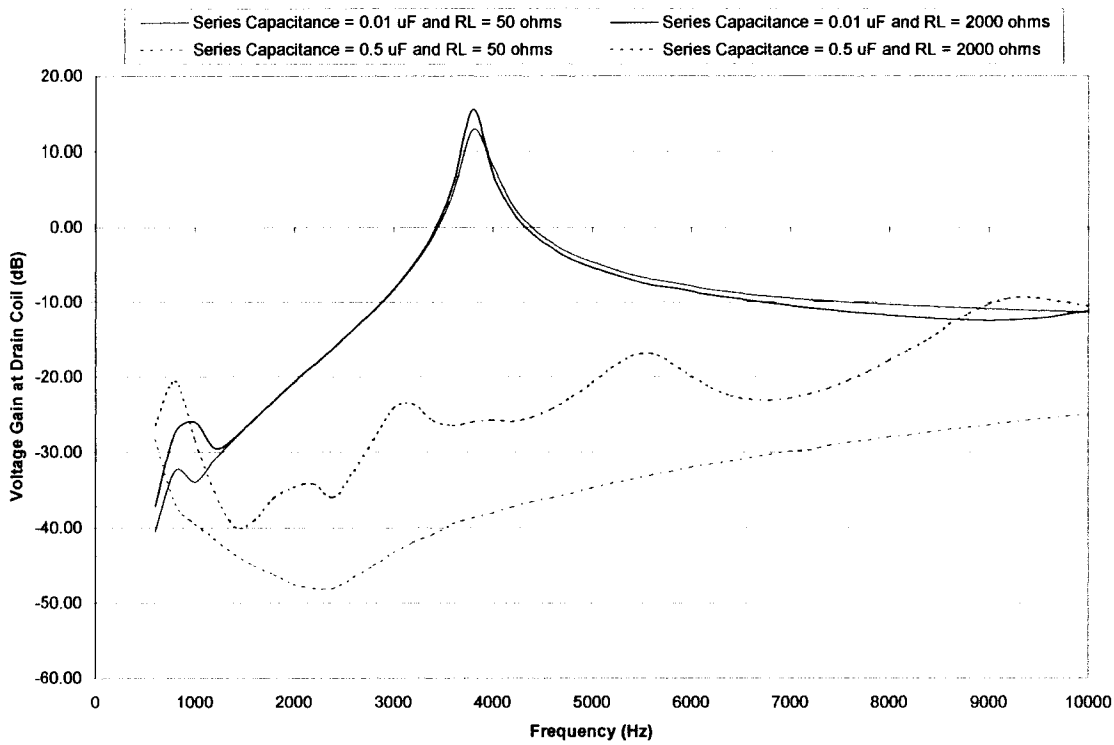

Figure 22. Comparison of frequency responses measured at the drain coil of a single-frequency resonant coupling system with large and small values of line tuner series capacitance and impedance-matching transformer (IMT) terminating resistance. RL = IMT terminating resistance.

Reproduced with permission of the copyright owner. Further reproduction prohibited without permission.

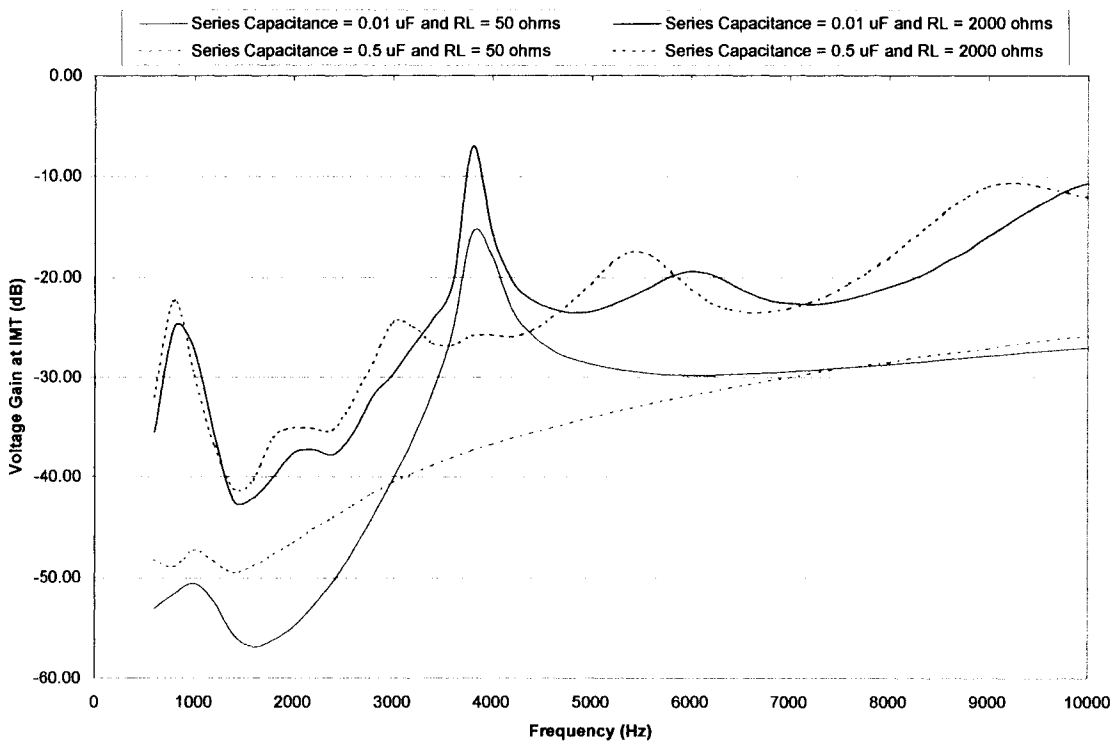

Figure 23. Comparison of frequency responses measured at the impedance-matching transformer (IMT) of a single-frequency resonant coupling system with large and small values of line tuner series capacitance and IMT terminating resistance. RL = IMT terminating resistance.

Reproduced with permission of the copyright owner. Further reproduction prohibited without permission.

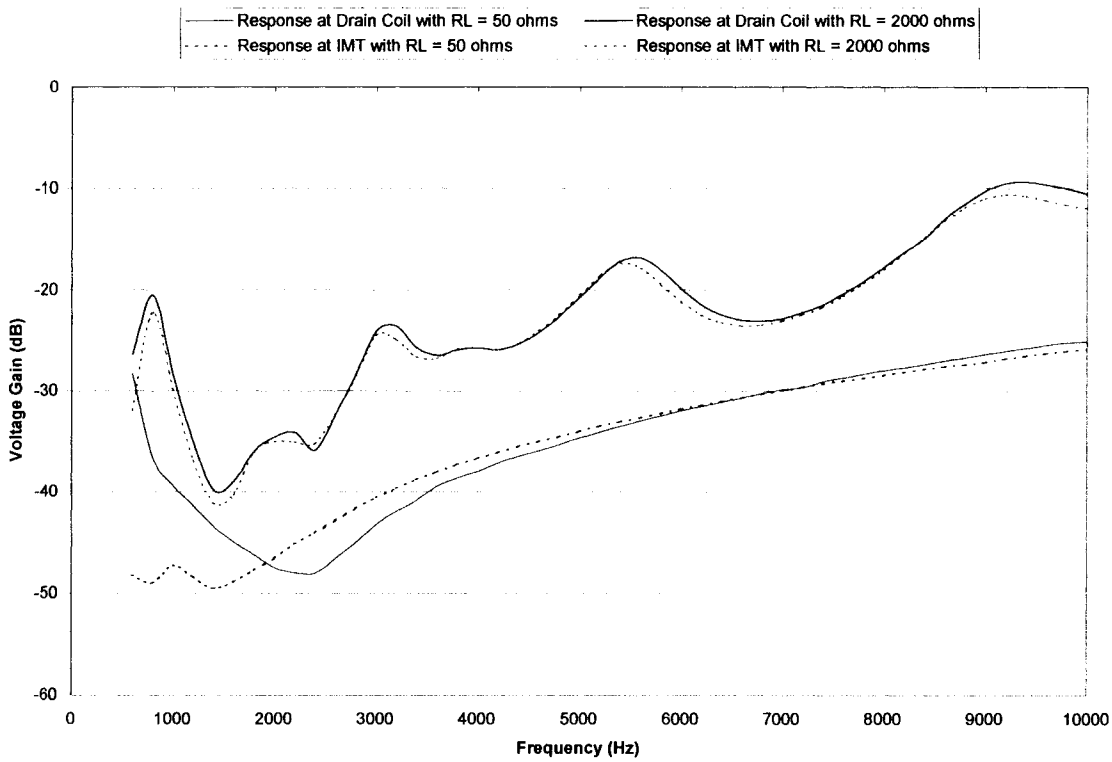

Figure 24. Comparison of frequency responses measured at the drain coil and impedance-matching transformer (IMT) of a single-frequency resonant coupling system with a large-valued line tuner series capacitance. The line tuner series capacitance was approximately 0.5 μF. RL = IMT terminating resistance.

Reproduced with permission of the copyright owner. Further reproduction prohibited without permission.

24 show that the terminating resistance of the IMT had a significant effect on frequency response at both the drain coil and the IMT when the series capacitance of the line tuner was large; however, the voltage gain remained relatively low throughout the harmonic frequency band. When the line tuner series capacitance is large, such as when the high-frequency tuning capacitor of a single-frequency system is disabled, the IMT magnetizing reactance becomes the dominant reactance in the circuit at frequencies in the harmonic frequency band. Since the IMT magnetizing reactance is nonlinear and produces currents at harmonics of the forcing frequency, the frequency response of the system becomes oscillatory. Furthermore, as shown in Figure 24, when the IMT terminating resistance is large and when the line tuner series capacitance is large, the frequency responses at the drain coil and IMT are approximately equal. Essentially, a small-valued IMT termination resistance squelches the effects of the IMT magnetizing reactance.

The frequency response measurements for the two-frequency resonant system are shown in Figures 25 and 26. Figure 25 shows the frequency responses measured at the drain coil and each IMT with small values of line tuner series capacitance in each tuning leg. The responses are similar to those of the single-frequency system with a small-valued line tuner series capacitance; that is, voltage gain at the drain coil exceeded 0 dB. Another similarity to the single-frequency system response is that, when the series capacitance of one of the tuning legs is large, voltage gain is drastically reduced at the drain coil as shown in Figure 26. Thus, as with the single-frequency resonant system, a possible solution for mitigating harmonic frequency interference in a two-frequency resonant system is to increase the series capacitance in one of the tuning legs.

Reproduced with permission of the copyright owner. Further reproduction prohibited without permission.

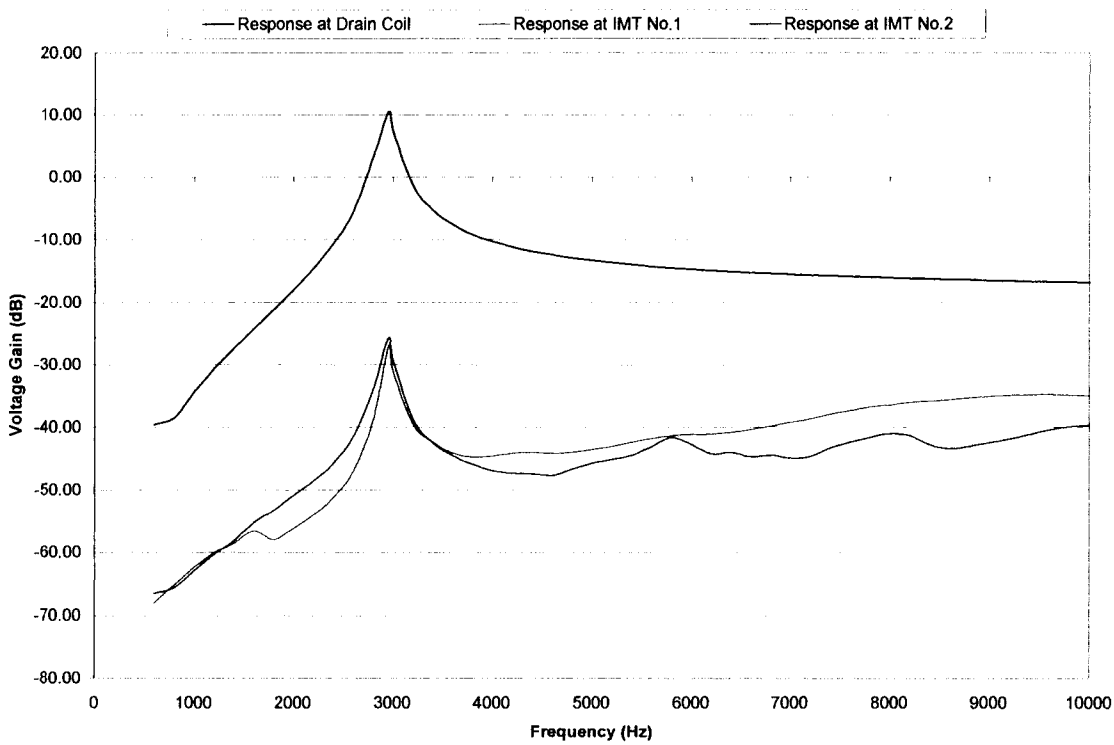

Figure 25. Comparison of frequency responses measured at the drain coil and impedance-matching transformers (IMTs) of a two-frequency resonant coupling system with a small-valued line tuner series capacitance in each tuning leg. One of the IMTs was terminated into a carrier receiver having an input impedance of approximately 1 MΩ at frequencies in the harmonic frequency band, and the other IMT was terminated into two parallel receivers having an equivalent input resistance of approximately 1.16 kΩ. The series capacitance of each tuning leg was approximately 0.01 μF.

Reproduced with permission of the copyright owner. Further reproduction prohibited without permission.

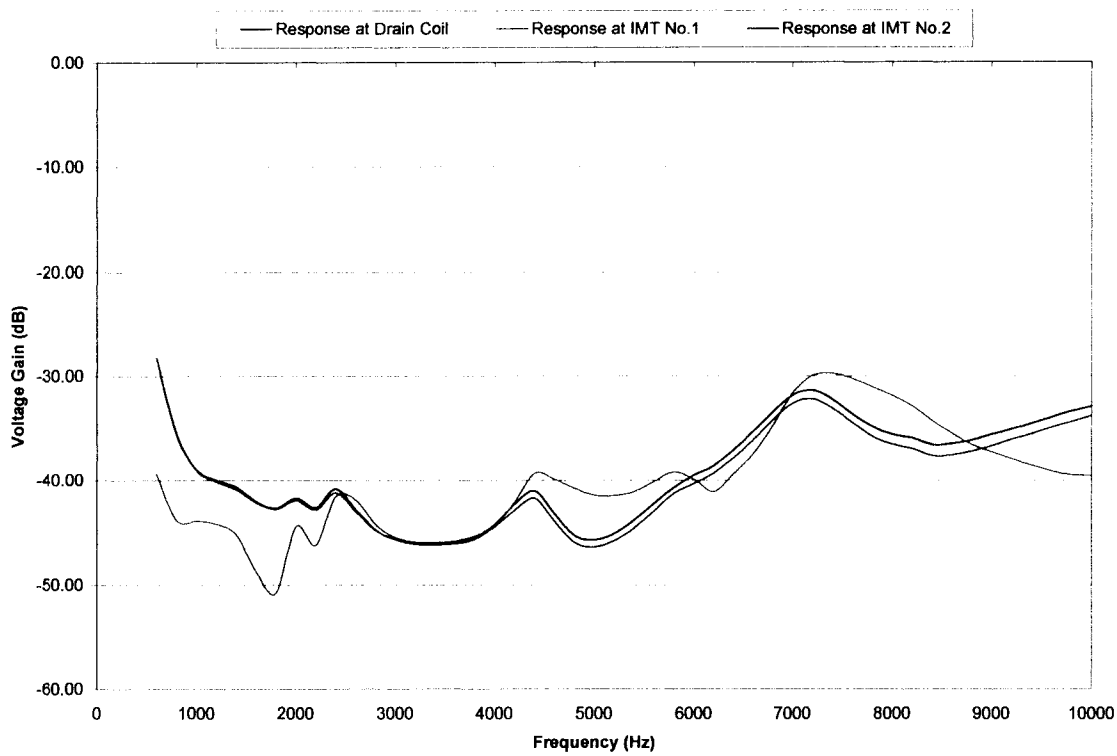

Figure 26. Comparison of frequency responses measured at the drain coil and impedance-matching transformers (IMTs) of a two-frequency resonant coupling system with a small-valued line tuner series capacitance in one tuning leg and a large-valued line tuner series capacitance in the other tuning leg. One of the IMTs was terminated into a carrier receiver having an input impedance of approximately 1 MΩ at frequencies in the harmonic frequency band, and the other IMT was terminated into two parallel receivers having an equivalent input resistance of approximately 1.16 kΩ. The series capacitance of the tuning leg with IMT No.1 was approximately 0.01 μF, and the series capacitance of the tuning leg with IMT No.2 was approximately 0.5 μF.

Reproduced with permission of the copyright owner. Further reproduction prohibited without permission.

The frequency response measurements for the second-order wideband system are shown in Figure 27. The voltage gain remained relatively low throughout the harmonic frequency band except at the low-order switching frequency of the parallel combination of the drain coil and line tuner impedances. The only series capacitance used in the second-order wideband line tuner is the 60-Hz blocking capacitor, which has a relatively large value. For the second-order wideband system tested, the blocking capacitor had a value of 0.1 μF. Thus, the second-order wideband system's response was similar to that of the resonant type systems with large values of line tuner series capacitance. Also, comparing the frequency response measurements of voltage gain at the primary of the IMT illustrated in Figure 27 with those measurements given in Table 6 reveals that a difference exists. The difference in gain measurements is a result of different values used for the inductance that is in parallel with the primary of the IMT for the second-order wideband system. For the measurements presented in Table 6, this parallel inductance was set at approximately 0.84 mH, whereas the inductance was set at approximately 0.179 mH for the frequency response measurements shown in Figure 27. Of course, the smaller inductance in parallel with the primary of the IMT will result in lower voltage gain at the IMT as shown in Figure 27.

Reproduced with permission of the copyright owner. Further reproduction prohibited without permission.

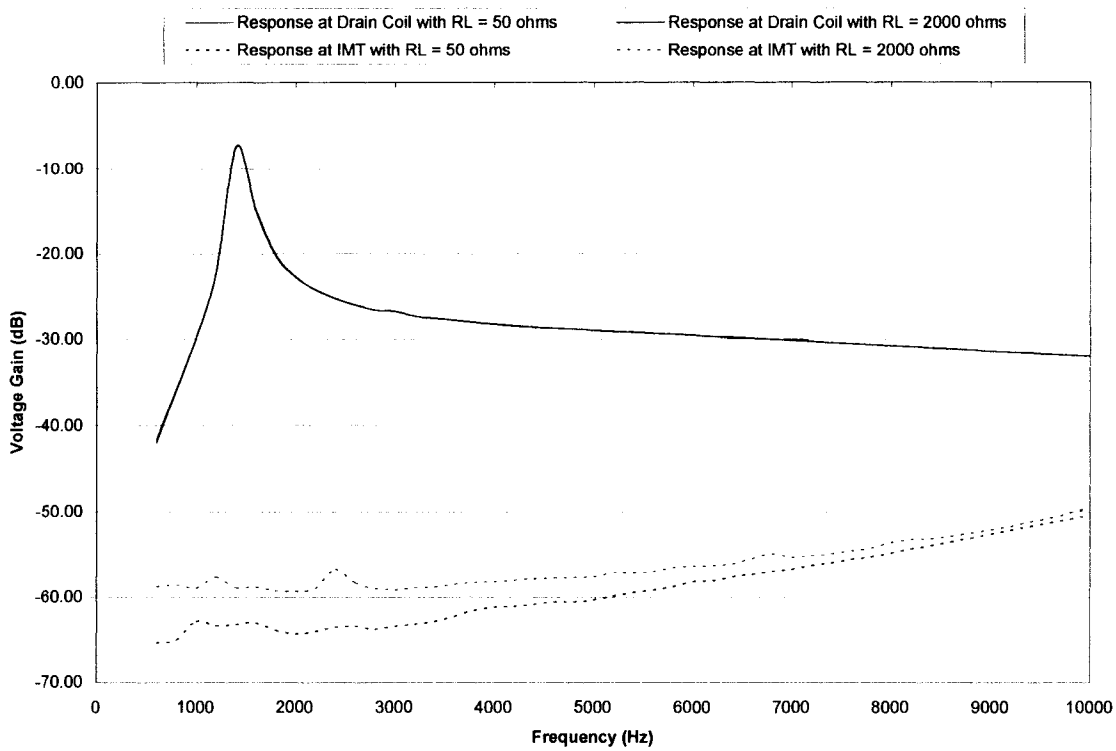

Figure 27. Comparison of frequency responses measured at the drain coil and impedance-matching transformer (IMT) of a second-order wideband coupling system with large and small values of IMT terminating resistance. RL = IMT terminating resistance.

Reproduced with permission of the copyright owner. Further reproduction prohibited without permission.

CHAPTER 3

PLC COUPLING SYSTEM MODELING

The coupling systems were modeled using a combination of PSpice and state-space methods. PSpice modeling was used to eliminate nonessential system components and develop simplified models of the coupling systems. After the negligible components were eliminated, state-space models of the coupling systems were developed for frequency response analysis. Also considered was the effect of the coupling capacitor voltage transformation circuitry on coupling system modeling.

Effect of Coupling Capacitor Voltage Transformer Voltage Transformation Circuitry on Coupling System Frequency Response in the Harmonic Frequency Band

Most applications also utilize the coupling capacitor in conjunction with voltage transformation circuitry, known as a coupling capacitor voltage transformer (CCVT), to provide power system frequency voltage for protective relaying and metering purposes. A CCVT is designed such that the voltage transformation circuitry does not affect normal carrier frequency operation. However, since the 600-Hz to 10-kHz harmonic frequency band is considerably lower than the carrier frequency band is, the effect of the voltage transformation circuitry on frequency response at the drain coil was investigated to determine if the voltage transformation circuitry could be neglected in the coupling system models. Others such as Vermeulen, Dann, and van Rooijen (1995) have investigated the frequency response characteristics of CCVTs at harmonic frequencies; however, their

Reproduced with permission of the copyright owner. Further reproduction prohibited without permission.

work did not focus on the response characteristics at the drain coil, which is of importance in regard to PLC coupling systems.

As practically all CCVTs share the same basic design, the type of CCVT chosen for analysis was one for which circuit component data were available. The CCVT circuit analyzed was that of a Westinghouse type PCA-5 CCVT (Westinghouse Electric, 1967) designed for operation at a system voltage level of 230 kV. The circuit analysis was performed using PSpice and consisted of performing frequency response simulations measuring voltage gain at the drain coil with and without the dominant voltage transformation circuit components.

The simplified CCVT circuit is shown in Figure 28. The dominant voltage transformation circuit component is that of the compensating reactor, which is designated as L_{cr} in the circuit of Figure 28. The compensating reactor is used to achieve resonance at

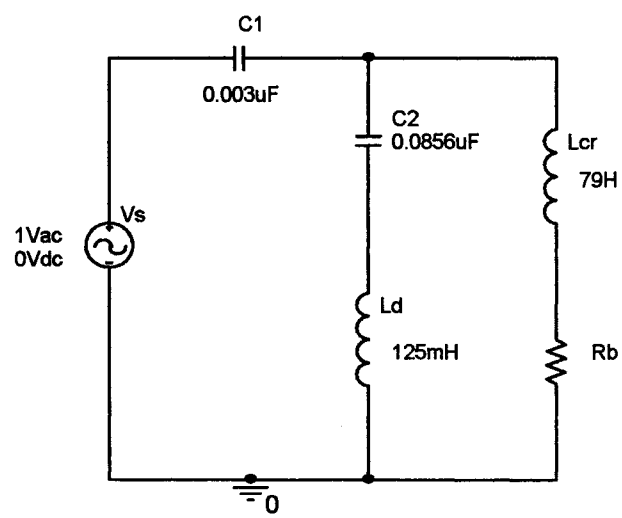

Figure 28. PSpice model of simplified circuit for a Westinghouse type PCA-5 coupling capacitor voltage transformer. C1 = high-voltage capacitor; C2 = intermediate-voltage capacitor; Ld = drain coil; Lcr = compensating reactor; Rb = burden resistance.

Reproduced with permission of the copyright owner. Further reproduction prohibited without permission.

60 Hz to eliminate phase angle shift between the transmission line voltage and the voltage applied to the primary of the CCVT voltage transformer. The capacitive voltage divider exists between the capacitors C_1 and C_2 shown in the circuit of Figure 28. The voltage across C_2 is the voltage impressed on the primary of the CCVT voltage transformer, which is approximately 5 kV for the Westinghouse type PCA-5 CCVT. Typical CCVT voltage transformer burdens, designated as R_b in Figure 28, are in the hundred-kilo-ohm range as seen on the primary side of the voltage transformer. Thus, the compensating reactor does not significantly affect the voltage level applied to the primary of the voltage transformer, which is represented by R_b in the simplified circuit of Figure 28. To eliminate phase shift between the transmission line voltage and the voltage applied to the primary of the voltage transformer, the compensating reactor must be tuned to resonate with the parallel combination of C_1 and C_2, which is the Thevenin equivalent capacitance in series with the compensating reactor. For the type PCA-5 CCVT considered here, the compensating reactor required an inductance of approximately 79 H to resonate at 60 Hz with the Thevenin equivalent series capacitance of approximately 0.0886 μF.

The effect of the voltage transformation circuitry on frequency response at the drain coil was investigated by using PSpice to perform a frequency scan from 1 Hz to 10 kHz on the circuit shown in Figure 28. The frequency scans were performed with the burden resistance, R_b, set to 1 Ω and 10 MΩ. With the burden at 1 Ω, the compensating reactor inductance was essentially placed in parallel with the leg of the circuit containing the drain coil. With the burden at 10 MΩ, the compensating reactor inductance was essentially removed from the circuit, leaving only the coupling capacitor and drain coil. The measure of comparison was the simulated voltage gain at the drain coil, which is desig-

Reproduced with permission of the copyright owner. Further reproduction prohibited without permission.

nated as L_d in Figure 28. The results of the two frequency scans are shown in Figure 29. As Figure 29 illustrates, the small burden resistance resulted in a voltage spike at approximately 60 Hz, which is where the series reactor resonates with the coupling capacitance. However, at frequencies above 300 Hz, the two responses shown in Figure 29 are practically equal.

Although a CCVT designed for one particular system voltage level was analyzed, the analysis can be readily extended to other voltage levels such as 115 kV and 500 kV; that is, to accommodate different voltage levels, only the small-valued capacitance, C_1, typically changes. Thus, the inductance of the compensating reactor does not change significantly. For example, a type PCA-5 CCVT designed for 115 kV has a C_1 capacitance of 0.006 μF, which results in only changing the compensating reactor inductance to approximately 77 H. On the basis of the analysis of the effect of the voltage transformation circuitry components on frequency response at the drain coil, the voltage transformation circuitry can be neglected when the coupling systems are being modeled at frequencies in the harmonic frequency band.

PSpice Modeling

PSpice modeling of the coupling systems was performed in two stages. First, detailed models were developed. The detailed models included parameters such as capacitor leakage resistance, inductor winding resistance, and full PSpice transformer modeling of the IMT. Data from simulations using these detailed models was then compared to measured data to validate the models. After validation of the detailed models was accomplished, simplified models were developed. The purpose of the simplified models was to

Reproduced with permission of the copyright owner. Further reproduction prohibited without permission.

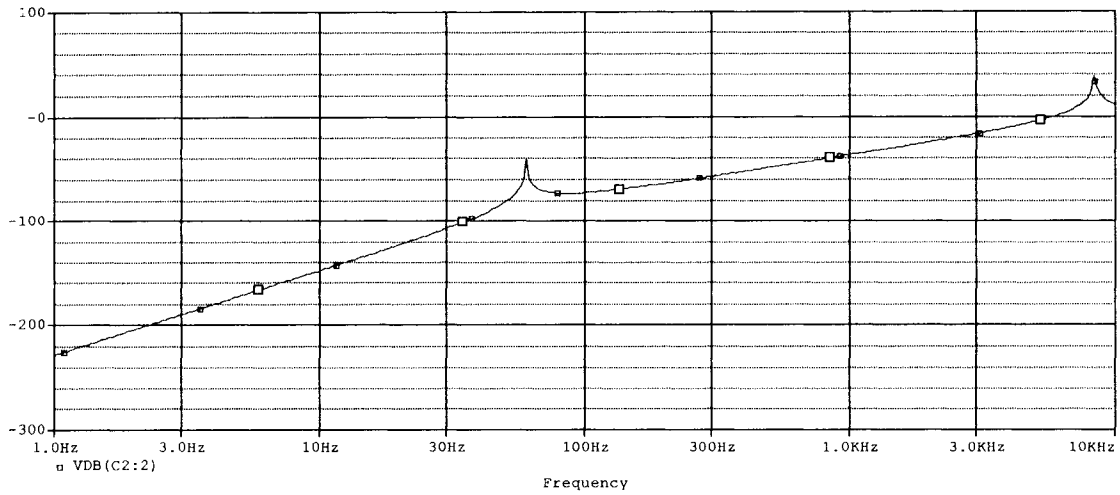

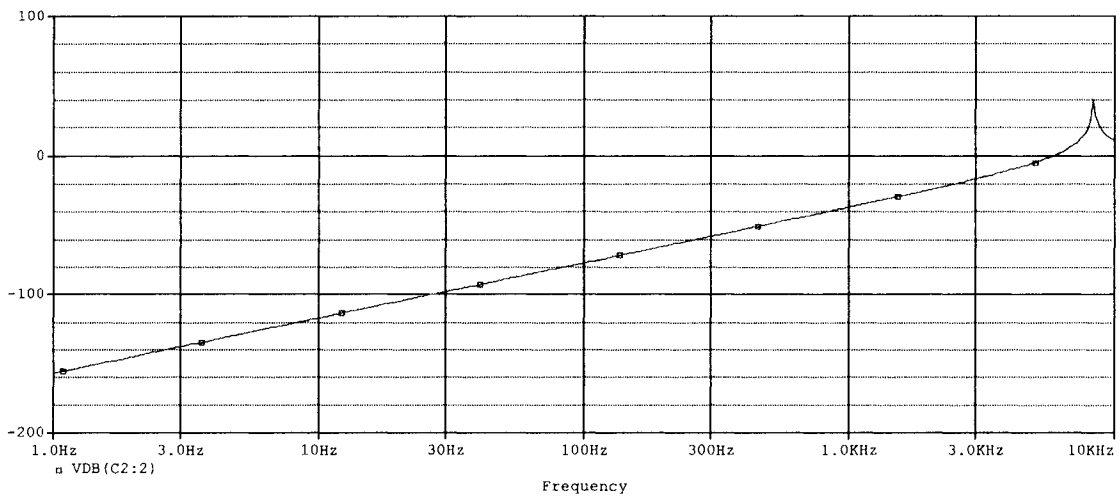

Figure 29. Frequency response comparison illustrating the effect of coupling capacitor voltage transformation circuitry on frequency response at the drain coil. The upper plot is the voltage gain at the drain coil in units of dB with the voltage transformer burden equal to 1 Ω. The lower plot is the voltage gain at the drain coil in units of dB with the voltage transformer burden equal to 10 MΩ. For both responses, the voltage gain at the drain coil was referenced to the source voltage.

Reproduced with permission of the copyright owner. Further reproduction prohibited without permission.

eliminate system parameters that had values that were not readily available. In particular, parameters such as capacitor leakage resistance and inductor winding resistance were eliminated in the simplified models. Also, the IMT model was reduced to an inductor in parallel with a resistance. This IMT model is similar to the low-frequency model for an output transformer given by Fitzgerald et al. (1990). As with the detailed models, data from the PSpice simulations using the simplified models were compared to measurements for validation.

Model validation consisted of running time domain simulations and comparing simulated voltage levels to measured voltage levels obtained from the peak voltage gain measurements described in chapter 2; that is, the model simulations were run at frequencies corresponding to those where a voltage peak occurred at the drain coil. The simulated voltage levels at the drain coil and primary of the IMT were then compared to the measured voltage levels obtained at those frequencies.

Acquisition of Coupling System Component Data for Use With Models

The detailed models included component parameters such as capacitor leakage resistance and inductor winding resistance, including IMT winding resistance, all of which were acquired through measurement. The IMT parameters were obtained from IMT winding inductance and resistance measurements that are described in chapter 2. The winding resistance and inductance of the line tuner inductors were measured using an LCR meter with a test frequency of 1 kHz. The leakage resistance of the capacitors was calculated using Equation 8, which was derived by rearranging an equation provided by Wolf and Smith (1990) for a parallel equivalent circuit model of a capacitor. The dissipa-

Reproduced with permission of the copyright owner. Further reproduction prohibited without permission.

tion factors of the capacitors, along with their capacitance, were measured using an LCR meter with a test frequency of 1 kHz. Equation 8 is

$$R_p = \frac{1}{\omega CD}, \tag{8}$$

where

R_p is the capacitor parallel leakage resistance,

ω is the angular frequency in radians per second,

C is the capacitance, and

D is the dissipation factor.

Data for the drain coils was obtained from the drain coil tests that are described in chapter 2. The inductance of each drain coil was measured, and the actual measured inductance was used for all PSpice simulations. For drain coil resistance, the range of frequencies and resistances from the drain coil tests was used with an interpolation function in Matlab to calculate drain coil resistance at a particular frequency. The drain coil resistance used in the simulations was the interpolated resistance at the frequency of the forcing voltage of each simulation, where the frequency of the forcing voltage corresponded to the frequency where a voltage peak occurred at the drain coil as obtained from the peak voltage gain measurements described in chapter 2. The interpolated drain coil resistance for each frequency used in the simulations is provided in Appendix B.

Reproduced with permission of the copyright owner. Further reproduction prohibited without permission.

Detailed PSpice Models

The detailed model of the single-frequency resonant system is shown in Figure 30.

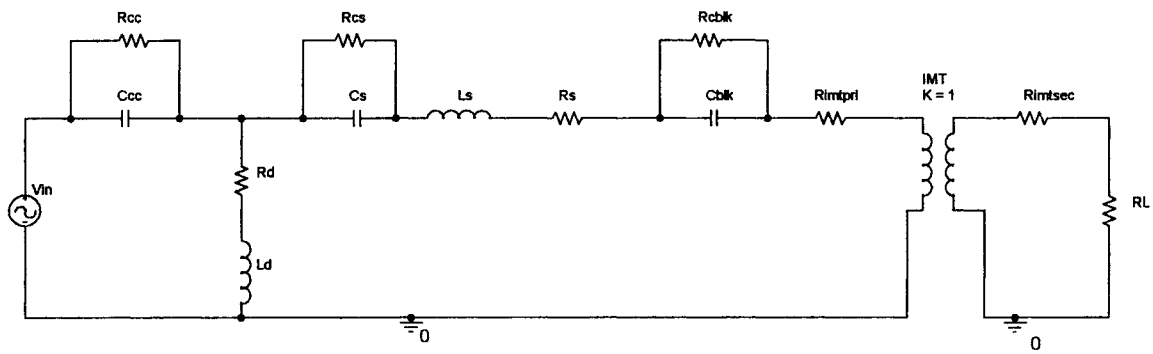

Figure 30. Detailed PSpice model of a single-frequency resonant coupling system.

Descriptions of the detailed single-frequency model components are as follows:

- C_{cc} is the coupling capacitor.
- R_{cc} is the leakage resistance of the coupling capacitor.
- L_d is the drain coil.
- R_d is the drain coil resistance.
- C_s is the line tuner series capacitor.
- R_{cs} is the leakage resistance of the line tuner series capacitor.
- L_s is the line tuner series inductor.
- R_s is the resistance of the line tuner series inductor.
- C_{blk} is the 60-Hz blocking capacitor.
- R_{cblk} is the leakage resistance of the blocking capacitor.

Reproduced with permission of the copyright owner. Further reproduction prohibited without permission.

- R_{imtpri} is the resistance of the primary winding of the IMT.
- R_{imtsec} is the resistance of the secondary winding of the IMT.
- RL is the IMT terminating resistance.

The detailed model of the two-frequency resonant system is shown in Figure 31. Descriptions of the detailed two-frequency model components are as follows:

- C_{cc} is the coupling capacitor.
- R_{cc} is the leakage resistance of the coupling capacitor.
- L_d is the drain coil.
- R_d is the drain coil resistance.
- C_{s1} and C_{s2} are the line tuner series capacitors.
- R_{cs1} and R_{cs2} are the leakage resistances of the line tuner series capacitors.
- L_{s1} and L_{s2} are the line tuner series inductors.
- R_{s1} and R_{s2} are the resistances of the line tuner series inductors.
- C_{p1} and C_{p2} are the line tuner parallel trap capacitors.
- R_{cp1} and R_{cp2} are the leakage resistances of the line tuner parallel trap capacitors.
- L_{p1} and L_{p2} are the line tuner parallel trap inductors.
- R_{p1} and R_{p2} are the resistances of the line tuner parallel trap inductors.
- C_{blk1} and C_{blk2} are the 60-Hz blocking capacitors.
- R_{cblk1} and R_{cblk2} are the leakage resistances of the blocking capacitors.
- $R_{imt1pri}$ and $R_{imt2pri}$ are the resistances of the primary windings of the IMTs.
- $R_{imt1sec}$ and $R_{imt2sec}$ are the resistances of the secondary windings of the IMTs.
- RL1 and RL2 are the IMT terminating resistances.

Reproduced with permission of the copyright owner. Further reproduction prohibited without permission.

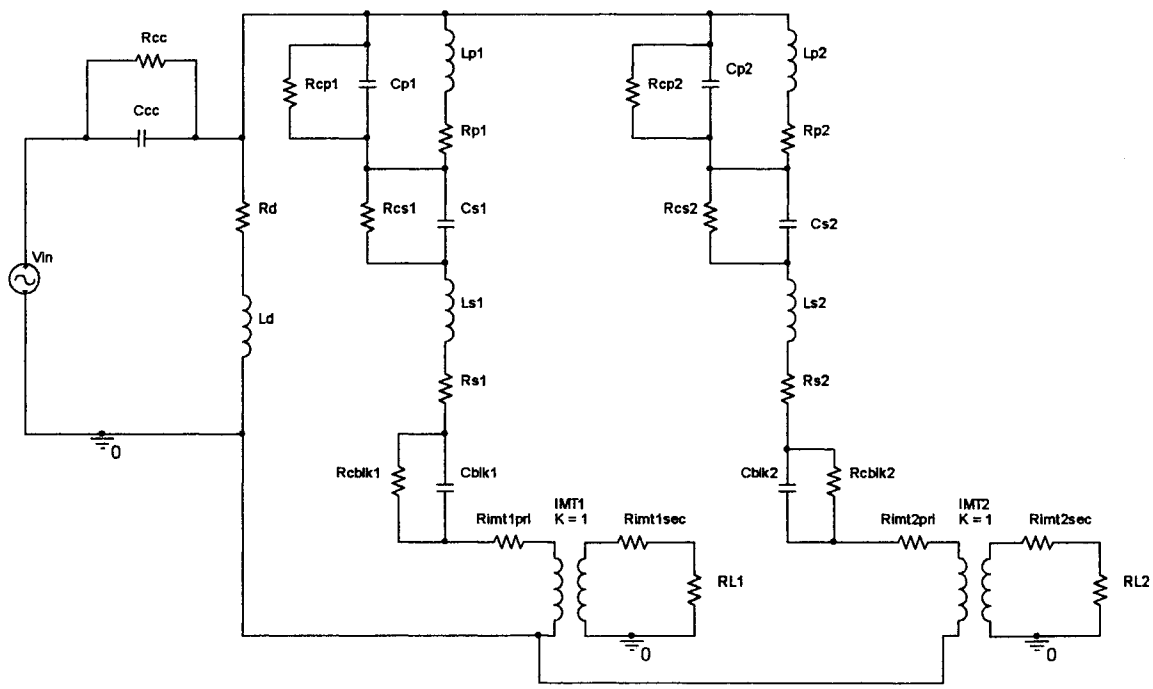

Figure 31. Detailed PSpice model of a two-frequency resonant coupling system.

Reproduced with permission of the copyright owner. Further reproduction prohibited without permission.

The detailed model of the second-order wideband system is shown in Figure 32.

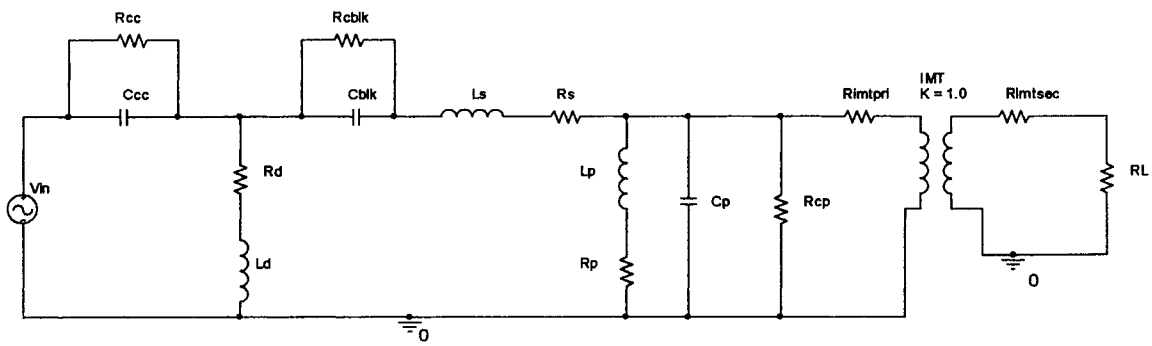

Figure 32. Detailed PSpice model of a second-order wideband coupling system.

Descriptions of the detailed second-order wideband model components are as follows:

- C_{cc} is the coupling capacitor.
- R_{cc} is the leakage resistance of the coupling capacitor.
- L_d is the drain coil.
- R_d is the drain coil resistance.
- L_s is the line tuner series inductor.
- R_s is the resistance of the line tuner series inductor.
- C_p is the line tuner parallel capacitor.
- R_{cp} is the leakage resistance of the line tuner parallel capacitor.
- L_p is the line tuner parallel inductor.
- R_p is the resistance of the line tuner parallel inductor.
- C_{blk} is the 60-Hz blocking capacitor.
- R_{cblk} is the leakage resistance of the blocking capacitor.

Reproduced with permission of the copyright owner. Further reproduction prohibited without permission.

- R_{imtpri} is the resistance of the primary winding of the IMT.
- R_{imtsec} is the resistance of the secondary winding of the IMT.
- RL is the IMT terminating resistance.

Simplified PSpice Models

As stated previously, the purpose of the simplified models was to eliminate system parameters that had values that were not readily available. For example, parameters such as capacitor conductance and inductor winding resistance can only be determined by measurement, so they are eliminated in the simplified models. Also, the IMT model was reduced to that of an inductor in parallel with a resistance, where the inductor represents the self-inductance of the primary winding of the IMT and where the resistance represents the IMT terminating resistance reflected to the primary side of the IMT.

The simplified model of the single-frequency resonant system is shown in Figure 33.

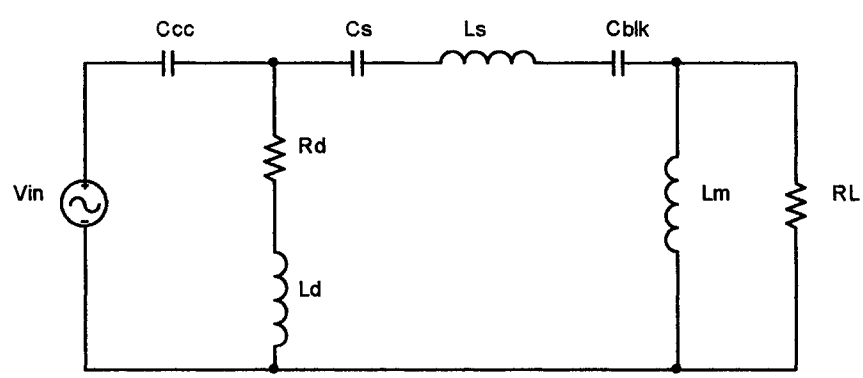

Figure 33. Simplified PSpice model of a single-frequency resonant coupling system.

Reproduced with permission of the copyright owner. Further reproduction prohibited without permission.

Descriptions of the simplified single-frequency model components are as follows:

- C_{cc} is the coupling capacitor.
- L_d is the drain coil.
- R_d is the drain coil resistance.
- C_s is the line tuner series capacitor.
- L_s is the line tuner series inductor.
- C_{blk} is the 60-Hz blocking capacitor.
- L_m is the inductance of the primary winding of the IMT.
- RL is the IMT terminating resistance reflected to the primary side of the IMT.

The simplified model of the two-frequency resonant system is shown in Figure 34. Descriptions of the simplified two-frequency model components are as follows:

- C_{cc} is the coupling capacitor.
- L_d is the drain coil.
- R_d is the drain coil resistance.
- C_{s1} and C_{s2} are the line tuner series capacitors.
- L_{s1} and L_{s2} are the line tuner series inductors.
- C_{p1} and C_{p2} are the line tuner parallel trap capacitors.
- L_{p1} and L_{p2} are the line tuner parallel trap inductors.
- C_{blk1} and C_{blk2} are the 60-Hz blocking capacitors.
- L_{m1} and L_{m2} are the inductances of the primary windings of the IMTs.
- RL1 and RL2 are the IMT terminating resistances reflected to the primary side of the IMT.

Reproduced with permission of the copyright owner. Further reproduction prohibited without permission.

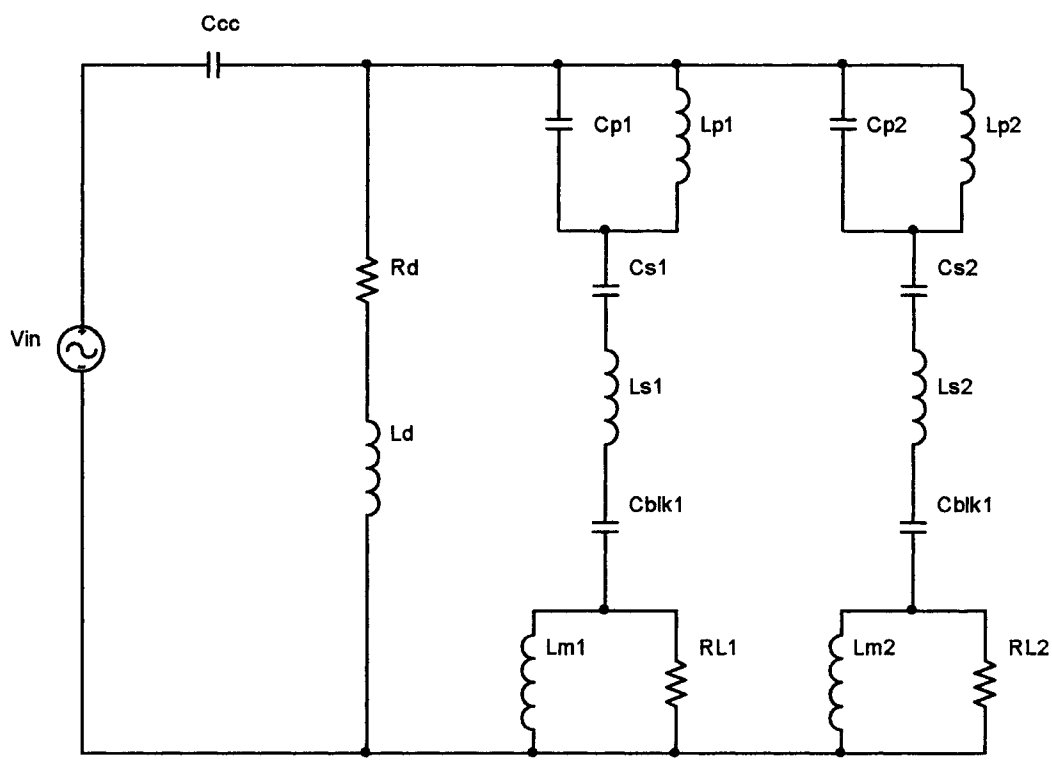

Figure 34. Simplified PSpice model of a two-frequency resonant coupling system.

Reproduced with permission of the copyright owner. Further reproduction prohibited without permission.

The simplified model of the second-order wideband system is shown in Figure 35.

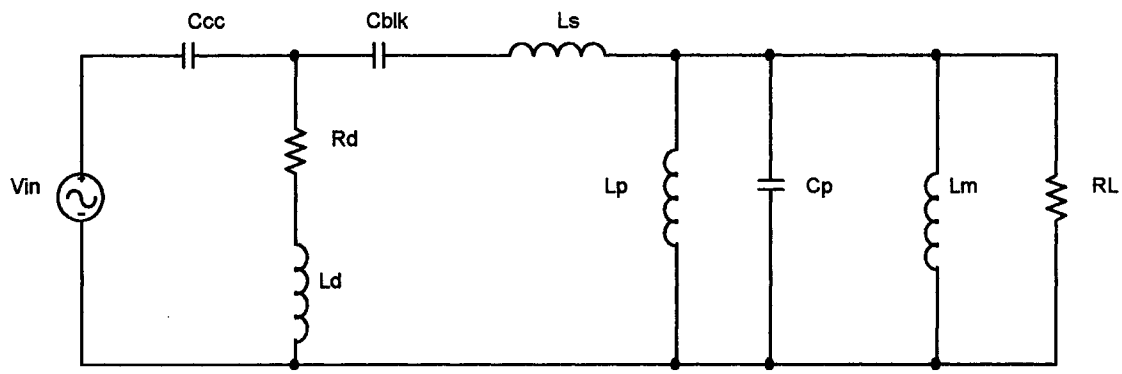

Figure 35. Simplified PSpice model of a second-order wideband coupling system.

Descriptions of the simplified second-order wideband model components are as follows:

- C_{cc} is the coupling capacitor.
- L_d is the drain coil.
- R_d is the drain coil resistance.
- L_s is the line tuner series inductor.
- C_p is the line tuner parallel capacitor.
- L_p is the line tuner parallel inductor.
- C_{blk} is the 60-Hz blocking capacitor.
- L_m is the inductance of the primary winding of the IMT.
- RL is the IMT terminating resistance reflected to the primary side of the IMT.

Reproduced with permission of the copyright owner. Further reproduction prohibited without permission.

Comparison of Detailed and Simplified PSpice Models to Measured Data

The comparison of the detailed and simplified PSpice models to measured data was made by calculating the percentage of error between measured and simulated voltage levels at the drain coil and primary of the IMT. The percentage of error between measured and simulated voltage levels was calculated as

$$Percent\ Error = \frac{Measured - Simulated}{Measured} \cdot 100\%. \tag{9}$$

Comparisons of the percentage of error between measured data and simulated data for the detailed and simplified PSpice models are shown in Table 7. As Table 7 indicates, the percentage of error achieved with the simplified models was less than 10% in most every case. Thus, the simplified models were deemed suitable for use in state-space modeling. The measured and simulated data used for model validation are provided in Appendix B.

State-Space Modeling

State-space modeling was chosen as a method for analyzing the frequency response characteristics of the coupling systems. State-space modeling was chosen because of the generality and versatility of the models. With a software package such as Matlab, the models could be used for both time-domain and frequency-domain analysis. Also, multiple systems could be analyzed using batch processing.

Reproduced with permission of the copyright owner. Further reproduction prohibited without permission.

Table 7

Percentage-of-Error Comparison Between PSpice Model Simulations and Measurements

Coupling system	Coupling capacitance (μF)	Drain coil inductance (mH)	Drain coil voltage error for detailed model (%)	Drain coil voltage error for simplified model (%)	IMT primary voltage error for detailed model (%)	IMT primary voltage error for simplified model (%)
Single-freq	0.006850	125	-1.61	-3.04	3.80	3.38
Single-freq	0.003458	125	0.36	-1.21	0.65	0.10
Single-freq	0.001717	125	2.88	1.26	0.02	-0.58
Single-freq	0.006850	25	8.91	7.95	4.01	4.47
Single-freq	0.003458	25	8.88	7.75	3.42	3.78
Single-freq	0.001717	25	8.90	7.70	3.55	3.82
Single-freq	0.006850	10	9.59	8.68	4.10	4.80
Single-freq	0.003458	10	7.00	5.87	2.10	2.64
Single-freq	0.001717	10	5.07	3.83	1.18	1.67
Two-freq	0.006850	125	5.26	2.72	8.27	6.92
Two-freq	0.003458	125	5.66	2.73	4.98	3.22
Two-freq	0.001717	125	7.44	4.42	4.71	2.74
Two-freq	0.006850	25	6.98	4.97	3.11	2.31
Two-freq	0.003458	25	9.01	6.83	4.56	3.61
Two-freq	0.001717	25	10.57	8.34	5.66	4.61
Two-freq	0.006850	10	10.30	8.42	5.36	4.77
Two-freq	0.003458	10	9.98	7.86	5.28	4.50
Two-freq	0.001717	10	9.57	7.32	5.41	4.44
Wideband.	0.006850	125	-3.75	-12.95	-0.80	-9.72
Wideband	0.003458	125	-4.26	-13.89	1.62	-7.47
Wideband	0.001717	125	-4.38	-14.14	0.49	-8.88
Wideband	0.006850	25	-7.08	-12.74	-7.65	-13.37
Wideband	0.003458	25	-4.40	-9.94	-5.24	-10.89
Wideband	0.001717	25	-3.04	-8.49	-2.98	-8.51
Wideband	0.006850	10	7.81	5.75	7.14	5.05
Wideband	0.003458	10	7.49	5.29	7.15	4.91
Wideband	0.001717	10	9.42	7.32	8.24	6.09

Note: The impedance-matching transformer (IMT) voltage for the two-frequency system is that of IMT2 shown in the two-frequency model of Figure 31. freq = frequency.

Reproduced with permission of the copyright owner. Further reproduction prohibited without permission.

The general form of the state-space model consists of a state equation and an output equation. The state equation (Nise. 1992) is

$$\dot{\mathbf{x}} = \mathbf{Ax} + \mathbf{Bu}, \tag{10}$$

and the output equation (Nise) is

$$\mathbf{y} = \mathbf{Cx} + \mathbf{Du}. \tag{11}$$

In Equations 10 and 11,

$\dot{\mathbf{x}}$ is the derivative of the state vector with respect to time,

$\mathbf{y}$ is the output vector,

$\mathbf{x}$ is the state vector,

$\mathbf{u}$ is the input or control vector,

$\mathbf{A}$ is the system matrix,

$\mathbf{B}$ is the input coupling matrix,

$\mathbf{C}$ is the output matrix, and

$\mathbf{D}$ is the feed-forward matrix.

General Narrowband Resonant Coupling System State-Space Model

In lieu of developing separate state-space models for both the single-frequency and two-frequency systems, a more general model was developed as shown in Figure 36.

Reproduced with permission of the copyright owner. Further reproduction prohibited without permission.

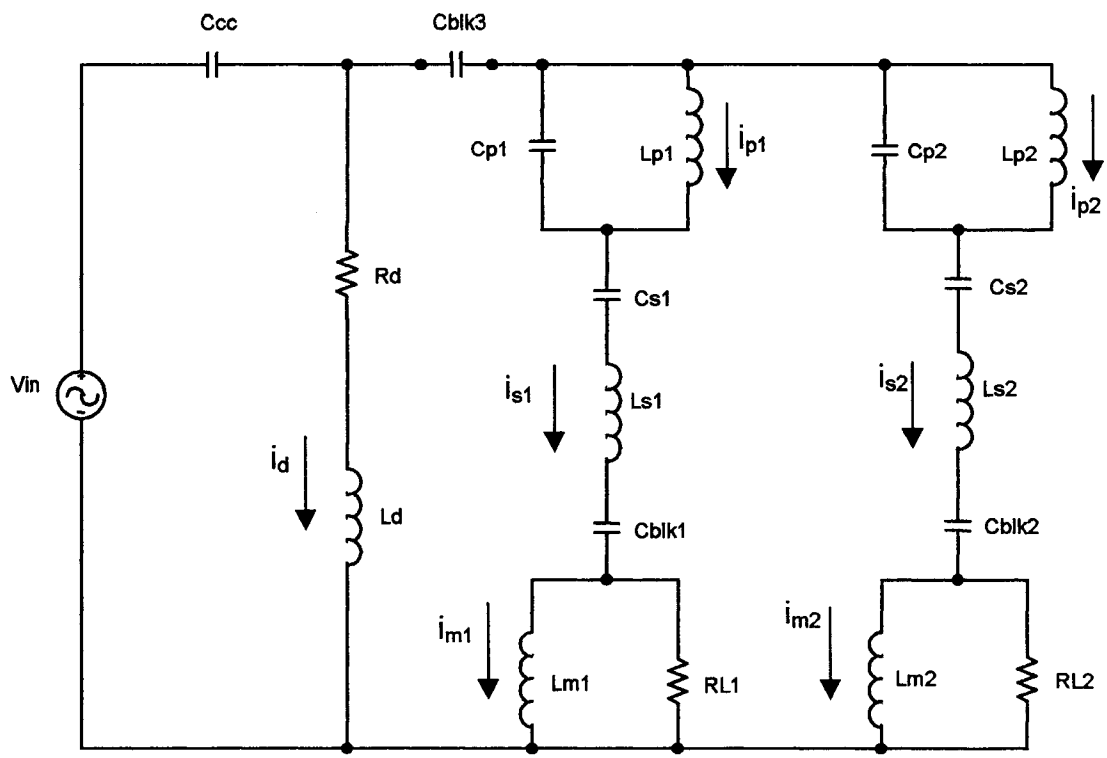

Figure 36. Schematic of narrowband resonant coupling system used for developing state-space model.

Reproduced with permission of the copyright owner. Further reproduction prohibited without permission.

The model is identical to the simplified PSpice model of the two-frequency system but has an additional capacitance in series with both tuning legs to accommodate a wider variety of narrowband resonant systems. For example, this additional capacitance will allow the model to be used for systems that utilize only one 60-Hz blocking capacitance in series with both tuning legs, as opposed to those systems that have a blocking capacitor in each tuning leg.

A set of state equations for the general narrowband resonant system can be written as follows (refer to Figure 36):

$$\dot{v}_{\mathrm{Ccc}} = \frac{1}{C_{\mathrm{CC}}}\left(i_{\mathrm{d}} + i_{\mathrm{s1}} + i_{\mathrm{s2}}\right), \tag{12}$$

$$\dot{v}_{\mathrm{Cblk3}} = \frac{1}{C_{\mathrm{blk3}}}\left(i_{\mathrm{s1}} + i_{\mathrm{s2}}\right), \tag{13}$$

$$\dot{v}_{\mathrm{Cp1}} = \frac{1}{C_{\mathrm{p1}}}\left(i_{\mathrm{s1}} - i_{\mathrm{p1}}\right), \tag{14}$$

$$\dot{v}_{\mathrm{Cs1}} = \frac{1}{C_{\mathrm{s1}}}\left(i_{\mathrm{s1}}\right), \tag{15}$$

$$\dot{v}_{\mathrm{Cblk1}} = \frac{1}{C_{\mathrm{blk1}}}\left(i_{\mathrm{s1}}\right), \tag{16}$$

Reproduced with permission of the copyright owner. Further reproduction prohibited without permission.

$$\dot{v}_{\mathrm{Cp2}} = \frac{1}{C_{\mathrm{p2}}}\left(i_{\mathrm{s2}} - i_{\mathrm{p2}}\right), \tag{17}$$

$$\dot{v}_{\mathrm{Cs2}} = \frac{1}{C_{\mathrm{s2}}}\left(i_{\mathrm{s2}}\right), \tag{18}$$

$$\dot{v}_{\mathrm{Cblk2}} = \frac{1}{C_{\mathrm{blk2}}}\left(i_{\mathrm{s2}}\right), \tag{19}$$

$$\dot{i}_{\mathrm{d}} = \frac{1}{L_{\mathrm{d}}}\left(v_{\mathrm{in}} - v_{\mathrm{Ccc}} - i_{\mathrm{d}} R_{\mathrm{d}}\right), \tag{20}$$

$$\dot{i}_{\mathrm{s1}} = \frac{1}{L_{\mathrm{s1}}}\left(v_{\mathrm{in}} - v_{\mathrm{Ccc}} - v_{\mathrm{Cblk3}} - v_{\mathrm{Cp1}} - v_{\mathrm{Cs1}} - v_{\mathrm{Cblk1}} - i_{\mathrm{s1}} RL1 + i_{\mathrm{m1}} RL1\right), \tag{21}$$

$$\dot{i}_{\mathrm{p1}} = \frac{1}{L_{\mathrm{p1}}}\left(v_{\mathrm{Cp1}}\right), \tag{22}$$

$$\dot{i}_{\mathrm{m1}} = \frac{1}{L_{\mathrm{m1}}}\left(v_{\mathrm{RL1}}\right) = \frac{RL1}{L_{\mathrm{m1}}}\left(i_{\mathrm{s1}} - i_{\mathrm{m1}}\right), \tag{23}$$

$$\dot{i}_{\mathrm{s2}} = \frac{1}{L_{\mathrm{s2}}}\left(v_{\mathrm{in}} - v_{\mathrm{Ccc}} - v_{\mathrm{Cblk3}} - v_{\mathrm{Cp2}} - v_{\mathrm{Cs2}} - v_{\mathrm{Cblk2}} - i_{\mathrm{s2}} RL2 + i_{\mathrm{m2}} RL2\right), \tag{24}$$

$$\dot{i}_{\mathrm{p2}} = \frac{1}{L_{\mathrm{p2}}}\left(v_{\mathrm{Cp2}}\right), \tag{25}$$

Reproduced with permission of the copyright owner. Further reproduction prohibited without permission.

and,

$$\dot{i}_{m2} = \frac{1}{L_{m2}}\left(v_{RL2}\right) = \frac{RL2}{L_{m2}}\left(i_{s2} - i_{m2}\right). \tag{26}$$

Letting the state vector be

$$\mathbf{x} = \left[v_{Ccc} \quad v_{Cblk1} \quad v_{Cblk2} \quad v_{Cblk3} \quad v_{Cs1} \quad v_{Cs2} \quad v_{Cp1} \quad v_{Cp2} \quad i_d \quad i_{s1} \quad i_{s2} \quad i_{p1} \quad i_{p2} \quad i_{m1} \quad i_{m2}\right]^T \tag{27}$$

results in a system matrix of

$$\mathbf{A} = \begin{bmatrix}
0 & 0 & 0 & 0 & 0 & 0 & 0 & 0 & \frac{1}{C_{CC}} & \frac{1}{C_{CC}} & \frac{1}{C_{CC}} & 0 & 0 & 0 & 0 \\
0 & 0 & 0 & 0 & 0 & 0 & 0 & 0 & 0 & \frac{1}{C_{blk1}} & 0 & 0 & 0 & 0 & 0 \\
0 & 0 & 0 & 0 & 0 & 0 & 0 & 0 & 0 & 0 & \frac{1}{C_{blk2}} & 0 & 0 & 0 & 0 \\
0 & 0 & 0 & 0 & 0 & 0 & 0 & 0 & 0 & \frac{1}{C_{blk3}} & \frac{1}{C_{blk3}} & 0 & 0 & 0 & 0 \\
0 & 0 & 0 & 0 & 0 & 0 & 0 & 0 & 0 & \frac{1}{C_{s1}} & 0 & 0 & 0 & 0 & 0 \\
0 & 0 & 0 & 0 & 0 & 0 & 0 & 0 & 0 & 0 & \frac{1}{C_{s2}} & 0 & 0 & 0 & 0 \\
0 & 0 & 0 & 0 & 0 & 0 & 0 & 0 & 0 & \frac{1}{C_{p1}} & 0 & \frac{-1}{C_{p1}} & 0 & 0 & 0 \\
0 & 0 & 0 & 0 & 0 & 0 & 0 & 0 & 0 & 0 & \frac{1}{C_{p2}} & 0 & \frac{-1}{C_{p2}} & 0 & 0 \\
\frac{-1}{L_d} & 0 & 0 & 0 & 0 & 0 & 0 & 0 & \frac{-R_d}{L_d} & 0 & 0 & 0 & 0 & 0 & 0 \\
\frac{-1}{L_{s1}} & \frac{-1}{L_{s1}} & 0 & \frac{-1}{L_{s1}} & \frac{-1}{L_{s1}} & 0 & \frac{-1}{L_{s1}} & 0 & 0 & \frac{-RL1}{L_{s1}} & 0 & 0 & 0 & \frac{RL1}{L_{s1}} & 0 \\
\frac{-1}{L_{s2}} & 0 & \frac{-1}{L_{s2}} & \frac{-1}{L_{s2}} & 0 & \frac{-1}{L_{s2}} & 0 & \frac{-1}{L_{s2}} & 0 & 0 & \frac{-RL2}{L_{s2}} & 0 & 0 & 0 & \frac{RL2}{L_{s2}} \\
0 & 0 & 0 & 0 & 0 & 0 & \frac{1}{L_{p1}} & 0 & 0 & 0 & 0 & 0 & 0 & 0 & 0 \\
0 & 0 & 0 & 0 & 0 & 0 & 0 & \frac{1}{L_{p2}} & 0 & 0 & 0 & 0 & 0 & 0 & 0 \\
0 & 0 & 0 & 0 & 0 & 0 & 0 & 0 & 0 & \frac{RL1}{L_{m1}} & 0 & 0 & 0 & \frac{-RL1}{L_{m1}} & 0 \\
0 & 0 & 0 & 0 & 0 & 0 & 0 & 0 & 0 & 0 & \frac{RL2}{L_{m2}} & 0 & 0 & 0 & \frac{-RL2}{L_{m2}}
\end{bmatrix} \tag{28}$$

Reproduced with permission of the copyright owner. Further reproduction prohibited without permission.

and an input coupling vector of

$$\mathbf{B} = \begin{bmatrix} 0 & 0 & 0 & 0 & 0 & 0 & 0 & 0 & \frac{1}{L_d} & \frac{1}{L_{s1}} & \frac{1}{L_{s2}} & 0 & 0 & 0 & 0 \end{bmatrix}^T . \tag{29}$$

The output equation for calculating drain coil voltage is

$$v_{drain} = \begin{bmatrix} -1 & 0 & 0 & 0 & 0 & 0 & 0 & 0 & 0 & 0 & 0 & 0 & 0 & 0 & 0 \end{bmatrix} \begin{bmatrix} v_{Ccc} \\ v_{Cblk1} \\ v_{Cblk2} \\ v_{Cblk3} \\ v_{Cs1} \\ v_{Cs2} \\ v_{Cp1} \\ v_{Cp2} \\ i_d \\ i_{s1} \\ i_{s2} \\ i_{p1} \\ i_{p2} \\ i_{m1} \\ i_{m2} \end{bmatrix} + [1] v_{in} . \tag{30}$$

Second-Order Wideband Coupling System State-Space Model

The equivalent circuit of the second-order wideband system used for developing the state-space model is shown in Figure 37. A set of state equations for the second-order wideband coupling system can be written as Equations 31 through 37 (refer to Figure 37).

Reproduced with permission of the copyright owner. Further reproduction prohibited without permission.

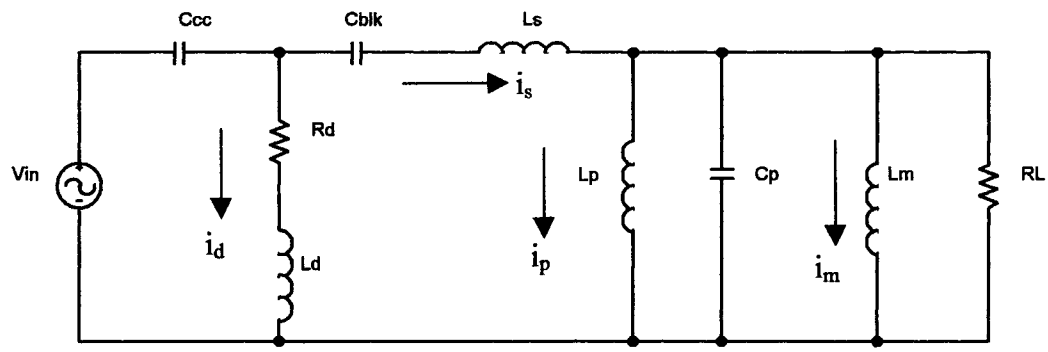

Figure 37. Schematic of second-order wideband coupling system used for developing state-space model.

$$\dot{v}_{\mathrm{Ccc}} = \frac{1}{C_{\mathrm{CC}}}\left(i_{\mathrm{d}} + i_{\mathrm{s}}\right), \tag{31}$$

$$\dot{v}_{\mathrm{Cblk}} = \frac{1}{C_{\mathrm{blk}}}\left(i_{\mathrm{s}}\right), \tag{32}$$

$$\dot{v}_{\mathrm{Cp}} = \frac{1}{C_{\mathrm{p}}}\left(i_{\mathrm{s}} - i_{\mathrm{p}} - i_{\mathrm{m}} - \frac{v_{\mathrm{Cp}}}{RL}\right), \tag{33}$$

$$\dot{i}_{\mathrm{d}} = \frac{1}{L_{\mathrm{d}}}\left(v_{\mathrm{in}} - v_{\mathrm{Ccc}} - i_{\mathrm{d}} R_{\mathrm{d}}\right), \tag{34}$$

$$\dot{i}_{\mathrm{s}} = \frac{1}{L_{\mathrm{s}}}\left(v_{\mathrm{in}} - v_{\mathrm{Ccc}} - v_{\mathrm{Cblk}} - v_{\mathrm{Cp}}\right), \tag{35}$$

Reproduced with permission of the copyright owner. Further reproduction prohibited without permission.

$$\dot{i}_{\mathrm{p}} = \frac{1}{L_{\mathrm{p}}}\left(v_{\mathrm{Cp}}\right), \tag{36}$$

and,

$$\dot{i}_{\mathrm{m}} = \frac{1}{L_{\mathrm{m}}}\left(v_{\mathrm{Cp}}\right). \tag{37}$$

Letting the state vector be

$$\mathbf{x} = \begin{bmatrix} v_{\mathrm{Ccc}} & v_{\mathrm{Cblk}} & v_{\mathrm{Cp}} & i_{\mathrm{d}} & i_{\mathrm{s}} & i_{\mathrm{p}} & i_{\mathrm{m}} \end{bmatrix}^{\mathrm{T}} \tag{38}$$

results in a system matrix of

$$\mathbf{A} = \begin{bmatrix} 0 & 0 & 0 & \frac{1}{C_{\mathrm{CC}}} & \frac{1}{C_{\mathrm{CC}}} & 0 & 0 \\ 0 & 0 & 0 & 0 & \frac{1}{C_{\mathrm{blk}}} & 0 & 0 \\ 0 & 0 & \frac{-1}{C_{\mathrm{p}}RL} & 0 & \frac{1}{C_{\mathrm{p}}} & \frac{-1}{C_{\mathrm{p}}} & \frac{-1}{C_{\mathrm{p}}} \\ \frac{-1}{L_{\mathrm{d}}} & 0 & 0 & \frac{-R_{\mathrm{d}}}{L_{\mathrm{d}}} & 0 & 0 & 0 \\ \frac{-1}{L_{\mathrm{s}}} & \frac{-1}{L_{\mathrm{s}}} & \frac{-1}{L_{\mathrm{s}}} & 0 & 0 & 0 & 0 \\ 0 & 0 & \frac{1}{L_{\mathrm{p}}} & 0 & 0 & 0 & 0 \\ 0 & 0 & \frac{1}{L_{\mathrm{m}}} & 0 & 0 & 0 & 0 \end{bmatrix} \tag{39}$$

and an input coupling vector of

Reproduced with permission of the copyright owner. Further reproduction prohibited without permission.

$$\mathbf{B} = \begin{bmatrix} 0 & 0 & 0 & \frac{1}{L_d} & \frac{1}{L_s} & 0 & 0 \end{bmatrix}^T . \tag{40}$$

The output equation for calculating drain coil voltage is

$$v_{drain} = \begin{bmatrix} -1 & 0 & 0 & 0 & 0 & 0 & 0 \end{bmatrix} \begin{bmatrix} v_{Ccc} \\ v_{Cblk} \\ v_{Cp} \\ i_d \\ i_s \\ i_p \\ i_m \end{bmatrix} + [1] v_{in} . \tag{41}$$

Comparison of Measured Frequency Response to Simulated Frequency Response

The frequency responses of the coupling systems were calculated using the state-space models and compared to the measured frequency responses obtained from the frequency response tests described in chapter 2. The Matlab routines used to calculate the frequency responses are provided in Appendix B, and the measured frequency response data to which the calculated responses are compared are from the frequency response tests described in chapter 2.

Comparisons of calculated and measured frequency responses for each of the coupling systems are shown in Figures 38 through 42. As shown in the figures, the state-space models can produce estimations of the frequency responses of the coupling systems with practical accuracy, particularly when calculating voltage gain at the drain coil.

Reproduced with permission of the copyright owner. Further reproduction prohibited without permission.

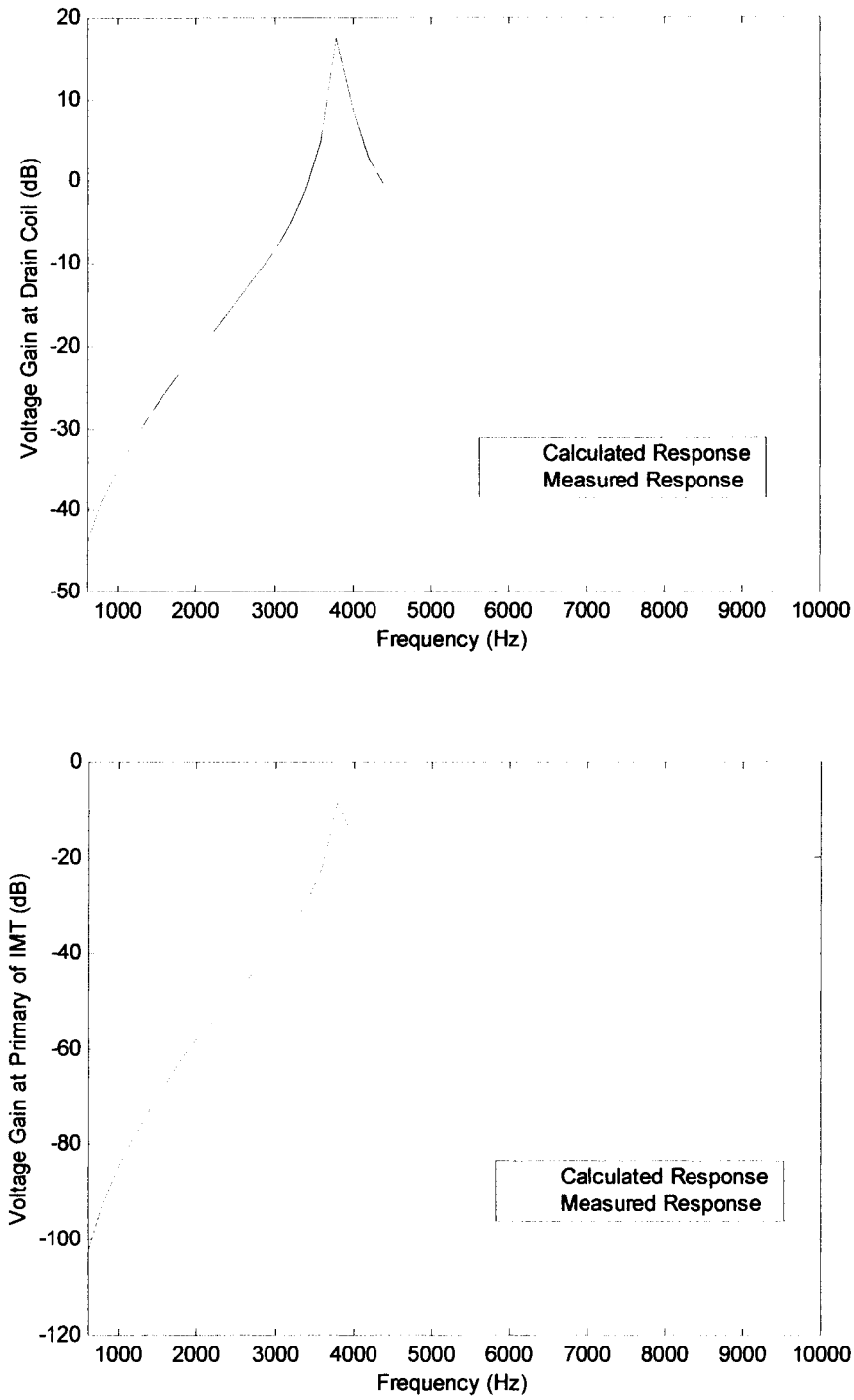

Figure 38. Calculated and measured frequency responses at the drain coil and impedance-matching transformer (IMT) of a single-frequency coupling system with the IMT terminated into 2,000 Ω.

Reproduced with permission of the copyright owner. Further reproduction prohibited without permission.

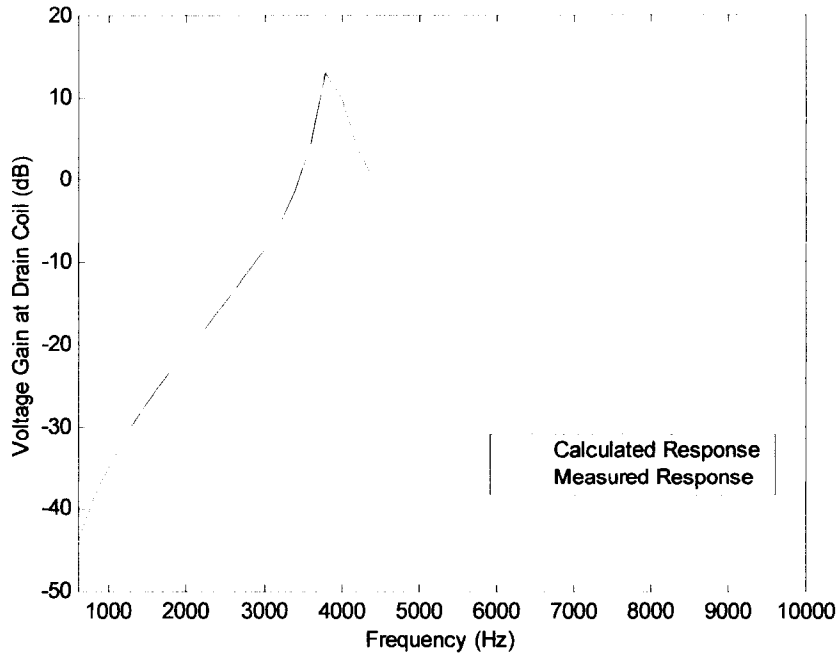

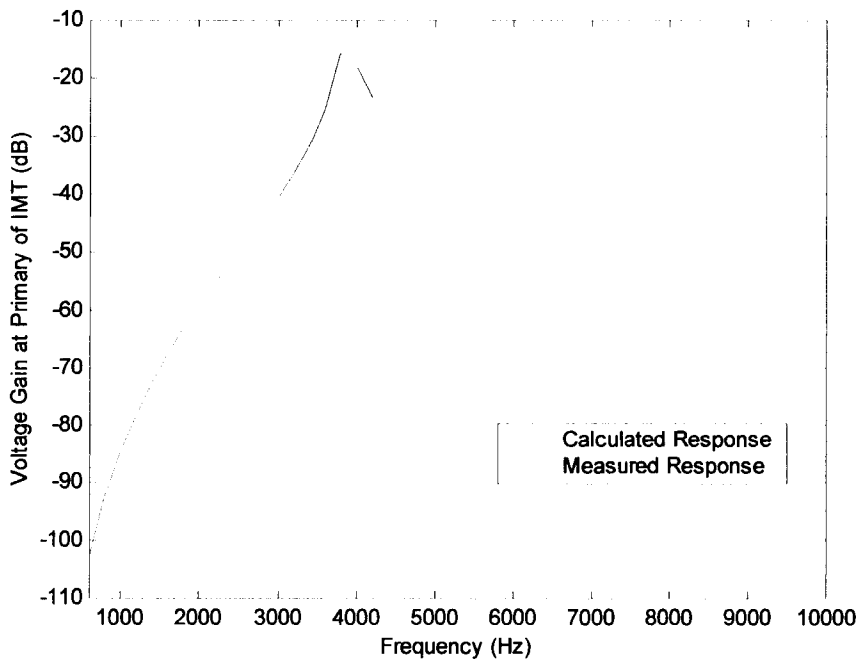

Figure 39. Calculated and measured frequency responses at the drain coil and impedance-matching transformer (IMT) of a single-frequency coupling system with the IMT terminated into 50 Ω.

Reproduced with permission of the copyright owner. Further reproduction prohibited without permission.

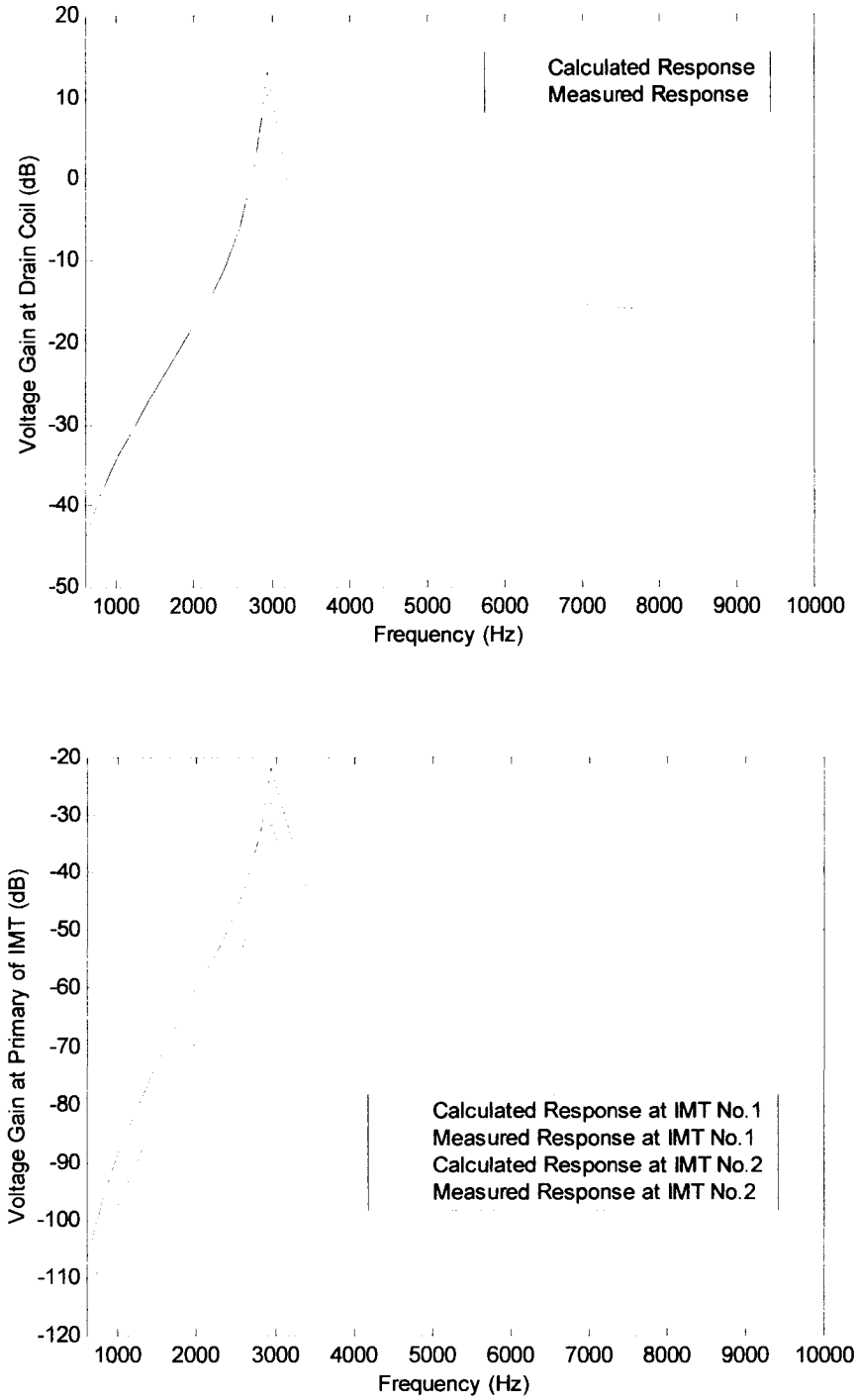

Figure 40. Calculated and measured frequency responses at the drain coil and each impedance-matching transformer (IMT) of a two-frequency coupling system with each IMT terminated into a high resistance.

Reproduced with permission of the copyright owner. Further reproduction prohibited without permission.

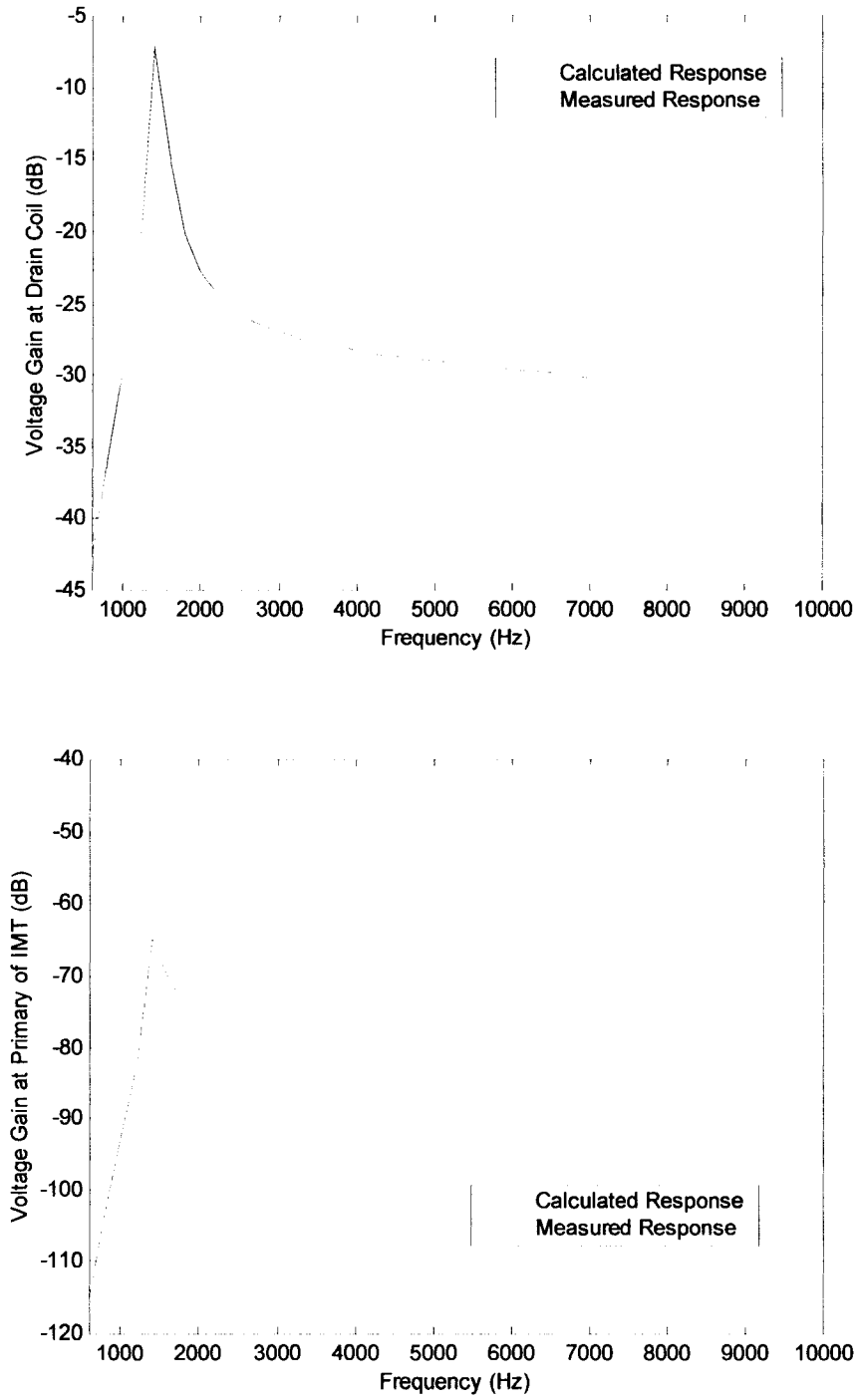

Figure 41. Calculated and measured frequency responses at the drain coil and impedance-matching transformer (IMT) of a second-order wideband coupling system with the IMT terminated into 2,000 Ω.

Reproduced with permission of the copyright owner. Further reproduction prohibited without permission.

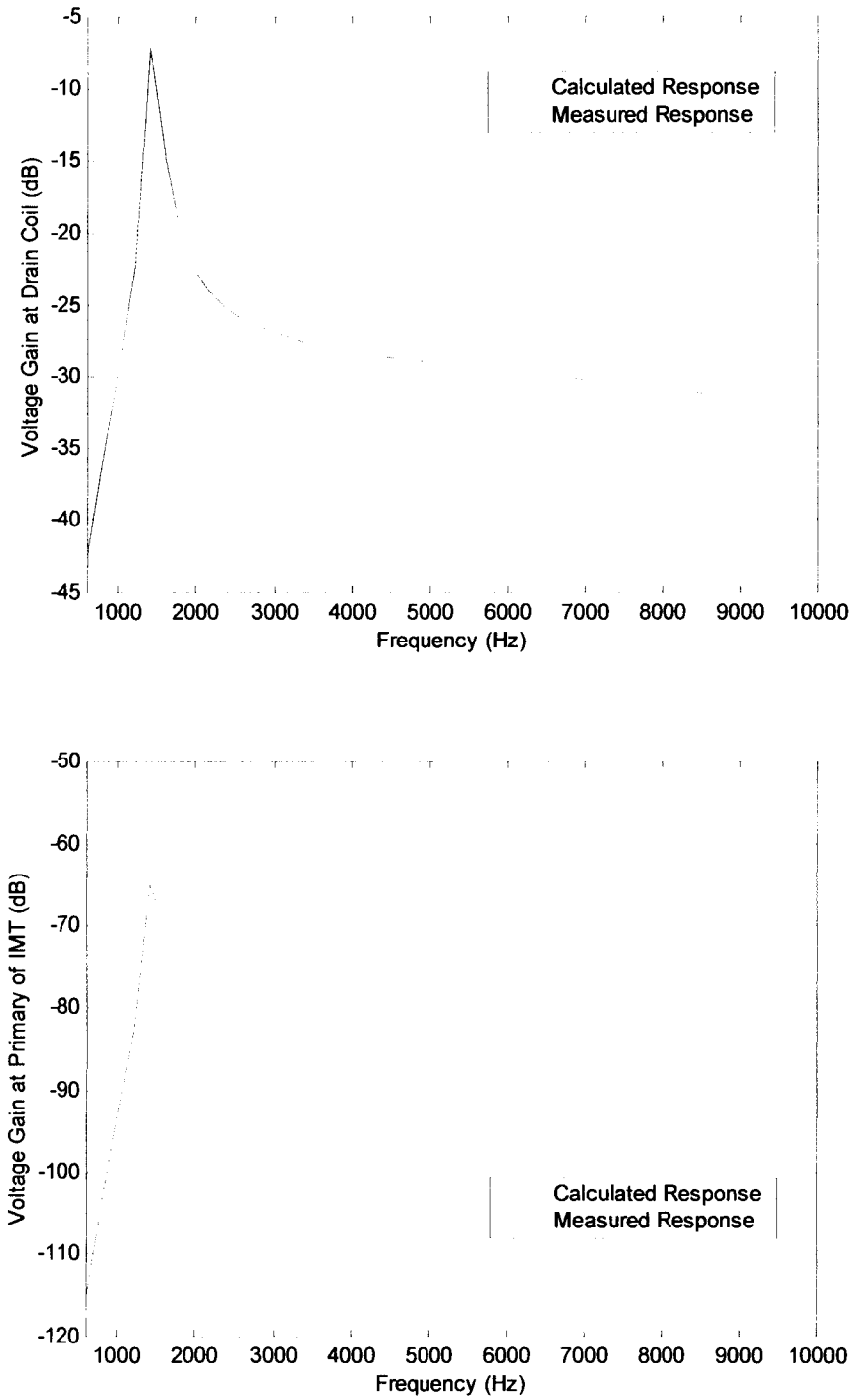

Figure 42. Calculated and measured frequency responses at the drain coil and impedance-matching transformer (IMT) of a second-order wideband coupling system with the IMT terminated into 50 Ω.

Reproduced with permission of the copyright owner. Further reproduction prohibited without permission.

However, the narrowband resonant model does lose accuracy when calculating the response at the primary of the IMT when the IMT is terminated into a high resistance. The loss of accuracy with the high IMT termination resistance is a result of the IMT exciting current's becoming the dominant current component of the line tuner circuit branch. This limitation of the models is discussed further in the following section of this chapter, where the effect of a high-valued line tuner series capacitance on the IMT current is also discussed. For the narrowband resonant systems of Figures 38 through 40, the high-frequency tuning capacitor was enabled, which resulted in a small-valued line tuner series capacitance. The aforementioned IMT exciting current does not significantly affect the frequency response of the wideband coupling system because the primary winding of the IMT in a wideband system is shunted by the small inductance of the parallel LC tuning unit that is in parallel with the primary winding of the IMT. The lower frequency discrepancies between the measured and calculated responses at the primary of the IMT for the wideband system shown in Figures 41 and 42 resulted from limitations of the meter used to measure voltage. The voltage levels developed at the primary of the IMT approached the minimum resolution of the meter used to measure voltage, which had a resolution of 1 mV. Furthermore, the meter used was not frequency selective, so a broadband voltage level was measured. Thus, extraneous noise induced into the test circuit could also have affected the measurements at the low voltage levels being measured.

Limitations of Models

The simplified PSpice and corresponding state-space models are not intended for frequencies higher than those in the harmonic frequency band since the IMT is simply

Reproduced with permission of the copyright owner. Further reproduction prohibited without permission.

modeled as an inductance in parallel with a resistance. At higher frequencies such as PLC frequencies, the leakage inductance of the IMT can be significant. Also, the actual magnetizing inductance of the IMT is nonlinear. However, this inductance is modeled as a linear inductance representing the self-inductance of the primary winding of the IMT (Fitzgerald et al., 1990). Thus, in cases where the IMT magnetizing reactance becomes a dominant reactance, the models lose accuracy. In particular, the IMT magnetizing reactance becomes significant when the series capacitance of the line tuner is relatively large and when the IMT is terminated into high impedance. For example, a single-frequency narrowband resonant system with the high-frequency tuning capacitor disabled and the IMT terminated into a carrier receiver with an input impedance of several kilo-ohms results in a case where the IMT magnetizing reactance becomes dominant. When the IMT magnetizing reactance becomes the dominant reactance in the circuit, the dominant current in the circuit becomes that of the IMT exciting current. Figure 43 illustrates the discrepancies between simulated and measured frequency responses for a system with the aforementioned characteristics by providing a comparison between the calculated and measured frequency responses at the drain coil and primary of the IMT for a single-frequency system. The single-frequency system had a line tuner series capacitance of 0.5 μF, and the IMT was terminated into a carrier receiver with an input resistance of 2,000 Ω. As shown in Figure 43, the nonlinearity of the IMT magnetizing inductance results in an oscillatory frequency response with higher gain than that of the calculated frequency response using the single-frequency state-space model. Although the models lose accuracy when the IMT magnetizing inductance becomes dominant, harmonic frequency interference would generally be mild in these cases anyway because voltage gain remains

Reproduced with permission of the copyright owner. Further reproduction prohibited without permission.

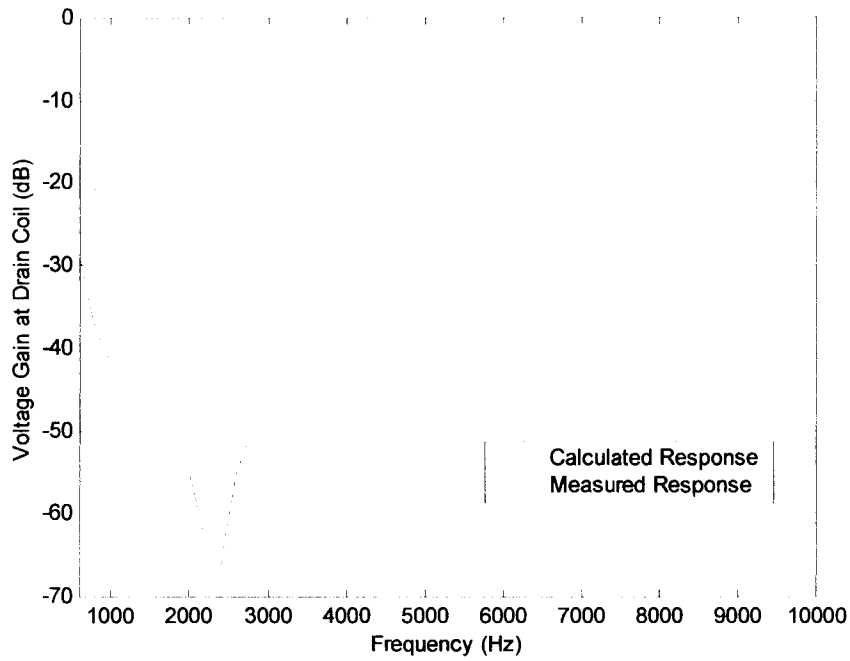

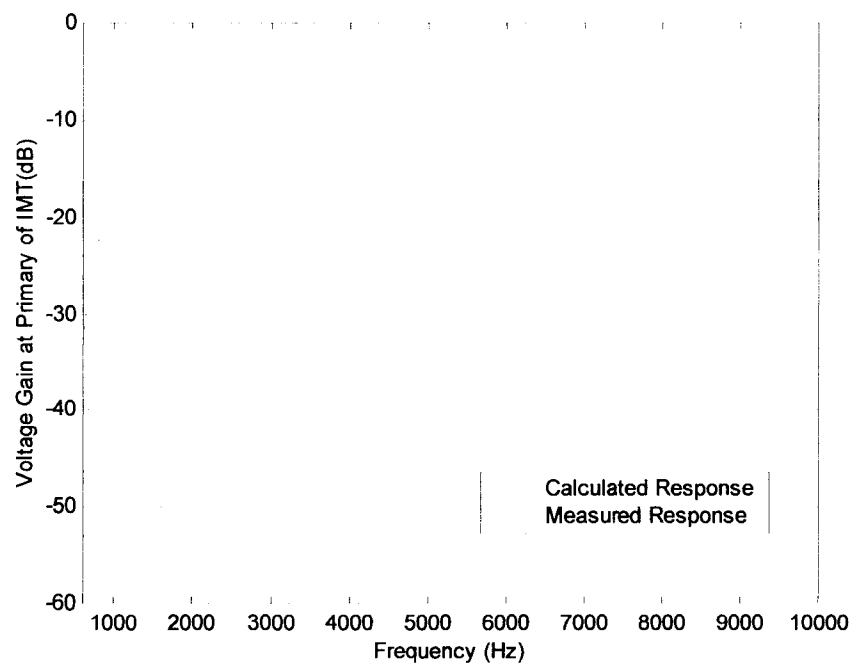

Figure 43. Calculated and measured frequency responses at the drain coil and impedance-matching transformer (IMT) of a single-frequency coupling system when the IMT magnetizing reactance is dominant.

Reproduced with permission of the copyright owner. Further reproduction prohibited without permission.

relatively low throughout the harmonic frequency band.

To show the difficulties that would arise in modeling the nonlinearity of the IMT, Figures 44 and 45 show waveforms and frequency spectrums of the IMT primary voltage at frequencies of 3 kHz and 4 kHz, respectively. The waveform measurements were taken during the single-frequency system's frequency response measurements shown in Figure 43. As shown by the waveforms and frequency spectrums of Figures 44 and 45, the magnitude and the frequency content of the IMT exciting current change with the frequency of the exciting voltage. For example, with the source voltage frequency at 3 kHz, the dominant IMT voltage component was the 9th harmonic at 27 kHz. However, with the source voltage frequency at 4 kHz, the IMT had dominant components of the 5th, 7th, and 9th harmonics at 20 kHz, 28 kHz, and 36 kHz, respectively.

Reproduced with permission of the copyright owner. Further reproduction prohibited without permission.

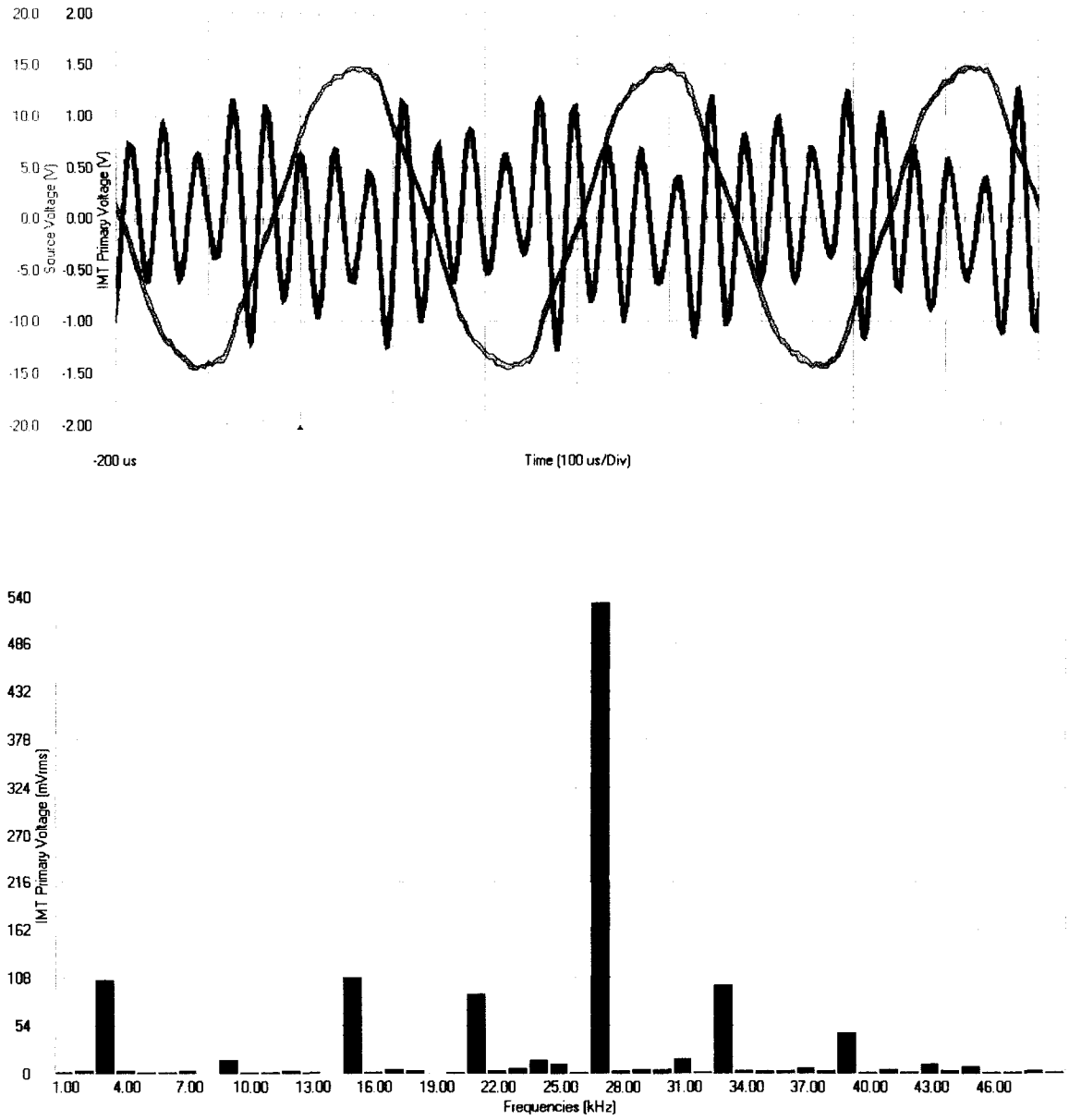

Figure 44. Waveform and frequency spectrum of impedance-matching transformer (IMT) primary voltage with source voltage frequency of 3 kHz.

Reproduced with permission of the copyright owner. Further reproduction prohibited without permission.

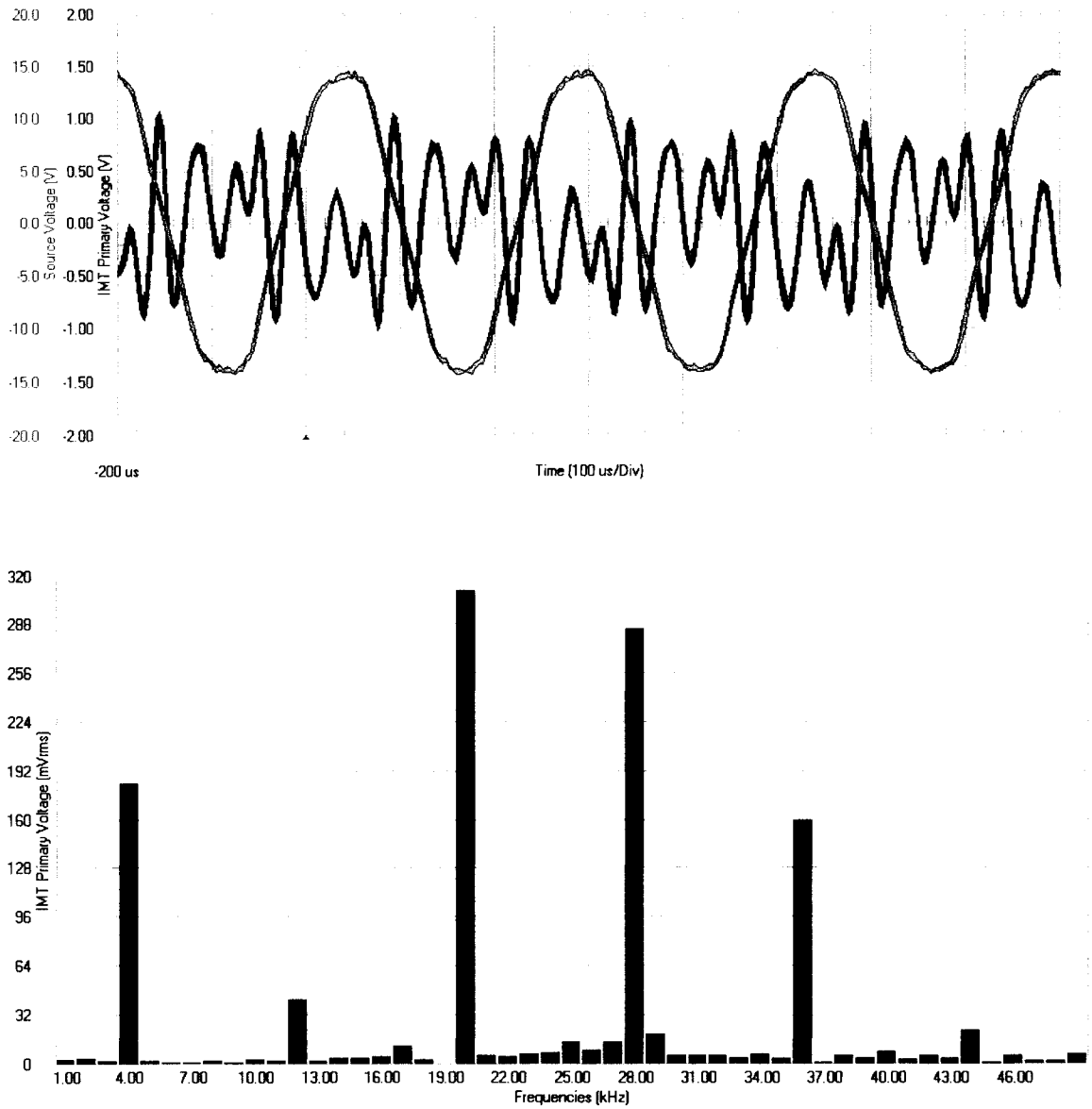

Figure 45. Waveform and frequency spectrum of impedance-matching transformer (IMT) primary voltage with source voltage frequency of 4 kHz.

Reproduced with permission of the copyright owner. Further reproduction prohibited without permission.

CHAPTER 4

MITIGATION OF HARMONIC FREQUENCY INTERFERENCE

This chapter presents a method of mitigating harmonic frequency interference that consists of altering certain system components to reduce voltage gain in the harmonic frequency band. The system components to be altered for harmonic frequency interference mitigation are identified, and a general description of the effects on frequency response of altering the system components is also provided. Furthermore, application of the method of interference mitigation presented does not require taking a transmission line out of service. Also considered are the effects of altering system components on other coupling system functions such as line tuning and impedance matching at carrier frequencies. Finally, an example of harmonic frequency interference mitigation on an actual 230-kV coupling system is presented.

Identifying and Altering Coupling System Components for Mitigation of Harmonic Frequency Interference

Identification of the system components to alter for mitigation of harmonic frequency interference begins with the generalized equivalent circuits of a coupling system shown in Figure 46. The circuits can represent any of the three coupling systems studied herein. Voltage gain at Z_{teq} is a function of the voltage divider between the coupling capacitor impedance and Z_{teq} (refer to Figure 46). The voltage gain at Z_{teq} can be written as

Reproduced with permission of the copyright owner. Further reproduction prohibited without permission.

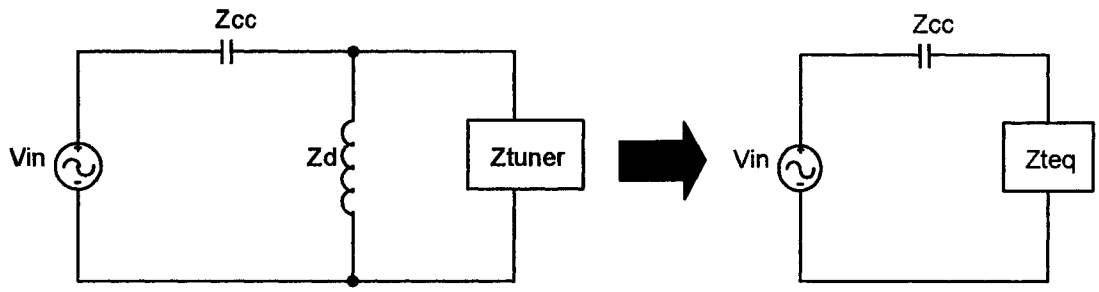

Figure 46. Generalized equivalent circuits for a coupling system. Vin = harmonic voltage distortion at the coupling system location; Zcc = coupling capacitor impedance; Zd = drain coil impedance; Ztuner = line tuner impedance; Zteq = equivalent impedance formed by the parallel combination of the drain coil and line tuner impedances.

$$A_{teq} = 20 \cdot \mathrm{Log}_{10}\left[\left|\frac{V_{teq}}{V_{in}}\right|\right] \mathrm{dB}, \tag{42}$$

where

$$V_{teq} = \left(\frac{Z_{teq}}{Z_{teq} + Z_{cc}}\right) \cdot V_{in}. \tag{43}$$

Substituting Equation 43 into Equation 42 yields

$$A_{teq} = 20 \cdot \mathrm{Log}_{10}\left[\left|\frac{Z_{teq}}{Z_{teq} + Z_{cc}}\right|\right] \mathrm{dB}, \tag{44}$$

which is the voltage gain expressed in dB at the drain coil in terms of the drain coil, line tuner, and coupling capacitor impedances. As Equation 44 shows, harmonic frequency

Reproduced with permission of the copyright owner. Further reproduction prohibited without permission.

interference mitigation basically consists of reducing Z_{teq} in the harmonic frequency band. Since Z_{teq} is the parallel combination of the drain coil and line tuner impedances, decreasing the drain coil impedance, decreasing the line tuner impedance, or decreasing both impedances will reduce Z_{teq}. Obviously, decreasing the drain coil inductance will reduce the drain coil impedance. The line tuner impedance, however, consists of a combination of inductive and capacitive reactances. Nevertheless, if component values typically used in line-tuning equipment are taken into consideration, the dominant components that can be altered for reducing the line tuner impedance in the harmonic frequency band can be readily identified.

The single-frequency resonant line tuner's components consist of an IMT and a tuning inductor in series with the net capacitance composed of the series combination of the 60-Hz blocking capacitor and the high-frequency tuning capacitor if enabled. The tuning inductor reactance will typically be small at harmonic frequencies, especially for tuning inductors tuned for carrier frequencies above 100 kHz, and thus can be neglected at frequencies in the harmonic frequency band. The dominant inductive reactance in the harmonic frequency band is the self-inductance of the primary winding of the IMT. However, the inductance of the IMT cannot be altered because altering the IMT primary winding inductance would require changing the impedance-matching tap setting, which could prevent acceptable impedance matching. Therefore, the dominant line tuner reactance in the harmonic frequency band that is available to alter is the line tuner's net capacitive reactance. Of course, decreasing the line tuner's impedance by decreasing the capacitive reactance requires increasing the line tuner's net capacitance consisting of the series combination of the-60 Hz blocking capacitor and high-frequency tuning capacitor.

Reproduced with permission of the copyright owner. Further reproduction prohibited without permission.

The single-frequency resonant line tuner simplifications previously described can be applied to the two-frequency line tuner. The inductive reactance of the IMTs for the two-frequency line tuner cannot be altered for the same reasons that this reactance cannot be altered for the single-frequency line tuner. The reactance of the parallel trap circuits in the tuning legs of the two-frequency line tuner can be neglected at frequencies in the harmonic frequency band because these trap circuits are tuned to resonate at carrier frequencies. Thus, the reactance of the parallel trap circuits will be a small inductive reactance at frequencies in the harmonic frequency band; therefore, the same reasoning used to eliminate the inductive reactance of the tuning inductor also applies to the small inductive reactance of the parallel trap circuits. Thus, as with the single-frequency line tuner, the dominant line tuner reactances in the harmonic frequency band that can be altered are the series capacitive reactances, which consist of the 60-Hz blocking capacitor and the high-frequency tuning capacitor in each tuning leg.

Analysis of the second-order wideband tuner also reveals that the dominant line tuner reactance in the harmonic frequency band is the tuner's capacitive reactance, which consists of the 60-Hz blocking capacitor. For the wideband tuner, the parallel LC circuit that is in parallel with the primary of the IMT is tuned to resonate at carrier frequencies and thus will present a small inductive reactance at harmonic frequencies. This small inductive reactance also shunts the inductive reactance of the primary winding of the IMT; as a result, the inductive reactance of the IMT need not even be considered as a component to alter. Also, as with the resonant type tuners, the inductive reactance of the series tuning inductor will also present a small inductive reactance at harmonic frequencies and thus can be neglected. Therefore, as was the case with the resonant type tuners, decreas-

Reproduced with permission of the copyright owner. Further reproduction prohibited without permission.

ing the line tuner's capacitive reactance by increasing the capacitance provides the means by which the wideband line tuner's impedance can be decreased in the harmonic frequency band.

Effect of Altering Drain Coil Inductance and Line Tuner Capacitance on Voltage Gain at the Drain Coil

A single-frequency coupling system is used to illustrate the effect of altering the line tuner series capacitance and drain coil inductance on voltage gain at the drain coil. The equivalent circuit for the system is shown in Figure 47. In the circuit, the line tuner series capacitance, C_s, represents the net line tuner capacitance consisting of the 60-Hz blocking capacitor and the high-frequency tuning capacitor if enabled.

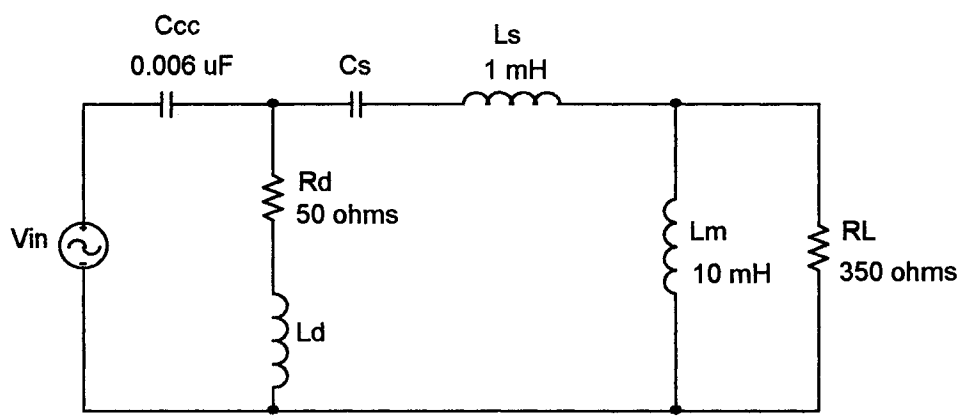

Figure 47. Single-frequency coupling system model for illustrating the effects of various combinations of drain coil inductance and line tuner series capacitance on voltage gain at the drain coil. Ccc = coupling capacitance; Rd = drain coil resistance; Ld = drain coil inductance; Cs = line tuner series capacitance; Ls = line tuner series inductance; Lm = impedance-matching transformer (IMT) magnetizing inductance; RL = load resistance reflected to primary of IMT.

Reproduced with permission of the copyright owner. Further reproduction prohibited without permission.

Using the general state-space model for resonant type coupling systems from chapter 3, the frequency response of the system was calculated using various combinations of large and small values of drain coil inductance and line tuner capacitance. The calculated frequency responses are shown in Figure 48. As the figure shows, the primary effect of altering the drain coil inductance and line tuner capacitance is that of shifting the low-order switching frequency of Z_{teq} to either end of the harmonic frequency band. The low-order switching frequency was described in chapter 2 as the lowest frequency at which the impedance formed by the parallel combination of the drain coil and line tuner impedances, which is Z_{teq}, switches from an inductive impedance to a capacitive impedance. In other words, the low-order switching frequency is the lowest frequency at which Z_{teq} exhibits a parallel resonance. At frequencies below the low-order switching frequency, the reactance of Z_{teq} is inductive. When Z_{teq} is inductive, the voltage gain at the drain coil will exhibit a peak prior to the low-order switching frequency because the inductive reactance of Z_{teq} will be in series with the capacitive reactance of the coupling capacitor. Shifting the low-order switching frequency of Z_{teq} to the lower end of the harmonic frequency band results in reduced voltage gain at the drain coil and line tuner because the capacitive reactance of the coupling capacitor will be large and because the inductive reactance of Z_{teq} will be small. Shifting the low-order switching frequency of Z_{teq} above the harmonic frequency band results in Z_{teq}'s remaining an inductive reactance throughout the harmonic frequency band, but the inductive reactance peak exhibited by Z_{teq} prior to the low-order switching frequency is outside the harmonic frequency band. Thus, the voltage gain at the drain coil does not exhibit a peak in the harmonic frequency band. As Figure 48 shows, a large line tuner capacitance shifts the low-order switching

Reproduced with permission of the copyright owner. Further reproduction prohibited without permission.

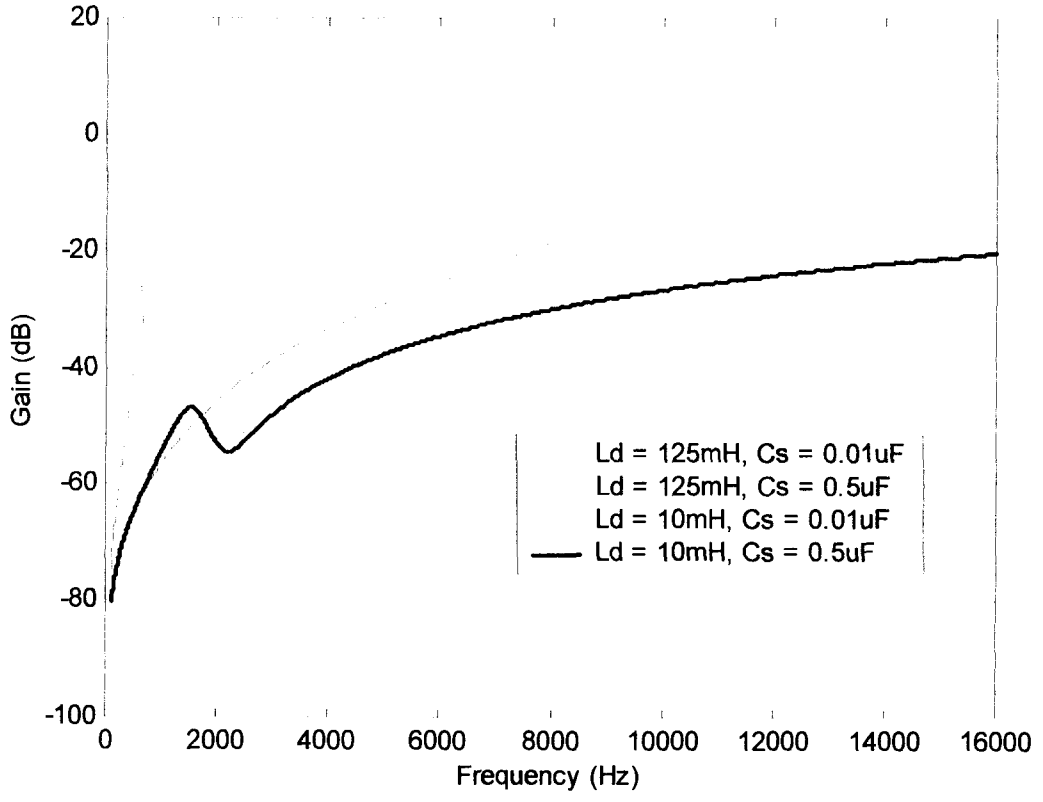

Figure 48. Comparison of voltage gain at drain coil of a single-frequency coupling system for various combinations of drain coil inductance and line tuner series capacitance. Ld = drain coil inductance; Cs = line tuner series capacitance.

Reproduced with permission of the copyright owner. Further reproduction prohibited without permission.

frequency of Z_{teq} to a lower frequency, whereas a small drain coil inductance shifts the low-order switching frequency to a higher frequency.

In summary, the response most immune to harmonic frequency interference is that obtained with a small drain coil inductance and a large line tuner series capacitance. However, the response obtained with a large drain coil inductance and a large line tuner series capacitance would also be satisfactory in most cases. Thus, for systems that have a large drain coil inductance, only changing the line tuner series capacitance would likely produce acceptable mitigation of harmonic frequency interference. Figure 48 also shows that systems that have a small-valued drain coil inductance, such as 10 mH, are not likely to experience problems, either, as voltage gain remains relatively low until the higher end of the harmonic frequency band. Thus, as mentioned previously, decreasing the drain coil inductance and/or increasing the line tuner series capacitance can provide mitigation of harmonic frequency interference. Determining the best method is dependent upon the particular application and consideration of the effects of altering the components on system operation at carrier frequencies, which is discussed in the following section.

Carrier Frequency Considerations When System Components Are Being Altered for Mitigation of Harmonic Frequency Interference

Although line tuner series capacitance and drain coil inductance are predominant components affecting frequency response in the harmonic frequency band, they can also affect other functions such as line tuning and impedance matching at carrier frequencies. Since harmonic interference mitigation requires increasing line tuner series capacitance and/or decreasing drain coil inductance, the effects of altering these components on system operation at carrier frequencies must be considered.

Reproduced with permission of the copyright owner. Further reproduction prohibited without permission.

Considerations When Increasing Line Tuner Series Capacitance

For the resonant type coupling systems, the line tuner series capacitance is the series combination of the 60-Hz blocking capacitor and, if enabled, the high-frequency tuning capacitor that is part of the series LC line-tuning unit. For resonant type coupling systems, the overall series capacitance of the line tuner is constrained by the minimum value achievable for the line tuner series inductance, which is dependent on the equivalent series inductance of the IMT at carrier frequencies. The equivalent series inductance of the IMT at carrier frequencies, which is dependent on the IMT tap setting, can be as high as several hundred micro-henries for older generation IMTs with toroidal cores. Thus, depending on carrier frequency and coupling capacitance, desired resonance between the line tuner and coupling capacitor at a particular carrier frequency may not be achievable without additional capacitive reactance provided by the line tuner series capacitance; that is, smaller values of line tuner series capacitance are required at higher carrier frequencies and/or larger values of coupling capacitance. Therefore, in some cases, mitigation of harmonic frequency interference by increasing line tuner series capacitance alone may not be satisfactory, and additional or alternative mitigation by reducing the drain coil inductance may be required. Figure 49 shows a plot of the additional series capacitance required to resonate with an inductance of 200 μH for coupling capacitance values of 0.003 μF and 0.006 μF, which are values commonly found at voltage levels of 230 kV and 115 kV, respectively.

Another consideration when line tuner series capacitance is being increased is that of voltage gain at the IMT. As shown by the frequency response measurements in chapter 2 for the resonant type coupling systems, a large-valued line tuner capacitance such as the

Reproduced with permission of the copyright owner. Further reproduction prohibited without permission.

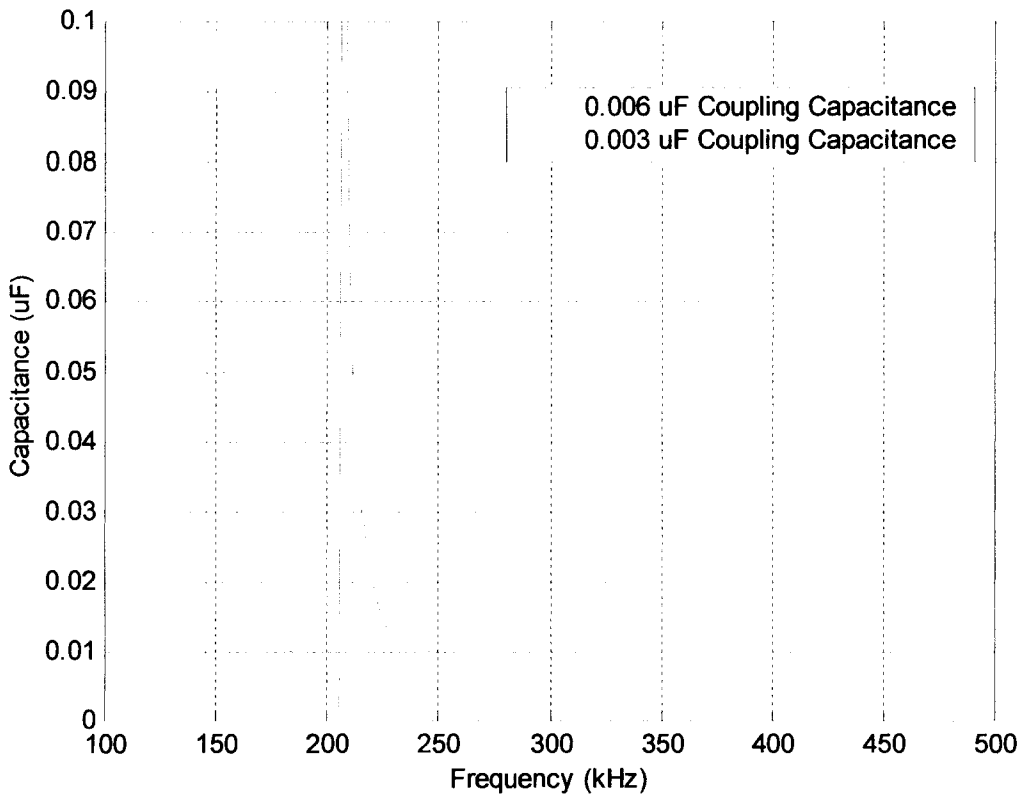

Figure 49. Plots showing additional line tuner series capacitance required to resonate with an inductance of 200 μH for coupling capacitance values of 0.003 μF and 0.006 μF.

Reproduced with permission of the copyright owner. Further reproduction prohibited without permission.

60-Hz blocking capacitance results in a voltage gain at the IMT that is approximately equal to that at the drain coil at frequencies in the harmonic frequency band. The voltage gain at the IMT and drain coil are approximately equal because the reactance of the large-valued 60-Hz blocking capacitance becomes very small at frequencies in the harmonic frequency band, which results in the IMT's being essentially in parallel with the drain coil. Thus, depending on the magnitude and frequency of the harmonic distortion at a coupling system's location, the IMT could possibly experience saturation problems resulting in impedance-matching problems at carrier frequencies despite the voltage gain's being relatively low at the drain coil. The aforementioned problem would not likely occur with the second-order wideband system because the parallel LC circuit that is in parallel with the primary of the IMT has very low impedance at frequencies in the harmonic frequency band. Thus, the primary of the IMT is effectively shunted at harmonic frequencies, which results in voltage levels at the IMT below that necessary to cause saturation.

Considerations When Decreasing Drain Coil Inductance

Drain coil inductance can affect impedance matching and line tuning at carrier frequencies; therefore, the effects of decreasing drain coil inductance on coupling system operation at carrier frequencies must also be considered. Figure 50 shows an equivalent circuit of a coupling system at carrier frequencies. Since it is assumed that the line tuner will be tuned to cancel the reactive part of the transmission line's characteristic impedance, the transmission line is represented as a characteristic resistance, R_0. The line tuner, which includes the IMT, is in series with the equivalent load impedance formed by the parallel combination of L_d, C_{cc}, and R_0. This equivalent load impedance, Z_{Leq}, can be

Reproduced with permission of the copyright owner. Further reproduction prohibited without permission.

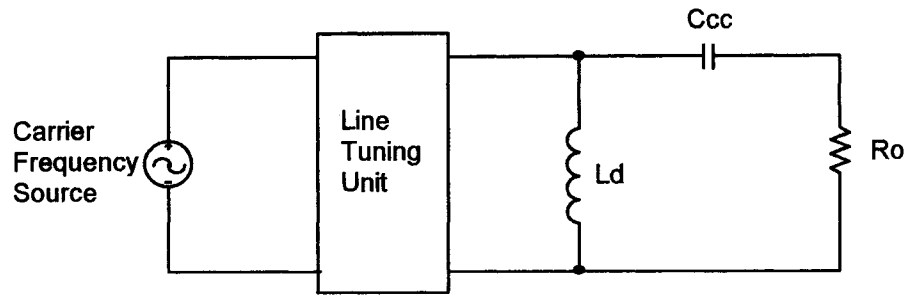

Figure 50. Equivalent circuit of coupling system at carrier frequencies. Ld = drain coil inductance; Ccc = coupling capacitance; Ro = characteristic resistance of the transmission line.

derived by first converting the components to impedances and forming the parallel combination of the impedances as

$$Z_{\mathrm{Leq}} = \frac{jX_{\mathrm{d}}(R_0 - jX_{\mathrm{cc}})}{R_0 - jX_{\mathrm{cc}} + jX_{\mathrm{d}}}, \tag{45}$$

where $X_{\mathrm{d}} = \omega L_{\mathrm{d}}$ and $X_{\mathrm{cc}} = 1/(\omega C_{\mathrm{cc}})$. Rationalizing the denominator of Equation 45 yields

$$Z_{\mathrm{Leq}} = \frac{X_{\mathrm{d}}X_{\mathrm{cc}} + jR_0X_{\mathrm{d}}}{R_0 + j(X_{\mathrm{d}} - X_{\mathrm{cc}})} \cdot \frac{R_0 - j(X_{\mathrm{d}} - X_{\mathrm{cc}})}{R_0 - j(X_{\mathrm{d}} - X_{\mathrm{cc}})}, \tag{46}$$

which expands to

$$Z_{\mathrm{Leq}} = \frac{R_0X_{\mathrm{d}}X_{\mathrm{cc}} + jX_{\mathrm{d}}R_0^{\,2} - jX_{\mathrm{d}}X_{\mathrm{cc}}(X_{\mathrm{d}} - X_{\mathrm{cc}}) + R_0X_{\mathrm{d}}(X_{\mathrm{d}} - X_{\mathrm{cc}})}{R_0^2 + (X_{\mathrm{d}} - X_{\mathrm{cc}})^2}. \tag{47}$$

Reproduced with permission of the copyright owner. Further reproduction prohibited without permission.

Expanding further and combining terms yield

$$Z_{\mathrm{Leq}} = \frac{R_0 X_{\mathrm{d}}^{\ 2} + jX_{\mathrm{d}}[R_0^{\ 2} - X_{\mathrm{cc}}(X_{\mathrm{d}} - X_{\mathrm{cc}})]}{R_0^2 + (X_{\mathrm{d}} - X_{\mathrm{cc}})^2}. \tag{48}$$

Equation 48 can be reduced to the form of $Z_{\mathrm{Leq}} = R_{\mathrm{Leq}} + jX_{\mathrm{Leq}}$, where

$$R_{\mathrm{Leq}} = \frac{R_0 X_{\mathrm{d}}^{\ 2}}{R_0^{\ 2} + (X_{\mathrm{d}} - X_{\mathrm{cc}})^2} \tag{49}$$

and

$$X_{\mathrm{Leq}} = \frac{X_{\mathrm{d}}(R_0^{\ 2} + X_{\mathrm{cc}}^{\ 2} - X_{\mathrm{d}} X_{\mathrm{cc}})}{R_0^{\ 2} + (X_{\mathrm{d}} - X_{\mathrm{cc}})^2}. \tag{50}$$

In Equations 49 and 50, R_{Leq} is the resistance that the IMT matches to the communication equipment internal resistance, and X_{Leq} is the reactance to which the line tuner is tuned to cancel at the carrier frequency.

To determine the effect of lowering the drain coil inductance on impedance matching at carrier frequencies, an assumption is first made that the line tuner is tuned to cancel X_{Leq} so that the IMT is matching the communication equipment resistance to the equivalent load resistance, R_{Leq}, within the carrier frequency band of operation for a particular coupling system. Thus, determining the effect of lowering drain coil inductance on impedance matching becomes an analysis of the effect of lowering drain coil inductance

Reproduced with permission of the copyright owner. Further reproduction prohibited without permission.

on R_{Leq}. R_{Leq} will exhibit the behavior of a parallel LCR circuit that asymptotically approaches a minimum value as frequency increases past the resonant frequency of the drain coil and coupling capacitor, which, of course, is $f = 1/(2\pi\sqrt{L_d C_{cc}})$ (refer to Equation 49). For R_{Leq}, the minimum value approached as frequency increases past the resonant frequency is R_0, which is the characteristic resistance of the transmission line. The aforementioned behavior is illustrated in Figure 51. Figure 51 shows plots of R_{Leq} versus frequency for various values of drain coil inductance. The plots were created using Equation 49, with $R_0 = 300\ \Omega$ and $C_{cc} = 0.003\ \mu F$. As shown in Figure 51, R_{Leq} can achieve a high value at frequencies around the resonant frequency of the drain coil and coupling capacitor. Equation 49 can be used to determine the value of R_{Leq} at this resonant frequency where the reactances, X_d and X_{cc}, are equal; this value is given by

$$R_{Leq} = \frac{X_d^{\ 2}}{R_0} = \frac{L_d}{C_{cc} R_0}. \tag{51}$$

Lowering the drain coil inductance shifts the resonant frequency of the drain coil and coupling capacitor higher into the carrier frequency band, which shifts the maximum value of R_{Leq} higher into the carrier frequency band. If a carrier signal's frequency were near this resonant frequency, the high value of R_{Leq} would likely exceed the maximum impedance tap of an IMT, thereby preventing impedance matching. Similarly, if a carrier signal's frequency were below the resonant frequency of the drain coil and coupling capacitor, the value of R_{Leq} could exceed the minimum impedance tap of an IMT. Also, at frequencies below the resonant frequency of the drain coil and coupling capacitor, R_{Leq}

Reproduced with permission of the copyright owner. Further reproduction prohibited without permission.

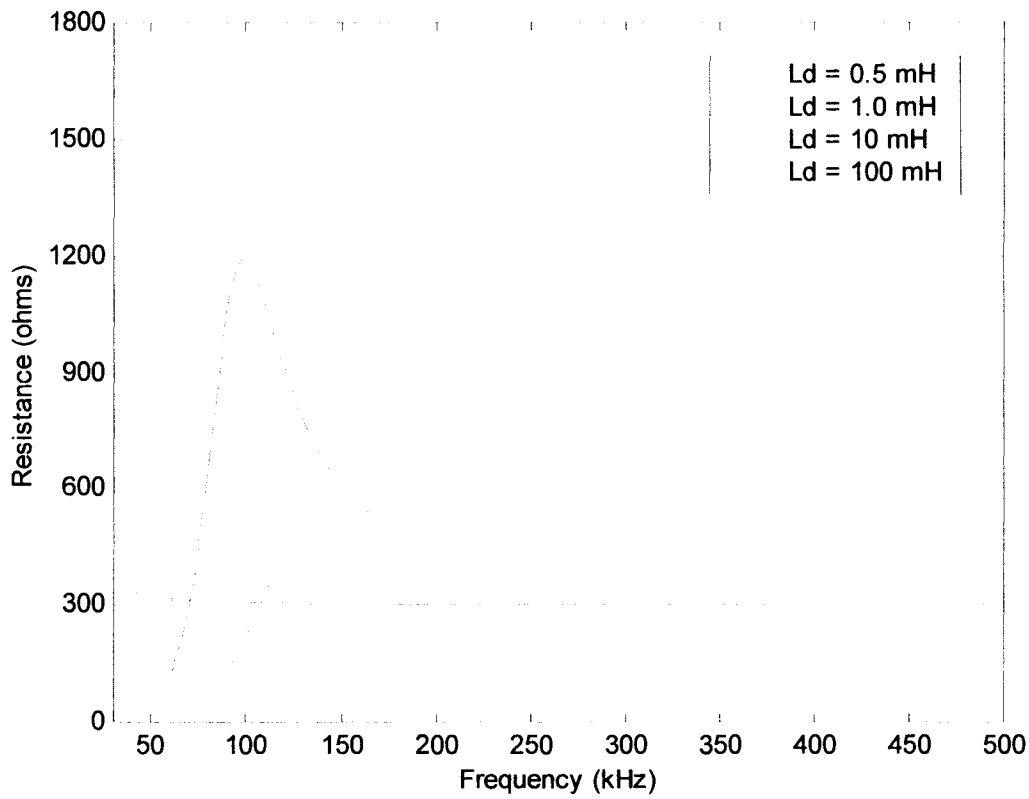

Figure 51. Plots of equivalent load resistance versus frequency for various values of drain coil inductance. The plots were created using Equation 49 with a transmission line characteristic resistance of 300 Ω and a coupling capacitance of 0.003 μF. Ld = drain coil inductance.

Reproduced with permission of the copyright owner. Further reproduction prohibited without permission.

has a steep rate of change with frequency, which would make impedance matching difficult using an IMT with discrete taps. Therefore, for the types of coupling systems studied herein, drain coil inductance should not be decreased to the point that the resonant frequency of the drain coil and coupling capacitor is within the carrier frequency band of operation for a particular coupling system. Furthermore, the drain coil inductance must be large enough to allow R_{Leq} to fall within the tap range of the IMT. Manufacturers of coupling system equipment indicate that the drain coil should ideally have an inductance that results in R_{Leq}'s approaching R_0 at frequencies below or near the minimum carrier frequency of 30 kHz so that their equipment is usable over the entire carrier frequency band. This result is achievable with larger values of drain coil inductance, which explains why most drain coils have an inductance of 10 mH or higher.

In addition to the effect on impedance matching, smaller values of drain coil inductance can result in X_{Leq}'s being an inductive reactance further into the carrier frequency band, which means the line tuner's reactance will have to be capacitive to cancel X_{Leq}. Line-tuning equipment is designed with variable inductors for line tuning. Thus, drain coil inductance should not be decreased to the point that X_{Leq} is inductive in the carrier frequency band of operation for a particular coupling system. Figure 52 shows plots of X_{Leq} versus frequency for various values of drain coil inductance. As a general rule, the industry standard for PLC coupling capacitors (*Requirements for Power-Line Carrier Coupling Capacitors and Coupling Capacitor Voltage Transformers (CCVT)*, 1999) recommends that drain coil inductance be at least a factor of 13 times greater than the series inductance of the line tuner. However, using Equations 49 and 50, the effect of drain coil inductance on impedance matching and line tuning can be calculated.

Reproduced with permission of the copyright owner. Further reproduction prohibited without permission.

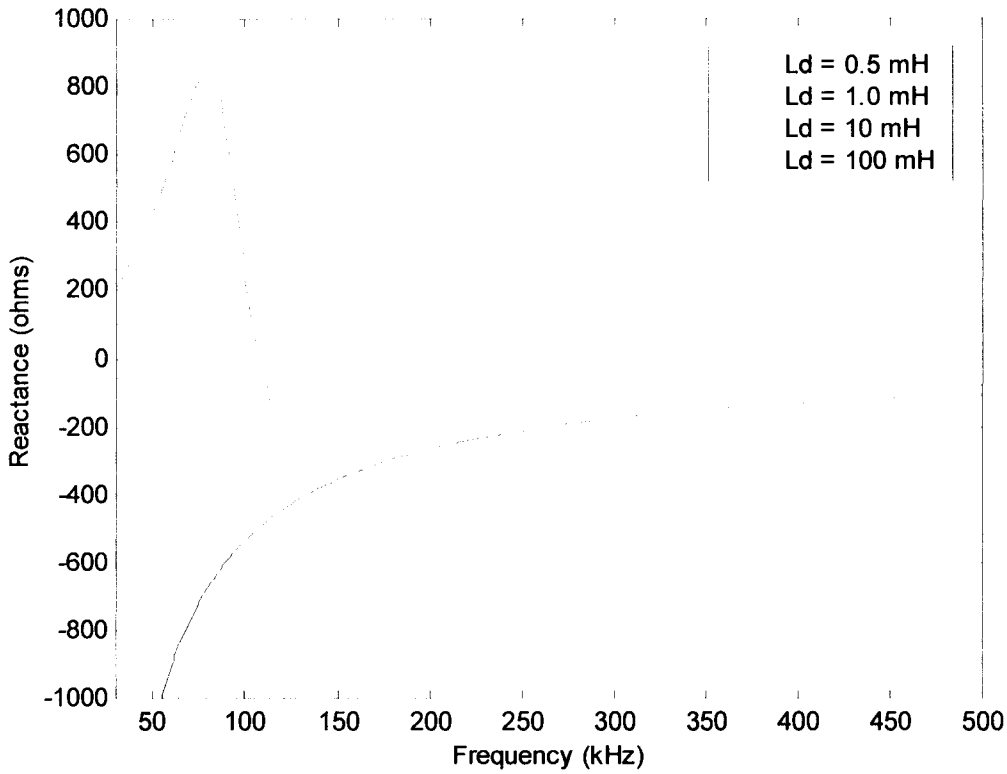

Figure 52. Plots of equivalent load reactance versus frequency for various values of drain coil inductance. The plots were created using Equation 50 with a transmission line characteristic resistance of 300 Ω and a coupling capacitance of 0.003 μF. Negative values indicate capacitive reactance, and positive values indicate inductive reactance. The line tuner reactance would be set opposite to that of the equivalent load reactance. Ld = drain coil inductance.

Reproduced with permission of the copyright owner. Further reproduction prohibited without permission.

Example of Altering Coupling System Components to Mitigate Harmonic Frequency Interference

To provide an example of altering the frequency response of a PLC coupling system to mitigate harmonic frequency interference, the 230-kV coupling system described in chapter 1 will be used. As described in chapter 1, the coupling system was severely affected by harmonic interference and thus provides an extreme case with which to illustrate the effectiveness of the mitigation methods presented. The coupling system on the 230-kV line is a two-frequency resonant system tuned to f_1 = 180 kHz and f_2 = 113 kHz. This particular system had the undesirable combination of a high-inductance drain coil with small series capacitance values in the line-tuning units. This combination resulted in a peak voltage gain at the drain coil of approximately 12 dB at 2,900 Hz as shown by the PSpice analysis and frequency response measurements of the system. The PSpice analysis and frequency response measurements of the system are presented in chapter 1, along with measurements illustrating the problems experienced with the system.

For interference mitigation, the drain coil inductance and/or the line tuner series capacitance could be altered. As shown by frequency response measurements, the series capacitance in only one tuning leg of a two-frequency system has to be increased to achieve the desired change in frequency response; thus, altering the line tuner series capacitance was the preferred method to avoid purchasing another drain coil. For the 113-kHz tuning leg, the high-frequency tuning capacitor was not needed for carrier frequency operation. Therefore, this small 0.01-μF capacitance could be disabled, leaving the much larger 0.5-μF 60-Hz blocking capacitor, which provided problem mitigation by increasing the series capacitance of the tuning branch. The two-frequency state-space model from chapter 3 was used to calculate the voltage gain response at the drain coil with and with-

Reproduced with permission of the copyright owner. Further reproduction prohibited without permission.

out the high-frequency tuning capacitor enabled. The system component values used with the state-space model can be obtained from the PSpice model of the system shown in Figure 6 in chapter 1. A comparison of the voltage gain responses with and without the high-frequency tuning capacitor enabled is shown in Figure 53. Also, Figure 54 shows measurements of the voltage levels taken across the drain coil of the 230-kV coupling system with and without the high-frequency tuning capacitor enabled. To verify that disabling the high-frequency tuning capacitor was actually mitigating the excessive voltage level shown by the upper waveform of Figure 54, the high-frequency tuning capacitor was enabled and disabled several times while observing the voltage waveform and verifying that the high voltage levels returned upon enabling the high-frequency tuning capacitor. The high-frequency signal content (and the resulting 1-kHz intermodulation) shown in the lower waveform of Figure 54 is that of two carrier signals at 112.6 kHz and 113.6 kHz that are received continuously by the 230-kV coupling system.

Reproduced with permission of the copyright owner. Further reproduction prohibited without permission.

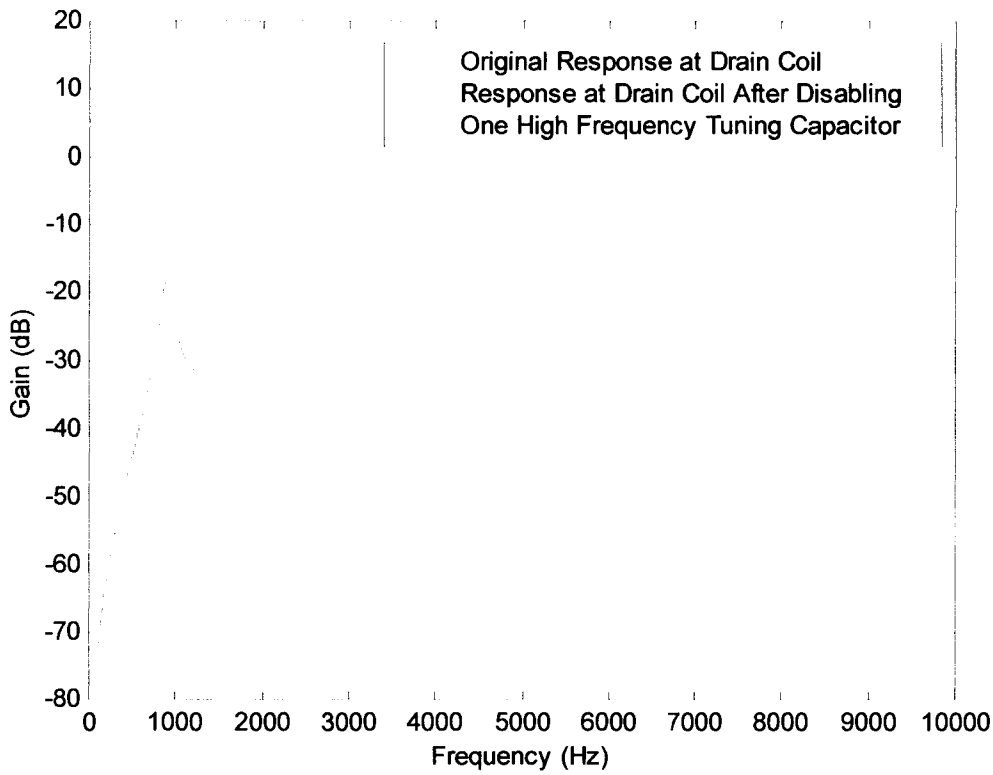

Figure 53. Comparison of calculated voltage gain at drain coil before and after disabling one of the high-frequency tuning capacitors in a 230-kV two-frequency coupling system.

Reproduced with permission of the copyright owner. Further reproduction prohibited without permission.

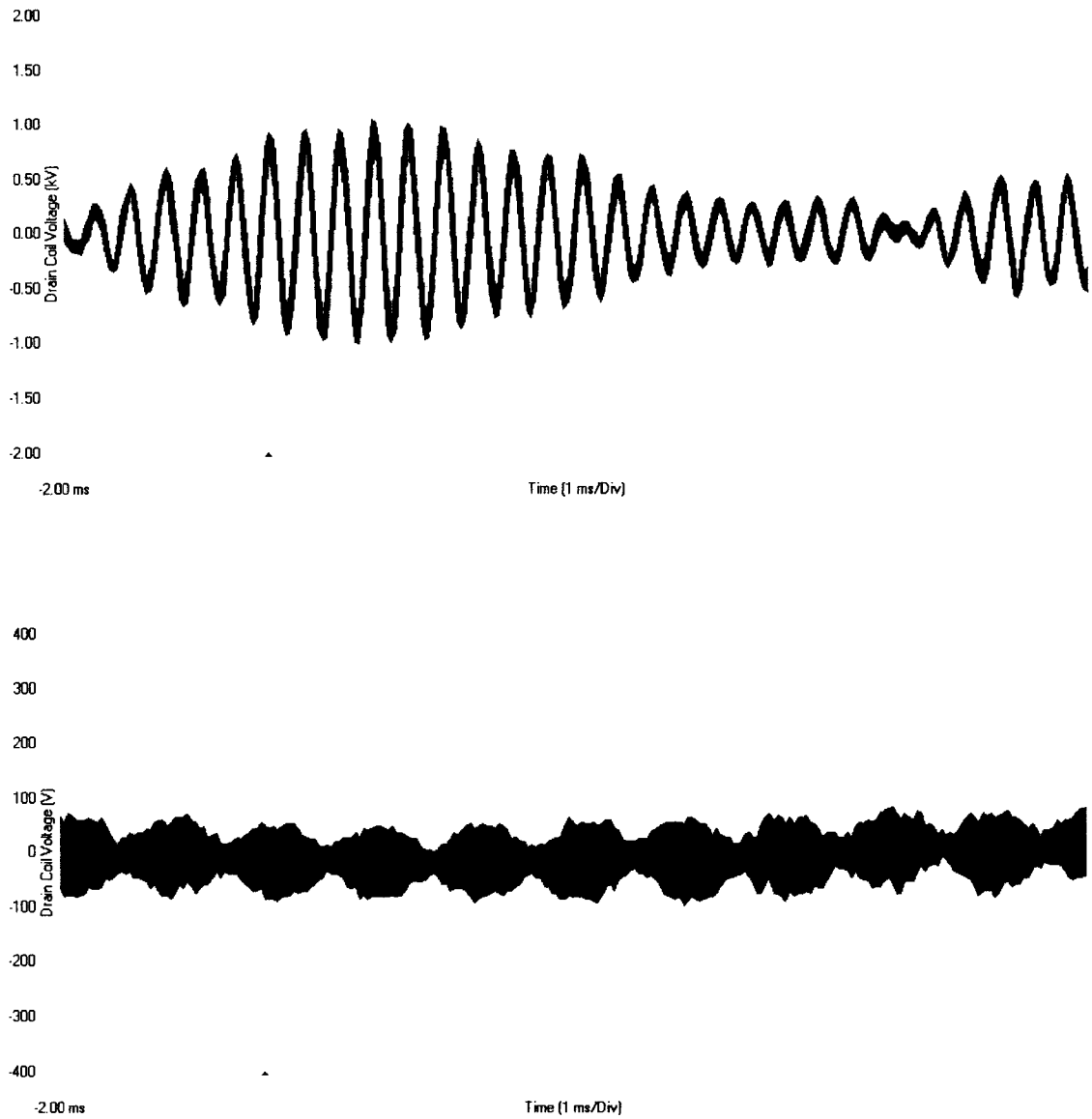

Figure 54. Waveforms of drain coil voltage on a 230-kV coupling system taken before and after alteration of line tuner series capacitance. The top waveform shows the drain coil voltage with the high-frequency tuning capacitor enabled in both tuning legs. The high-frequency tuning capacitor was set at 0.01 μF in each tuning leg. The bottom waveform shows the drain coil voltage with the high-frequency tuning capacitor enabled in only one tuning leg. Disabling one high-frequency tuning capacitor resulted in one tuning leg's having a series capacitance of approximately 0.01 μF and the other tuning leg's having a series capacitance of approximately 0.5 μF.

Reproduced with permission of the copyright owner. Further reproduction prohibited without permission.

CHAPTER 5

CONCLUSION

Summary of Research Goals and Results

The research was undertaken with the following three primary goals:

1. The first research goal was to obtain frequency response measurements of the coupling systems to acquire data for model validation and to gain a general understanding of the susceptibility of the various coupling system configurations to harmonic frequency interference.
2. The second goal of the research was to develop computer models suitable for estimating the frequency response of the coupling systems in the harmonic frequency band.
3. The third goal was to identify coupling system components that can be altered to provide mitigation of harmonic frequency interference.

The first goal of obtaining frequency response measurements was accomplished in two parts. First, measurements were made of the peak voltage gain in the harmonic frequency band for each of the three types of coupling systems studied. The peak voltage gain measurements were taken for each type of coupling system using three types of drain coils, as well as three values of capacitance corresponding to coupling capacitors found on the 115-kV, 230-kV, and 500-kV transmission systems. Voltage measurements were taken across the coupling capacitor, drain coil, and primary and secondary of the IMT to provide a broad range of data for model validation purposes. Second, the voltage gain response at the drain coil and primary of the IMT of each coupling system was

Reproduced with permission of the copyright owner. Further reproduction prohibited without permission.

measured from 600 Hz to 10 kHz at 200-Hz intervals using one value of coupling capacitance and drain coil inductance. To determine the effect of the IMT termination on frequency response, two widely different IMT terminations were used for the tests. From the frequency response measurements, the coupling systems most susceptible to harmonic frequency interference were identified as being single-frequency and two-frequency resonant systems applied with coupling capacitance values corresponding to those typically used on the 115-kV and 230-kV transmission systems. In particular, the single-frequency and two-frequency resonant systems were found to be most susceptible to harmonic frequency interference when they have the combination of a high-inductance drain coil, such as 125 mH, and a small line tuner series capacitance such as that of the high-frequency tuning capacitor. In addition to the aforementioned frequency response measurements, additional tests and measurements were performed to quantify some effects of harmonic frequency interference such as IMT saturation and its effect on impedance matching. The effects of IMT saturation were quantified by generating saturation curves for two types of IMTs at various frequencies spanning the harmonic frequency band. Then, using the IMT saturation curves, tests were performed to quantify the effect of IMT saturation on impedance matching using the percentage of reflected power as the quantifying measure.

The second research goal, that of developing computer models of the coupling systems, was also accomplished in two parts. First, detailed PSpice models of the coupling systems were developed and validated using measured data. The PSpice models were then simplified and revalidated using measured data. From the simplified PSpice models, state-space models of the coupling systems were developed for frequency re-

Reproduced with permission of the copyright owner. Further reproduction prohibited without permission.

sponse analysis. State-space modeling was chosen for frequency response analysis because of the versatility and generality of the state-space models. State-space modeling using a software package such as Matlab allowed for easy comparison of measured frequency response to calculated frequency response. Furthermore, batch processing could be used to compare variations in coupling system component values to analyze the effects of altering system component values. The models developed produced practically accurate and useful results, except in cases where the nonlinear IMT magnetizing reactance becomes a dominant reactance in the single-frequency and two-frequency resonant type coupling systems. The frequency response measurements indicated that the IMT magnetizing reactance becomes significant in the single-frequency and two-frequency coupling systems when the series capacitance of the line tuner is relatively large and when the IMT is terminated into high impedance such as a carrier receiver with an input impedance of several kilo-ohms. However, the frequency response measurements showed that, in these cases where the models lose accuracy, voltage gain remains relatively low, indicating that harmonic frequency interference would not likely be a problem in these particular cases.

The third goal, that of identifying the dominant coupling system components affecting frequency response in the harmonic frequency band, was accomplished through frequency response measurements, along with generalized analysis of the coupling systems; during this analysis, typical component values used with the systems were taken into consideration. The dominant coupling system components that can be altered to mitigate harmonic frequency interference were identified as being the drain coil inductance and the line tuner series capacitance. The analysis showed that decreasing drain coil inductance, increasing line tuner series capacitance, or using a combination of the two

Reproduced with permission of the copyright owner. Further reproduction prohibited without permission.

could mitigate harmonic frequency interference by reducing voltage gain and eliminating possible resonant conditions in the harmonic frequency band. The method of interference mitigation was validated by successful application on a 230-kV coupling system that was severely affected by harmonic frequency interference. Furthermore, application of the method of interference mitigation presented does not require that the transmission line be taken out of service.

Relating Harmonic Frequency Interference to Standard Harmonic Voltage Distortion Limits

Of particular interest was relating measured voltage levels from a coupling system affected by harmonic frequency interference to harmonic voltage distortion limits given in an industry standard for harmonic control in electric power systems (*IEEE Recommended Practices and Requirements for Harmonic Control in Electrical Power Systems*, 1992). The 230-kV coupling system discussed in the immediately preceding section and in chapter 1 will be used as an example. Using the voltage measurement and frequency spectrum from Figure 2 in conjunction with the measured frequency response plot from Figure 7, the phase-to-ground harmonic voltage level on the transmission line can be calculated as

$$V_{\text{Line}} = \frac{V_{\text{Drain}}}{10^{\frac{Gain(\text{dB})}{20}}}, \tag{52}$$

where V_{Line} is the phase-to-ground voltage on the transmission line and where V_{Drain} is the drain coil voltage.

Reproduced with permission of the copyright owner. Further reproduction prohibited without permission.

Figure 7 shows that the voltage gain at the drain coil for this 230-kV coupling system was approximately 12 dB. As the frequency spectrum of Figure 2 indicates, the drain coil voltage was composed primarily of 47th and 49th harmonics, with each being about 600 Vrms. Using Equation 52 with gain equal to 12 dB and drain coil voltage equal to 600 Vrms yields individual harmonic voltage levels for the 47th and 49th harmonics of approximately 150 Vrms phase to ground on the transmission line. A voltage level of 150 Vrms phase to ground equates to about 0.11% of the 230-kV system voltage, where the 230-kV system voltage is 132.79 kV phase to ground. The industry standard (*IEEE Recommended Practices and Requirements for Harmonic Control in Electrical Power Systems*, 1992) recommends an individual harmonic voltage distortion limit of 1.0% at 230 kV. Thus, although harmonic voltage distortion levels were far below the recommended limits, the 230-kV coupling system experienced severe problems.

Recommendations for Future Research in the Area of Harmonic Frequency Interference

The example of the immediately preceding section shows that PLC coupling systems are susceptible to harmonic frequency interference even when harmonic distortion levels are within standard specified limits. Therefore, a topic for future research in the area of harmonic frequency interference in PLC coupling systems would be that of improving the immunity of these systems to harmonic frequency interference using standard harmonic voltage distortion levels as a reference. In particular, narrowband resonant type coupling systems were shown to be most susceptible to harmonic frequency interference. Two predominant problems for these systems resulting from harmonic frequency interference are IMT saturation and excessive voltage levels imposed on carrier communica-

Reproduced with permission of the copyright owner. Further reproduction prohibited without permission.

tion equipment. Therefore, development of an optimization algorithm for these coupling systems that optimizes component values to meet a specified maximum voltage gain curve for the IMT in the harmonic frequency band would be useful in improving the immunity of these systems to harmonic frequency interference. The voltage gain constraints at the IMT should be based on IMT saturation data, as well as on voltage limitations of carrier communication equipment. Of course, the optimization of the system components must also meet the carrier frequency constraints of line tuning and impedance matching.

Another research topic of consideration is that of altering the configuration of resonant type coupling systems using existing components to produce a system less susceptible to harmonic frequency interference. Although other types of coupling systems, such as wideband coupling systems, are less susceptible to harmonic frequency interference, it would not necessarily be advantageous to simply convert a resonant type coupling system to a wideband system, particularly in the case of the two-frequency resonant coupling system. Wideband coupling systems require additional components such as hybrid isolation units to provide source isolation for the carrier transmitters. Thus, converting a narrowband resonant system to a wideband system would require additional components. However, the existing components of a narrowband resonant system could possibly be reconfigured to form a high-pass filter; in the case of the two-frequency system, the parallel trap circuits could still be used to provide source isolation.

Reproduced with permission of the copyright owner. Further reproduction prohibited without permission.

LIST OF REFERENCES

Crowley, M. A., & Parker, J. R. (1993, April). *The effect of customer generated noise upon power line carrier tuning*. Paper presented at the 47th annual Georgia Tech Protective Relaying Conference, Atlanta, GA.

Extech Instruments. (2003). *Passive component LCR meter model 380193 user's guide*. Waltham, MA: Author.

Fitzgerald, A. E., Kingsley, C., Jr., & Umans, S. D. (1990). Transformers. In *Electric machinery* (5th ed., pp. 50-94). New York: McGraw-Hill.

General Electric. (n.d.a). *Carrier current line tuning equipment type CL-2, Rev. A* (Instruction Book No. LBI-5579J). Lynchburg, VA: Author.

General Electric. (n.d.b). *Power line carrier line tuning equipment: Bandpass line tuners second order models* (Instruction Book No. LBI-37443A). Malvern, PA: Author.

General Electric. (n.d.c). *Power line carrier line tuning equipment: Resonant line tuner single frequency phase to ground* (Instruction Book No. LBI-19885B). Malvern, PA: Author.

General Electric. (n.d.d). *Power line carrier line tuning equipment: Resonant line tuner two frequency phase to ground* (Instruction Book No. LBI-19887B). Malvern, PA: Author.

Hayt, W. H., Jr. (1967). Transmission lines. In *Engineering electromagnetics* (2nd ed., pp. 365-394). New York: McGraw-Hill.

IEEE guide for power-line carrier applications (ANSI/IEEE 643-1980). (1980). New York: The Institute of Electrical and Electronics Engineers.

IEEE recommended practices and requirements for harmonic control in electrical power systems (IEEE 519-1992). (1992). New York: The Institute of Electrical and Electronics Engineers.

IEEE recommended practice for testing electronics transformers and inductors (IEEE 389-1996). (1996). New York: The Institute of Electrical and Electronics Engineers.

Reproduced with permission of the copyright owner. Further reproduction prohibited without permission.

Nise, N. S. (1992). System representation in the time domain. In *Control systems engineering* (pp. 111-148). Redwood City, CA: Benjamin/Cummings.

Podszeck, H.-K. (1972). *Carrier communication over power lines* (4th ed.). Berlin, Germany: Springer.

Power Line Carrier Practices Working Group (1995). Power line carrier practices and experiences. *IEEE Transactions on Power Delivery, 10*(2), 639-646.

Requirements for power-line carrier coupling capacitors and coupling capacitor voltage transformers (CCVT) (ANSI/NEMA C93.1-1999). (1999). Rosslyn, VA: National Electrical Manufacturers Association.

RFL Electronics. (2003). *Reflected power meter* (No. RFL RPM) [Brochure]. Boonton Township, NJ: Author.

Sanders, M. P., & Ray, R. E. (n.d.). *Power line carrier channel and application considerations for transmission line relaying* (Pulsar Document No. C045-P0597, p. 17). Coral Springs, FL: Pulsar Technologies.

Signalcrafters Tech. (n.d.). *Model 70 computing power/SWR meter owners manual*. East Hanover, NJ: Author.

Tatro, P. J., Adamson, K. A., Eitzmann, M. A., & Smead, M. (1993). Power line carrier interference from HVDC converter terminals. *IEEE Transactions on Power Delivery, 8*(3), 827-840.

Temes, L. (1979). Tuned circuits. In *Schaum's outline of theory and problems of electronic communication* (pp. 59-83). New York: McGraw-Hill.

Trench Limited. (n.d.). *Power line carrier line tuning equipment: Bandpass line tuners second order models* (Instruction Book No. GEK-90622B). Scarborough, Ontario, Canada: Author.

Vermeulen, H. J., Dann, L. R., & van Rooijen, J. (1995). Equivalent circuit modeling of a capacitive voltage transformer for power system harmonic frequencies. *IEEE Transactions on Power Delivery, 10*(4), 1743-1749.

Westinghouse Electric. (1967). *Instructions for coupling capacitor potential device type PCA-5* (Instruction Book No. 39-621-1). Bloomington, IN: Author.

Wolf, S., & Smith, R. (1990). Measurement of capacitance, inductance, and impedance. In *Student reference manual for electronic instrumentation laboratories* (pp. 296-332). Englewood Cliffs, NJ: Prentice-Hall.

Reproduced with permission of the copyright owner. Further reproduction prohibited without permission.

APPENDIX A

COUPLING SYSTEM TEST DATA

Reproduced with permission of the copyright owner. Further reproduction prohibited without permission.

Drain Coil Test Data

The purpose of the drain coil tests was to determine the frequency dependent resistance of each coil. As described in Chapter 2, the tests consisted of forming series LC resonant circuits using each drain coil and various capacitors to achieve resonance at various frequencies in the harmonic frequency band. A circuit was deemed resonant when maximum voltage was measured across the drain coil. At each resonant frequency, the 3 dB bandwidth of the voltage across the drain coil was measured. Using the 3 dB bandwidth of the drain coil voltage and the measured drain coil inductance, the resistance was calculated using Equation 1 from Chapter 2. For each drain coil, the resistance at 0 Hz and 1000 Hz was measured directly with a LCR meter. The inductance of each drain coil was also measured with the LCR meter using a test frequency of 1000 Hz. The test data for the 10 mH , 25 mH, and 125 mH drain coils is provided in Tables A1, A2, and A3, respectively.

Table A1

10-mH Drain Coil Test Data

Capacitance (μF)	Measured resonant frequency (Hz)	Voltage applied (Vrms)	Voltage across capacitor (Vrms)	Voltage across drain coil (Vrms)	3-dB bandwidth (Hz)	Resistance (Ω)
*	0	*	*	*	*	4.40
*	1000	*	*	*	*	8.63
0.3262	2583	5	63.3	63.6	206	15.57
0.0826	5142	10	142.0	140.8	378	28.57
0.0321	8325	10	132.1	132.8	633	47.85
0.0204	10464	10	120.9	121.1	871	65.84
0.0102	14835	10	103.0	103.0	1436	108.54

Note: The measured inductance of the 10-mH drain coil was 12.03 mH.
* indicates data not applicable.

Reproduced with permission of the copyright owner. Further reproduction prohibited without permission.

Table A2

25-mH Drain Coil Test Data

Capacitance (μF)	Measured resonant frequency (Hz)	Voltage applied (Vrms)	Voltage across capacitor (Vrms)	Voltage across drain coil (Vrms)	3-dB bandwidth (Hz)	Resistance (Ω)
*	0	*	*	*	*	8.30
*	1000	*	*	*	*	11.00
0.1524	2607	5	99.4	99.5	132	20.43
0.0460	4764	5	104.8	104.5	229	35.44
0.0204	7165	5	99.8	99.3	358	55.40
0.0102	10150	5	89.0	88.4	564	87.28

Note: The measured inductance of the 25-mH drain coil was 24.63 mH.
* indicates data not applicable.

Table A3

125-mH Drain Coil Test Data

Capacitance (μF)	Measured resonant frequency (Hz)	Voltage applied (Vrms)	Voltage across capacitor (Vrms)	Voltage across drain coil (Vrms)	3-dB bandwidth (Hz)	Resistance (Ω)
*	0	*	*	*	*	38.00
*	1000	*	*	*	*	48.00
0.0321	2522	5	138.6	138.4	89	69.40
0.0069	5453	5	208.7	207.9	130	101.37

Note: The measured inductance of the 125-mH drain coil was 124.1 mH.
* indicates data not applicable.

Data from Test to Determine Effect of Harmonic Frequency Interference on Impedance Matching at Carrier Frequencies

Described in Chapter 2, a test was devised to measure reflected power at carrier frequencies in the presence of harmonic frequency interference. The measurements from the test are presented in Table A4, and the test circuit is shown in Figure 14 of Chapter 2.

Reproduced with permission of the copyright owner. Further reproduction prohibited without permission.

Table A4

Measurements from Test to Determine Effect of Harmonic Frequency Interference on Impedance Matching at Carrier Frequencies

IMT core type	Harm. freq. (kHz)	V_{cgen} at f_c (V_{rms})	V_{cgen} at f_h (V_{rms})	V_{cab} at f_c (V_{rms})	V_{cab} at f_h (V_{rms})	V_{line} at f_c (V_{rms})	V_{line} at f_h (V_{rms})	V_{hgen} at f_c (V_{rms})	V_{hgen} at f_h (V_{rms})	V_{inc} at f_c (V_{rms})	V_{ref} at f_c (V_{rms})	RP_C (%)	RP_M (%)
Toroid	0.6	9.7	0.001	11.6	2.0	25.1	5.8	0.09	5.8	9.80	0.15	0.0	0.0
Toroid	0.6	9.7	0.001	11.2	3.0	25.2	8.8	0.09	8.8	9.90	0.51	0.3	0.1
Toroid	0.6	9.4	0.002	11.2	4.5	25.1	13.1	0.09	13.3	10.20	0.84	0.7	1.5
Toroid	0.6	6.9	0.004	11.6	5.1	21.0	16.1	0.07	16.8	11.60	4.21	13.2	45.0
Toroid	1.0	9.6	0.004	11.1	5.0	25.1	14.3	0.10	14.4	9.80	0.52	0.3	0.0
Toroid	1.0	9.4	0.005	11.2	6.9	25.2	20.1	0.10	20.2	10.10	0.77	0.6	0.5
Toroid	1.0	9.1	0.006	11.4	7.8	25.4	22.9	0.10	23.2	10.30	1.17	1.3	4.0
Toroid	1.0	8.4	0.007	11.8	8.4	25.0	25.4	0.11	25.8	10.90	2.50	5.3	33.0
Toroid	3.0	9.7	0.025	11.1	13.7	24.8	39.5	0.10	39.6	9.80	0.54	0.3	0.0
Toroid	3.0	9.6	0.043	11.1	15.6	24.9	45.1	0.10	45.3	9.90	0.53	0.3	0.1
Toroid	3.0	9.5	0.053	11.1	19.4	25.1	56.4	0.10	56.6	10.00	0.63	0.4	0.5
Toroid	3.0	7.6	0.073	11.2	25.3	23.1	75.8	0.08	78.1	11.60	3.85	11.1	21.0
Pot	0.6	9.4	0.003	9.2	6.8	25.3	18.9	0.13	18.9	9.82	0.35	0.1	0.0
Pot	0.6	9.5	0.003	9.3	7.9	25.4	21.7	0.13	21.8	9.79	0.35	0.1	0.0
Pot	0.6	9.4	0.004	9.3	10.7	25.2	29.4	0.13	29.6	9.77	0.55	0.3	1.0
Pot	0.6	9.2	0.004	9.0	11.6	24.4	32.0	0.13	32.3	9.74	1.21	1.5	9.0
Pot	1.0	9.5	0.009	9.3	11.8	25.5	32.4	0.13	32.6	9.77	0.31	0.1	0.0
Pot	1.0	9.5	0.010	9.4	13.6	25.5	37.5	0.12	37.6	9.76	0.31	0.1	0.0
Pot	1.0	9.5	0.013	9.3	17.5	25.3	48.4	0.13	48.5	9.77	0.40	0.2	0.5
Pot	1.0	9.2	0.015	9.0	19.4	24.6	53.4	0.12	53.9	9.63	1.18	1.5	8.0

Note: For all tests, the carrier frequency was set at 200 kHz. Descriptions of the table column headings are as follows:

- f_c designates carrier frequency,
- f_h designates harmonic frequency,
- V_{cgen} designates voltage at the terminals of the carrier frequency generator,
- V_{hgen} designates voltage at the terminals of the harmonic frequency generator,
- V_{cab} designates voltage at the low impedance terminals of the IMT,
- V_{line} designates voltage at the high impedance terminals of the IMT,
- V_{inc} designates incident voltage measured from the directional coupler,
- V_{ref} designates reflected voltage measured from the directional coupler,
- RP_C designates reflected power calculated from the incident and reflected voltage measurements, and
- RP_M designates reflected power measured by the reflectometer.
- IMT designates impedance-matching transformer.

Reproduced with permission of the copyright owner. Further reproduction prohibited without permission.

Peak Voltage Gain Test Data

The equivalent circuit for the single-frequency system showing the component values used for the peak voltage gain tests is shown in Figure A1. The measurements taken during the test are provided in Table A5.

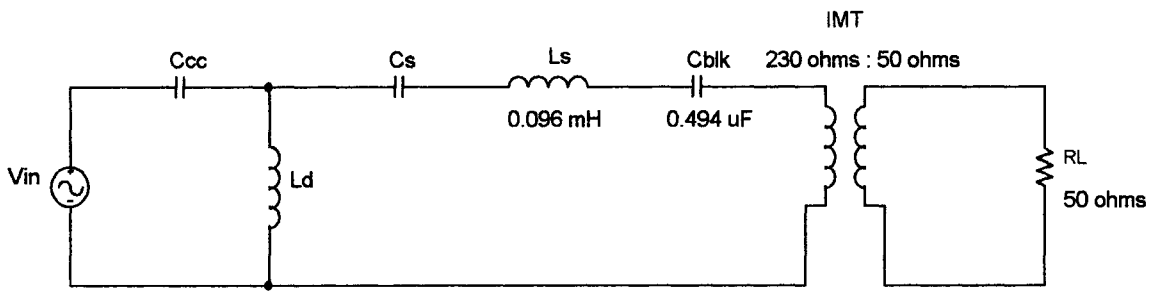

Figure A1. Equivalent circuit for the single-frequency system showing the component values used for the peak voltage gain tests.

Table A5

Measurements from Single-frequency Coupling System Peak Voltage Gain Tests

C_{CC} (μF)	C_S (μF)	L_d (mH)	Frequency of peak gain (Hz)	V_{in} (V_{rms})	V_{CC} (V_{rms})	V_{Ld} (V_{rms})	V_{IMThi} (V_{rms})	V_{IMTlo} (V_{rms})
0.006850	0.0102	12.03	11298	10	24.84	22.61	3.904	1.699
0.006850	0.0102	24.63	7757	10	40.32	38.73	4.230	1.844
0.006850	0.0102	124.10	3456	10	95.30	94.50	3.365	1.472
0.003458	0.0102	12.03	12565	10	15.26	11.20	2.200	0.953
0.003458	0.0102	24.63	8622	10	22.18	19.30	2.403	1.046
0.003458	0.0102	124.10	3852	10	54.80	53.40	2.168	0.946
0.001717	0.0102	12.03	13380	10	11.68	5.43	1.157	0.496
0.001717	0.0102	24.63	9190	10	14.20	9.40	1.269	0.549
0.001717	0.0102	124.10	4114	10	30.24	27.93	1.224	0.532
0.006850	*	12.03	1617	2	2.00	0.06	0.035	0.015
0.006850	*	24.63	1252	2	2.01	0.14	0.043	0.019
0.006850	*	124.10	618	2	1.99	0.24	0.016	0.007
0.003458	*	12.03	1619	2	1.99	0.03	0.018	0.008
0.003458	*	24.63	1258	2	2.00	0.07	0.022	0.010
0.003458	*	124.10	620	2	1.99	0.12	0.009	0.004
0.001717	*	12.03	1625	2	1.99	0.02	0.009	0.004
0.001717	*	24.63	1257	2	1.99	0.04	0.011	0.005
0.001717	*	124.10	621	2	2.01	0.06	0.005	0.002

* indicates that C_S was disabled.

Reproduced with permission of the copyright owner. Further reproduction prohibited without permission.

The equivalent circuit for the second-order wideband system showing the component values used for the peak voltage gain tests is shown in Figure A2. The measurements taken during the test are provided in Table A6.

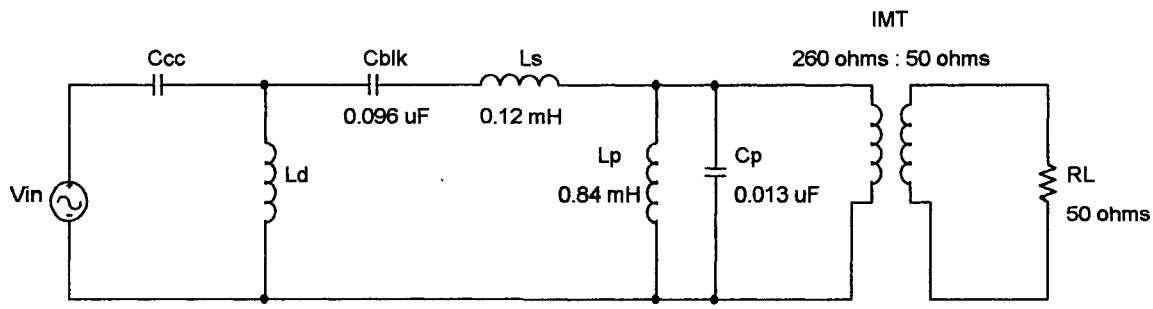

Figure A2. Equivalent circuit for the second-order wideband system showing the component values used for the peak voltage gain tests.

Table A6

Measurements from Second-Order Wideband Coupling System Peak Voltage Gain Tests

C_{CC} (μF)	L_d (mH)	Frequency of peak voltage gain (Hz)	V_{in} (V_{rms})	V_{CC} (V_{rms})	V_{Ld} (V_{rms})	V_{IMThi} (V_{rms})	V_{IMTlo} (V_{rms})
0.006850	12.03	4460	10	10.06	7.48	0.49	0.21
0.006850	24.63	3109	10	14.59	11.12	0.34	0.15
0.006850	124.10	1398	4	5.91	4.65	0.03	0.01
0.003458	12.03	4525	10	10.61	3.86	0.26	0.11
0.003458	24.63	3161	10	11.71	5.93	0.19	0.08
0.003458	124.10	1421	4	4.61	2.43	0.02	0.01
0.001717	12.03	4566	10	10.14	1.96	0.13	0.06
0.001717	24.63	3196	10	10.42	3.01	0.10	0.04
0.001717	124.10	1435	4	4.09	1.24	0.01	0.00

Reproduced with permission of the copyright owner. Further reproduction prohibited without permission.

The equivalent circuit for the two-frequency system showing the component values used for the peak voltage gain tests is shown in Figure A3. The measurements taken during the test are provided in Table A7.

Table A7

Measurements from Two-frequency Coupling System Peak Voltage Gain Tests

C_{CC} (μF)	C_{S2} (μF)	L_d (mH)	Frequency of peak voltage gain (Hz)	V_{in} (V_{rms})	V_{CC} (V_{rms})	V_{Ld} (V_{rms})	V_{IMT1hi} (V_{rms})	V_{IMT1lo} (V_{rms})	V_{IMT2hi} (V_{rms})	V_{IMT2lo} (V_{rms})
0.006850	0.01	12.03	8696	10	19.57	16.57	1.579	0.732	2.169	0.940
0.006850	0.01	24.63	6050	10	31.90	29.80	1.598	0.742	2.377	1.034
0.006850	0.01	124.10	2722	10	66.60	65.70	0.859	0.399	1.514	0.661
0.003458	0.01	12.03	9212	10	13.25	8.35	0.854	0.392	1.184	0.510
0.003458	0.01	24.63	6429	10	18.95	15.52	0.882	0.407	1.344	0.582
0.003458	0.01	124.10	2903	10	38.80	37.20	0.506	0.233	0.925	0.403
0.001717	0.01	12.03	9500	10	11.08	4.13	0.435	0.202	0.613	0.265
0.001717	0.01	24.63	6653	10	13.10	7.83	0.455	0.210	0.708	0.306
0.001717	0.01	124.10	3013	10	22.60	19.90	0.271	0.126	0.517	0.223
0.006850	**	12.03	1566	2	1.99	0.05	*	*	0.032	0.014
0.006850	**	24.63	1223	2	2.01	0.13	*	*	0.039	0.017
0.006850	**	124.10	610	2	1.99	0.23	*	*	0.015	0.007
0.003458	**	12.03	1562	2	2.00	0.03	*	*	0.016	0.007
0.003458	**	24.63	1229	2	2.00	0.07	*	*	0.020	0.009
0.003458	**	124.10	611	2	1.99	0.12	*	*	0.008	0.004
0.001717	**	12.03	1563	2	2.00	0.01	*	*	0.008	0.004
0.001717	**	24.63	1228	2	2.00	0.03	*	*	0.010	0.005
0.001717	**	124.10	612	2	1.98	0.06	*	*	0.004	0.002

* indicates no measurement taken.
** indicates that C_{S2} was disabled.

Frequency Response Measurement Data

The measurements taken during the single-frequency system test are provided in Tables A8, A9, A10, and A11. The equivalent circuit for the single-frequency system showing the component values used for the frequency response tests is shown in Figure A4.

Reproduced with permission of the copyright owner. Further reproduction prohibited without permission.

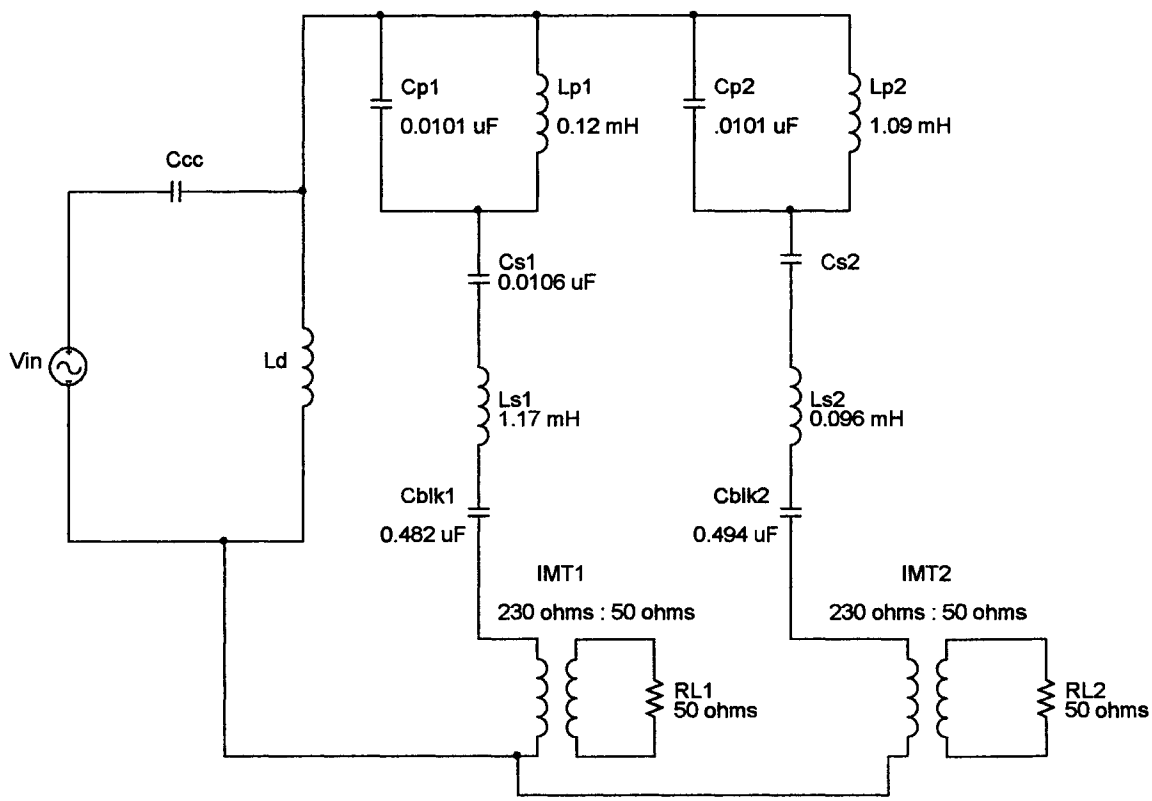

Figure A3. Equivalent circuit for the two-frequency system showing the component values used for the peak voltage gain tests.

Reproduced with permission of the copyright owner. Further reproduction prohibited without permission.

Table A8

Measurements from Single-frequency Coupling System Frequency Response Test with C_S = 0.0102 μF and RL = 2000 Ω

Frequency (Hz)	V_{in} (V_{rms})	V_{Ld} (V_{rms})	V_{IMThi} (V_{rms})
600	10.2000	0.1418	0.1706
800	10.2400	0.4390	0.5800
1000	10.2700	0.5140	0.4400
1200	10.3000	0.3440	0.1679
1400	10.3400	0.4090	0.0783
1600	10.3600	0.5440	0.0815
1800	10.3800	0.7250	0.1036
2000	10.3900	0.9590	0.1365
2200	10.4000	1.2510	0.1421
2400	10.4100	1.6390	0.1344
2600	10.4100	2.1660	0.1721
2800	10.4200	2.9130	0.2650
3000	10.4200	4.0300	0.3410
3200	10.4300	5.8900	0.4730
3400	10.4400	9.5400	0.6430
3600	10.4400	20.0300	0.9770
3800	10.4200	62.2000	4.6200
4000	10.4400	23.2300	1.7280
4200	10.4500	13.0800	1.0060
4400	10.4600	9.3900	0.8080
4600	10.4800	7.5100	0.7320
4800	10.4900	6.3500	0.6970
5000	10.5000	5.6100	0.7080
5200	10.5100	5.1600	0.7670
5400	10.5300	4.6800	0.8440
5600	10.5500	4.3500	0.9460
5800	10.5600	4.1700	1.0700
6000	10.5900	3.9600	1.1310
6200	10.6200	3.7400	1.0960
6400	10.6400	3.5900	0.9880
6600	10.6600	3.4500	0.8890
6800	10.6800	3.3030	0.8140
7000	10.7000	3.1910	0.7950
7200	10.7300	3.0880	0.7860
7400	10.7500	2.9970	0.8040
7600	10.7800	2.9180	0.8430
7800	10.8000	2.8420	0.8990
8000	10.8200	2.7800	0.9700
8200	10.8500	2.7210	1.0460
8400	10.8700	2.6720	1.1660
8600	10.8900	2.6330	1.3190
8800	10.9200	2.6090	1.4970
9000	10.9400	2.6010	1.7530
9200	10.9600	2.6180	2.0140
9400	10.9800	2.6670	2.3360
9600	11.0100	2.7550	2.6560
9800	11.0300	2.8850	2.9960
10000	11.0600	3.0540	3.2300

Reproduced with permission of the copyright owner. Further reproduction prohibited without permission.

Table A9

Measurements from Single-frequency Coupling System Frequency Response Test with C_S = 0.0102 μF and RL = 50 Ω

Frequency (Hz)	V_{in} (V_{rms})	V_{Ld} (V_{rms})	V_{IMThi} (V_{rms})
600	10.2000	0.0963	0.0227
800	10.2500	0.2460	0.0268
1000	10.2900	0.2060	0.0302
1200	10.3100	0.2920	0.0246
1400	10.3400	0.4010	0.0170
1600	10.3600	0.5380	0.0149
1800	10.3800	0.7230	0.0161
2000	10.3900	0.9550	0.0187
2200	10.4000	1.2410	0.0237
2400	10.4100	1.6250	0.0313
2600	10.4100	2.1530	0.0445
2800	10.4200	2.8940	0.0660
3000	10.4200	3.9700	0.1009
3200	10.4300	5.7600	0.1611
3400	10.4300	9.0700	0.2790
3600	10.4500	17.5800	0.5700
3800	10.4400	46.0000	1.7570
4000	10.4300	26.4100	1.3200
4200	10.4500	14.4300	0.7200
4400	10.4600	10.2300	0.5400
4600	10.4700	8.1400	0.4540
4800	10.4800	6.9000	0.4100
5000	10.4900	6.1000	0.3870
5200	10.5100	5.5400	0.3680
5400	10.5300	5.0600	0.3560
5600	10.5500	4.7300	0.3470
5800	10.5700	4.5200	0.3430
6000	10.5900	4.2800	0.3430
6200	10.6200	4.0600	0.3443
6400	10.6400	3.9100	0.3473
6600	10.6600	3.7900	0.3513
6800	10.6800	3.6800	0.3563
7000	10.7100	3.5900	0.3617
7200	10.7300	3.5100	0.3678
7400	10.7500	3.4480	0.3750
7600	10.7700	3.3880	0.3821
7800	10.8000	3.3340	0.3897
8000	10.8200	3.2850	0.3969
8200	10.8400	3.2410	0.4059
8400	10.8700	3.2030	0.4147
8600	10.8900	3.1650	0.4240
8800	10.9100	3.1330	0.4320
9000	10.9300	3.1020	0.4420
9200	10.9500	3.0760	0.4520
9400	10.9800	3.0520	0.4620
9600	11.0000	3.0310	0.4720
9800	11.0300	3.0100	0.4820
10000	11.0600	2.9920	0.4920

Reproduced with permission of the copyright owner. Further reproduction prohibited without permission.

Table A10

Measurements from Single-frequency Coupling System Frequency Response Test with C_S Disabled and RL = 2000 Ω

Frequency (Hz)	V_{in} (V_{rms})	V_{Ld} (V_{rms})	V_{IMThi} (V_{rms})
600	10.2000	0.4900	0.2570
800	10.2500	0.9650	0.7900
1000	10.2800	0.3890	0.3330
1200	10.3100	0.1801	0.1473
1400	10.3300	0.1047	0.0907
1600	10.3600	0.1162	0.0998
1800	10.3800	0.1645	0.1638
2000	10.3900	0.1930	0.1830
2200	10.4000	0.2040	0.1827
2400	10.4100	0.1664	0.1788
2600	10.4100	0.2500	0.2520
2800	10.4200	0.3970	0.3880
3000	10.4200	0.6470	0.6210
3200	10.4300	0.6900	0.5940
3400	10.4300	0.5390	0.4910
3600	10.4400	0.4970	0.4780
3800	10.4400	0.5270	0.5340
4000	10.4500	0.5420	0.5400
4200	10.4600	0.5300	0.5280
4400	10.4700	0.5670	0.5700
4600	10.4800	0.6430	0.6580
4800	10.5000	0.7740	0.7930
5000	10.5100	0.9610	0.9890
5200	10.5200	1.2080	1.2350
5400	10.5400	1.4530	1.4160
5600	10.5600	1.5090	1.3490
5800	10.5800	1.3120	1.1280
6000	10.6000	1.0720	0.9330
6200	10.6300	0.8980	0.7970
6400	10.6500	0.7980	0.7370
6600	10.6700	0.7540	0.7110
6800	10.6900	0.7490	0.7190
7000	10.7100	0.7720	0.7510
7200	10.7400	0.8280	0.8060
7400	10.7600	0.9090	0.8840
7600	10.7900	1.0300	1.0030
7800	10.8100	1.1830	1.1610
8000	10.8300	1.3960	1.3590
8200	10.8600	1.6580	1.6400
8400	10.8800	1.9480	1.9660
8600	10.9000	2.4400	2.3840
8800	10.9300	2.9010	2.7620
9000	10.9500	3.3500	3.0800
9200	10.9600	3.6800	3.2300
9400	11.0000	3.7700	3.1900
9600	11.0200	3.6400	3.0500
9800	11.0400	3.4600	2.8900
10000	11.0700	3.2600	2.7700

Reproduced with permission of the copyright owner. Further reproduction prohibited without permission.

Table A11

Measurements from Single-frequency Coupling System Frequency Response Test with C_S Disabled and RL = 50 Ω

Frequency (Hz)	V_{in} (V_{rms})	V_{Ld} (V_{rms})	V_{IMThi} (V_{rms})
600	10.2000	0.3910	0.0397
800	10.2500	0.1485	0.0365
1000	10.2700	0.1095	0.0444
1200	10.3100	0.0873	0.0393
1400	10.3200	0.0690	0.0346
1600	10.3400	0.0581	0.0375
1800	10.3700	0.0505	0.0427
2000	10.3900	0.0438	0.0487
2200	10.4000	0.0414	0.0573
2400	10.4000	0.0413	0.0652
2600	10.4100	0.0487	0.0751
2800	10.4100	0.0584	0.0862
3000	10.4200	0.0714	0.0973
3200	10.4300	0.0832	0.1082
3400	10.4300	0.0943	0.1195
3600	10.4400	0.1109	0.1305
3800	10.4400	0.1217	0.1420
4000	10.4500	0.1318	0.1527
4200	10.4600	0.1445	0.1635
4400	10.4700	0.1565	0.1745
4600	10.4800	0.1660	0.1851
4800	10.4900	0.1783	0.1965
5000	10.5000	0.1931	0.2088
5200	10.5200	0.2069	0.2215
5400	10.5400	0.2211	0.2336
5600	10.5500	0.2361	0.2459
5800	10.5800	0.2513	0.2590
6000	10.5900	0.2666	0.2722
6200	10.6200	0.2808	0.2849
6400	10.6400	0.2964	0.2985
6600	10.6700	0.3124	0.3119
6800	10.6900	0.3280	0.3254
7000	10.7100	0.3430	0.3394
7200	10.7200	0.3520	0.3532
7400	10.7600	0.3780	0.3673
7600	10.7800	0.3950	0.3820
7800	10.8100	0.4130	0.3960
8000	10.8300	0.4310	0.4090
8200	10.8500	0.4460	0.4260
8400	10.8800	0.4670	0.4410
8600	10.9000	0.4870	0.4560
8800	10.9200	0.5070	0.4680
9000	10.9500	0.5260	0.4820
9200	10.9600	0.5470	0.5040
9400	10.9900	0.5660	0.5190
9600	11.0200	0.5880	0.5370
9800	11.0400	0.6080	0.5520
10000	11.0500	0.6140	0.5680

Reproduced with permission of the copyright owner. Further reproduction prohibited without permission.

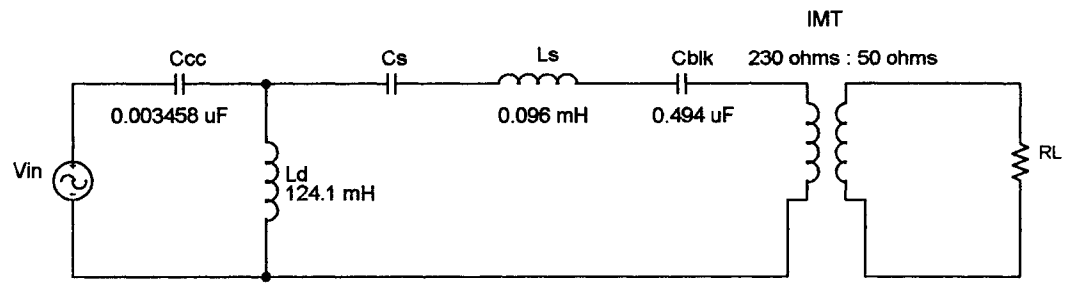

Figure A4. Equivalent circuit for the single-frequency system showing the component values used for the frequency response tests.

The equivalent circuit for the second-order wideband system showing the component values used for the frequency response tests is shown in Figure A5. The measurements taken during the second-order wideband system test are provided in Tables A12 and A13.

The equivalent circuit for the two-frequency system showing the component values used for the frequency response tests is shown in Figure A6. The measurements taken during the two-frequency system test are provided in Tables A14 and A15.

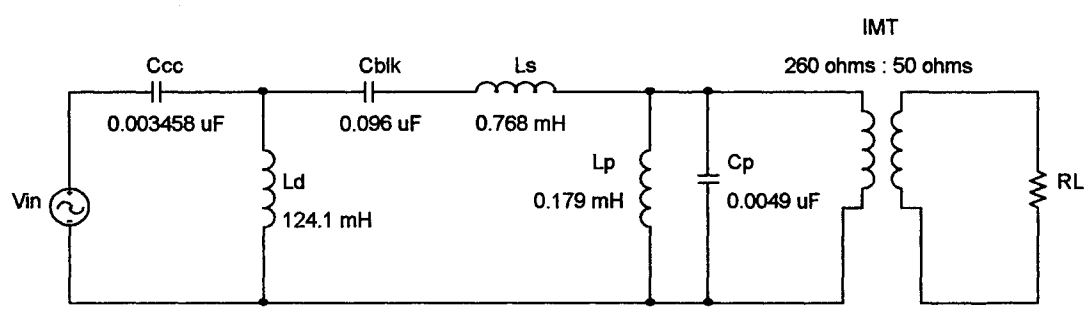

Figure A5. Equivalent circuit for the second-order wideband system showing the component values used for the frequency response tests.

Reproduced with permission of the copyright owner. Further reproduction prohibited without permission.

Table A12

Measurements from Second-Order Wideband Coupling System Frequency Response Test with RL = 2000 Ω

Frequency (Hz)	V_{in} (V_{rms})	V_{Ld} (V_{rms})	V_{IMThi} (V_{rms})
600	10.1900	0.0838	0.0118
800	10.2400	0.1663	0.0121
1000	10.2600	0.3347	0.0116
1200	10.3000	0.8040	0.0135
1400	10.3300	4.4100	0.0117
1600	10.3500	1.8470	0.0119
1800	10.3600	1.0090	0.0113
2000	10.3700	0.7500	0.0112
2200	10.3800	0.6340	0.0117
2400	10.3900	0.5650	0.0151
2600	10.4000	0.5200	0.0126
2800	10.4000	0.4860	0.0117
3000	10.4100	0.4760	0.0115
3200	10.4100	0.4450	0.0118
3400	10.4100	0.4360	0.0120
3600	10.4200	0.4230	0.0124
3800	10.4200	0.4110	0.0127
4000	10.4300	0.4020	0.0129
4200	10.4400	0.3920	0.0131
4400	10.4500	0.3860	0.0134
4600	10.4500	0.3820	0.0135
4800	10.4600	0.3770	0.0136
5000	10.4700	0.3720	0.0138
5200	10.4800	0.3680	0.0146
5400	10.5000	0.3630	0.0148
5600	10.5100	0.3590	0.0157
5800	10.5400	0.3550	0.0160
6000	10.5700	0.3500	0.0162
6200	10.5800	0.3450	0.0166
6400	10.6000	0.3430	0.0179
6600	10.6300	0.3390	0.0191
6800	10.6500	0.3350	0.0183
7000	10.6700	0.3310	0.0187
7200	10.6900	0.3270	0.0192
7400	10.7200	0.3220	0.0201
7600	10.7400	0.3187	0.0209
7800	10.7600	0.3152	0.0225
8000	10.7700	0.3114	0.0235
8200	10.8100	0.3085	0.0239
8400	10.8300	0.3048	0.0247
8600	10.8500	0.3004	0.0259
8800	10.8700	0.2959	0.0271
9000	10.8900	0.2918	0.0281
9200	10.9100	0.2882	0.0300
9400	10.9300	0.2859	0.0319
9600	10.9500	0.2827	0.0343
9800	10.9800	0.2783	0.0369
10000	11.0000	0.2751	0.0369

Reproduced with permission of the copyright owner. Further reproduction prohibited without permission.

Table A13

Measurements from Second-Order Wideband Coupling System Frequency Response Test with RL = 50 Ω

Frequency (Hz)	V_{in} (V_{rms})	V_{Ld} (V_{rms})	V_{IMThi} (V_{rms})
600	10.2000	0.0805	0.0055
800	10.2300	0.1632	0.0057
1000	10.2900	0.3338	0.0074
1200	10.3100	0.8000	0.0070
1400	10.3400	4.3700	0.0071
1600	10.3600	1.8870	0.0073
1800	10.3700	1.0210	0.0066
2000	10.3900	0.7560	0.0063
2200	10.3900	0.6320	0.0065
2400	10.3900	0.5620	0.0069
2600	10.4000	0.5160	0.0070
2800	10.4000	0.4850	0.0067
3000	10.4000	0.4740	0.0070
3200	10.4100	0.4450	0.0072
3400	10.4100	0.4340	0.0075
3600	10.4100	0.4230	0.0080
3800	10.4200	0.4130	0.0087
4000	10.4300	0.4040	0.0091
4200	10.4300	0.3960	0.0092
4400	10.4400	0.3890	0.0095
4600	10.4500	0.3810	0.0098
4800	10.4600	0.3770	0.0098
5000	10.4700	0.3710	0.0101
5200	10.4900	0.3650	0.0106
5400	10.5000	0.3620	0.0111
5600	10.5200	0.3570	0.0116
5800	10.5300	0.3540	0.0121
6000	10.5500	0.3510	0.0130
6200	10.5800	0.3450	0.0132
6400	10.6000	0.3410	0.0139
6600	10.6200	0.3380	0.0145
6800	10.6400	0.3350	0.0151
7000	10.6700	0.3300	0.0155
7200	10.6900	0.3270	0.0164
7400	10.7100	0.3223	0.0170
7600	10.7300	0.3189	0.0179
7800	10.7500	0.3150	0.0186
8000	10.7700	0.3115	0.0196
8200	10.8000	0.3080	0.0207
8400	10.8200	0.3033	0.0217
8600	10.8500	0.2994	0.0229
8800	10.8500	0.2951	0.0242
9000	10.8800	0.2916	0.0256
9200	10.9000	0.2879	0.0269
9400	10.9200	0.2846	0.0284
9600	10.9400	0.2808	0.0299
9800	10.9700	0.2776	0.0315
10000	10.9900	0.2742	0.0331

Reproduced with permission of the copyright owner. Further reproduction prohibited without permission.

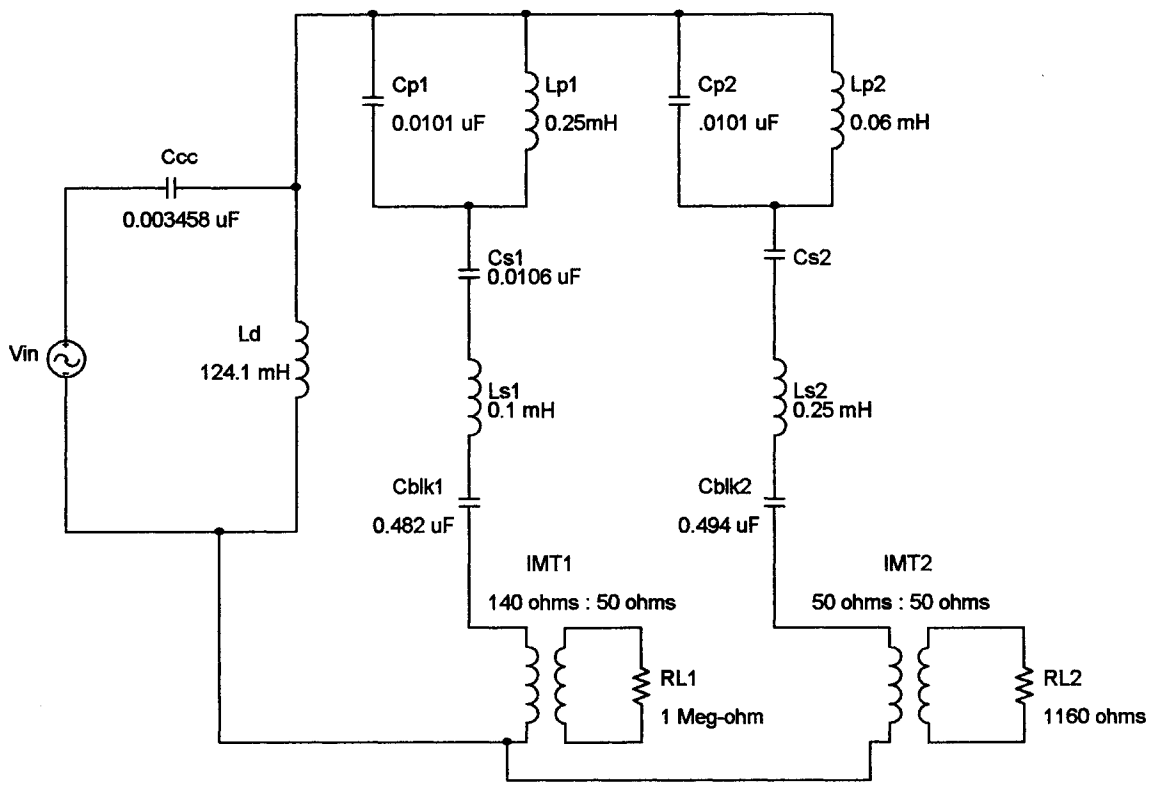

Figure A6. Equivalent circuit for the two-frequency system showing the component values used for the frequency response tests.

Reproduced with permission of the copyright owner. Further reproduction prohibited without permission.

Table A14

Measurements from Two-frequency Coupling System Frequency Response Test with C_{S2} = 0.01 μF

Frequency (Hz)	V_{in} (V_{rms})	V_{Ld} (V_{rms})	V_{IMT1hi} (V_{rms})	V_{IMT2hi} (V_{rms})
600	20.4000	0.2134	0.0081	0.0096
800	20.4800	0.2428	0.0113	0.0107
1000	20.5400	0.3960	0.0158	0.0148
1200	20.5800	0.6030	0.0205	0.0199
1400	20.6000	0.8830	0.0245	0.0257
1600	20.6200	1.2650	0.0307	0.0360
1800	20.6300	1.7980	0.0261	0.0449
2000	20.6300	2.5910	0.0322	0.0589
2200	20.6200	3.8300	0.0412	0.0769
2400	20.6200	6.0600	0.0561	0.1063
2600	20.6200	11.0000	0.0924	0.1747
2800	20.6200	30.1700	0.2382	0.4190
2950	20.5800	69.0000	0.9000	1.0720
3000	20.5900	46.3000	0.5710	0.7040
3200	20.6100	17.2300	0.2184	0.2401
3400	20.6100	11.0800	0.1576	0.1552
3600	20.6000	8.5100	0.1286	0.1225
3800	20.6100	7.1300	0.1191	0.1045
4000	20.6100	6.2600	0.1215	0.0930
4200	20.6100	5.6100	0.1292	0.0886
4400	20.6100	5.1800	0.1303	0.0879
4600	20.6200	4.8800	0.1280	0.0850
4800	20.6300	4.6100	0.1308	0.0955
5000	20.6400	4.4000	0.1365	0.1063
5200	20.6500	4.2500	0.1448	0.1146
5400	20.6700	4.0900	0.1565	0.1237
5600	20.6900	3.9500	0.1689	0.1444
5800	20.7100	3.8500	0.1783	0.1715
6000	20.7300	3.7700	0.1821	0.1507
6200	20.7400	3.6800	0.1838	0.1278
6400	20.7400	3.6100	0.1892	0.1302
6600	20.7500	3.5500	0.1992	0.1215
6800	20.7600	3.4990	0.2116	0.1251
7000	20.7900	3.4510	0.2277	0.1180
7200	20.8100	3.4060	0.2446	0.1230
7400	20.8400	3.3670	0.2656	0.1419
7600	20.8900	3.3340	0.2833	0.1591
7800	20.9500	3.3080	0.3035	0.1747
8000	21.0300	3.2830	0.3170	0.1872
8200	21.1000	3.2630	0.3360	0.1808
8400	21.1700	3.2430	0.3440	0.1534
8600	21.2200	3.2230	0.3540	0.1442
8800	21.3000	3.2060	0.3670	0.1495
9000	21.3600	3.1890	0.3790	0.1613
9200	21.4500	3.1750	0.3870	0.1737
9400	21.5100	3.1620	0.3910	0.1893
9600	21.6000	3.1490	0.3950	0.2055
9800	21.6800	3.1370	0.3900	0.2181
10000	21.7600	3.1270	0.3890	0.2262

Reproduced with permission of the copyright owner. Further reproduction prohibited without permission.

Table A15

Measurements from Two-frequency Coupling System Frequency Response Test with C_{S2} Disabled

Frequency (Hz)	V_{in} (V_{rms})	V_{Ld} (V_{rms})	V_{IMT1hi} (V_{rms})	V_{IMT2hi} (V_{rms})
600	20.3900	0.7910	0.2189	0.7890
800	20.4700	0.3400	0.1326	0.3450
1000	20.5200	0.2304	0.1317	0.2293
1200	20.5500	0.2050	0.1274	0.2020
1400	20.5800	0.1904	0.1133	0.1864
1600	20.6000	0.1633	0.0758	0.1619
1800	20.6100	0.1521	0.0596	0.1508
2000	20.6100	0.1695	0.1243	0.1659
2200	20.6200	0.1533	0.1015	0.1499
2400	20.6100	0.1879	0.1725	0.1801
2600	20.6200	0.1497	0.1662	0.1469
2800	20.6100	0.1192	0.1271	0.1188
3000	20.6100	0.1071	0.1098	0.1084
3200	20.6100	0.1024	0.1051	0.1033
3400	20.6000	0.1015	0.1042	0.1022
3600	20.6000	0.1034	0.1057	0.1028
3800	20.6100	0.1106	0.1118	0.1077
4000	20.6100	0.1272	0.1251	0.1239
4200	20.6100	0.1598	0.1640	0.1499
4400	20.6100	0.1833	0.2231	0.1699
4600	20.6200	0.1425	0.2084	0.1312
4800	20.6200	0.1124	0.1888	0.1042
5000	20.6300	0.1072	0.1756	0.0998
5200	20.6500	0.1156	0.1749	0.1066
5400	20.6500	0.1333	0.1822	0.1226
5600	20.6900	0.1607	0.2034	0.1474
5800	20.7000	0.1911	0.2270	0.1795
6000	20.7200	0.2198	0.2088	0.2001
6200	20.7300	0.2430	0.1833	0.2249
6400	20.7300	0.2910	0.2226	0.2660
6600	20.7400	0.3540	0.2767	0.3220
6800	20.7600	0.4400	0.3790	0.4030
7000	20.7800	0.5300	0.5450	0.4850
7200	20.8000	0.5600	0.6620	0.5110
7400	20.8500	0.5070	0.6780	0.4600
7600	20.8800	0.4310	0.6420	0.3920
7800	20.9400	0.3770	0.5890	0.3390
8000	21.0100	0.3470	0.5360	0.3120
8200	21.0800	0.3340	0.4780	0.2980
8400	21.1400	0.3130	0.4070	0.2780
8600	21.2000	0.3180	0.3550	0.2810
8800	21.2800	0.3310	0.3150	0.2930
9000	21.3500	0.3530	0.2920	0.3120
9200	21.4300	0.3760	0.2696	0.3350
9400	21.5000	0.4030	0.2535	0.3590
9600	21.5800	0.4320	0.2390	0.3870
9800	21.6600	0.4630	0.2294	0.4130
10000	21.7400	0.4910	0.2284	0.4400

Reproduced with permission of the copyright owner. Further reproduction prohibited without permission.

APPENDIX B

COUPLING SYSTEM MODELING AND SIMULATION DATA

Reproduced with permission of the copyright owner. Further reproduction prohibited without permission.

Comparison of Detailed and Simplified PSpice Model Simulations to Coupling System Measurements

As described in Chapter 3, PSpice model validation consisted of running time domain simulations using PSpice and comparing simulated voltage levels to measured voltage levels obtained from the peak voltage gain measurements described in Chapter 2. For the PSpice model simulations, the drain coil resistance used in the models was the interpolated resistance at the frequency of the forcing voltage of each simulation, where the frequency of the forcing voltage corresponded to the frequency where a voltage peak occurred at the drain coil as obtained from the peak voltage gain measurements. The range of frequencies and resistances from the drain coil tests were used with an interpolation function in Matlab to calculate drain coil resistance at the particular frequency of the forcing voltage for a simulation. The interpolated values of drain coil resistance used in the simulations are provided along with the simulated and measured data.

Comparison of Detailed PSpice Model Simulations to Measurements

The detailed models include component parameters such as capacitor leakage resistance and inductor winding resistance, including IMT winding resistance, all of which were acquired through measurement. The values for the capacitor leakage resistance and inductor winding resistance used with the detailed models are provided in Tables B1 and B2, respectively. The tables provide the measured values for these components along with their designation in the PSpice models.

The detailed PSpice models of the single-frequency, wideband, and two-frequency coupling systems are shown in Figures B1, B2, and B3, respectively. The measured and simulated values for voltage at the coupling capacitor and drain coil are

Reproduced with permission of the copyright owner. Further reproduction prohibited without permission.

provided in Table B3, and the measured and simulated values for voltage at the primary and secondary of the IMT are provided in Table B4.

Table B1

Capacitor Leakage Resistance Values Used with Detailed PSpice Models

Model Designation	Coupling System Model	Capacitance (μF)	Test Frequency (Hz)	Dissipation Factor	Parallel leakage resistance (MΩ)
Rcc	All three systems	0.006850	1000	0.0005	46.469
Rcc	All three systems	0.003458	1000	0.0007	65.750
Rcc	All three systems	0.001717	1000	0.0035	26.484
Rcs	Single-frequency	0.010200	1000	0.0011	14.185
Rcblk	Single-frequency	0.494000	1000	0.0046	0.070
Rcs1	Two-frequency	0.010560	1000	0.0006	25.119
Rcp1	Two-frequency	0.010100	1000	0.0010	15.758
Rcblk1	Two-frequency	0.482000	1000	0.0068	0.049
Rcs2	Two-frequency	0.010200	1000	0.0011	14.185
Rcp2	Two-frequency	0.010100	1000	0.0080	1.970
Rcblk2	Two-frequency	0.494000	1000	0.0046	0.070
Rcp	Wideband	0.013000	1000	0.0064	1.913
Rcblk	Wideband	0.096000	1000	0.0068	0.244

Note: Capacitance and dissipation factor values were measured with an LCR meter. The parallel leakage resistance was calculated from the dissipation factor using Equation 8 from chapter 3.

Table B2

Inductor Winding Resistance Values Used with Detailed PSpice Models

Model Designation	Coupling System Model	Test Frequency (Hz)	Inductance (mH)	Resistance (Ω)
Rs	Single-frequency	1000	0.0960	0.56
Rimtpri	Single-frequency	1000	8.4260	2.87
Rimtsec	Single-frequency	1000	1.6360	0.76
Rs1	Two-frequency	1000	1.1700	5.36
Rp1	Two-frequency	1000	0.1200	0.38
Rimt1pri	Two-frequency	1000	3.9160	1.61
Rimt1sec	Two-frequency	1000	0.8023	0.29
Rs2	Two-frequency	1000	0.0960	0.56
Rp2	Two-frequency	1000	1.0900	1.10
Rimt2pri	Two-frequency	1000	8.4260	2.87
Rimt2sec	Two-frequency	1000	1.6360	0.76
Rs	Wideband	1000	0.1200	0.12
Rp	Wideband	1000	0.8400	0.24
Rimtpri	Wideband	1000	24.2400	1.52
Rimtsec	Wideband	1000	4.5920	0.34

Note: Inductance and resistance values were measured with an LCR meter.

Reproduced with permission of the copyright owner. Further reproduction prohibited without permission.

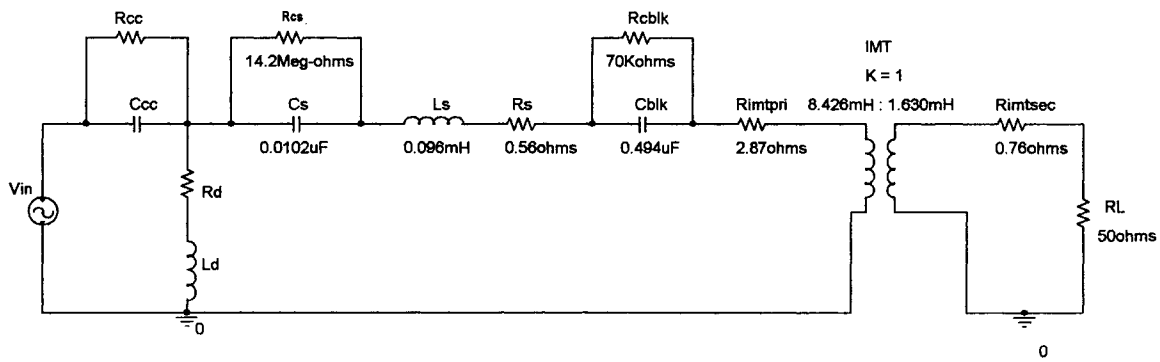

Figure B1. Detailed PSpice model of single-frequency coupling system.

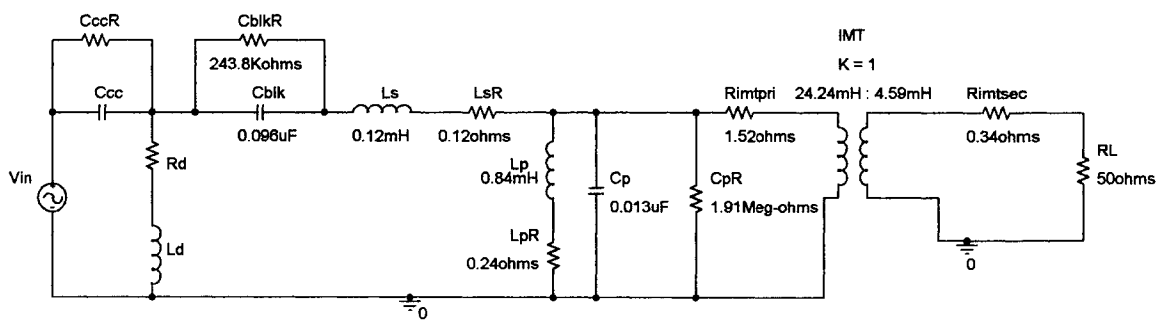

Figure B2. Detailed PSpice model of second-order wideband coupling system.

Reproduced with permission of the copyright owner. Further reproduction prohibited without permission.

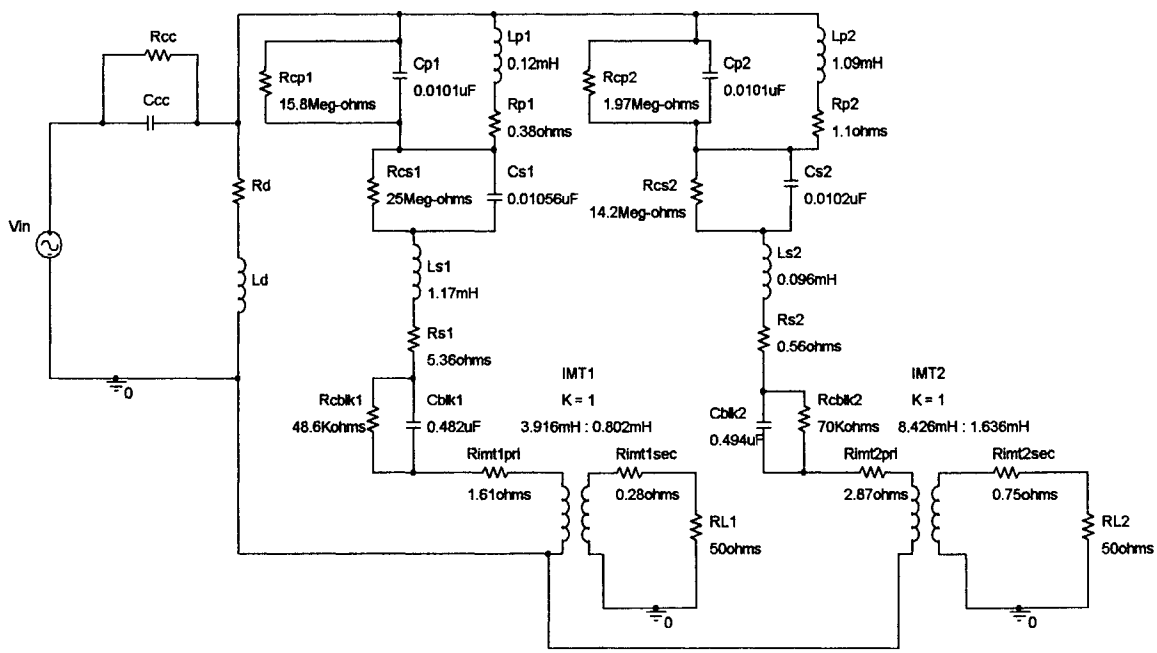

Figure B3. Detailed PSpice model of two-frequency coupling system.

Reproduced with permission of the copyright owner. Further reproduction prohibited without permission.

Table B3

Comparison of Detailed PSpice Model Simulations to Voltage Measurements at the Coupling Capacitor and Drain Coil

System Type	Ccc (μF)	Ld (mH)	Rd (Ω)	Freq-uency (Hz)	V_{in} (Vpk)	V_{CC} (Vpk)	Simu-lated V_{CC} (Vpk)	V_{Ld} (Vpk)	Simu-lated V_{Ld} (Vpk)
Wideband	0.006850	124.10	53.6	1398	5.66	8.36	9.36	6.58	6.82
Wideband	0.003458	124.10	53.9	1421	5.66	6.52	7.07	3.43	3.58
Wideband	0.001717	124.10	54.1	1435	5.66	5.79	6.10	1.75	1.83
Wideband	0.006850	24.63	23.9	3109	14.14	20.63	21.78	15.73	16.84
Wideband	0.003458	24.63	24.3	3161	14.14	16.56	16.23	8.39	8.76
Wideband	0.001717	24.63	24.5	3196	14.14	14.74	14.12	4.26	4.39
Wideband	0.006850	12.03	25.1	4460	14.14	14.23	12.72	10.58	9.75
Wideband	0.003458	12.03	25.4	4525	14.14	15.00	12.53	5.46	5.05
Wideband	0.001717	12.03	25.6	4566	14.14	14.34	13.06	2.77	2.51
Two-Freq.	0.006850	124.10	71.5	2722	14.14	94.19	88.58	92.91	88.03
Two-Freq.	0.003458	124.10	73.5	2903	14.14	54.87	51.31	52.61	49.63
Two-Freq.	0.001717	124.10	74.7	3013	14.14	31.96	29.07	28.14	26.05
Two-Freq.	0.006850	24.63	46.1	6050	14.14	45.11	38.95	42.14	39.20
Two-Freq.	0.003458	24.63	49.3	6429	14.14	26.80	22.42	21.95	19.97
Two-Freq.	0.001717	24.63	51.1	6653	14.14	18.53	15.93	11.07	9.90
Two-Freq.	0.006850	12.03	50.9	8696	14.14	27.68	20.81	23.43	21.02
Two-Freq.	0.003458	12.03	55.3	9212	14.14	18.74	14.88	11.81	10.63
Two-Freq.	0.001717	12.03	57.7	9500	14.14	15.67	13.72	5.84	5.28
Single-Freq.	0.006850	124.10	79.5	3456	14.14	134.77	135.70	133.64	135.80
Single-Freq.	0.003458	124.10	83.8	3852	14.14	77.50	76.10	75.52	75.25
Single-Freq.	0.001717	124.10	86.7	4114	14.14	42.77	40.82	39.50	38.36
Single-Freq.	0.006850	24.63	61.7	7757	14.14	57.02	49.38	54.77	49.89
Single-Freq.	0.003458	24.63	71.0	8622	14.14	31.37	27.27	27.29	24.87
Single-Freq.	0.001717	24.63	77.0	9190	14.14	20.08	18.07	13.29	12.11
Single-Freq.	0.006850	12.03	73.9	11298	14.14	35.13	28.28	31.98	28.91
Single-Freq.	0.003458	12.03	86.3	12565	14.14	21.58	18.27	15.84	14.73
Single-Freq.	0.001717	12.03	94.3	13380	14.14	16.52	15.02	7.68	7.29

Note: Frequency designates the frequency at which the peak voltage at the drain coil occurred, and the value for Rd is the interpolated value at that frequency.

Reproduced with permission of the copyright owner. Further reproduction prohibited without permission.

Table B4

Comparison of Detailed PSpice Model Simulations to Voltage Measurements at the Impedance-Matching Transformer (IMT)

System Type	Ccc (μF)	Ld (mH)	Rd (Ω)	Freq-uency (Hz)	V_{in} (Vpk)	V_{IMThi} (Vpk)	Simu-lated V_{IMThi} (Vpk)	V_{IMTlo} (Vpk)	Simu-lated V_{IMTlo} (Vpk)
Wideband	0.006850	124.10	53.6	1398	5.66	0.041	0.041	0.018	0.018
Wideband	0.003458	124.10	53.9	1421	5.66	0.023	0.022	0.010	0.010
Wideband	0.001717	124.10	54.1	1435	5.66	0.012	0.012	0.006	0.005
Wideband	0.006850	24.63	23.9	3109	14.14	0.483	0.520	0.211	0.223
Wideband	0.003458	24.63	24.3	3161	14.14	0.266	0.280	0.116	0.120
Wideband	0.001717	24.63	24.5	3196	14.14	0.139	0.143	0.061	0.062
Wideband	0.006850	12.03	25.1	4460	14.14	0.694	0.645	0.302	0.277
Wideband	0.003458	12.03	25.4	4525	14.14	0.371	0.345	0.162	0.148
Wideband	0.001717	12.03	25.6	4566	14.14	0.190	0.174	0.083	0.075
Two-Freq.	0.006850	124.10	71.5	2722	14.14	2.141	1.964	0.935	0.843
Two-Freq.	0.003458	124.10	73.5	2903	14.14	1.308	1.243	0.570	0.533
Two-Freq.	0.001717	124.10	74.7	3013	14.14	0.731	0.697	0.316	0.299
Two-Freq.	0.006850	24.63	46.1	6050	14.14	3.362	3.257	1.462	1.399
Two-Freq.	0.003458	24.63	49.3	6429	14.14	1.901	1.814	0.823	0.779
Two-Freq.	0.001717	24.63	51.1	6653	14.14	1.001	0.945	0.432	0.406
Two-Freq.	0.006850	12.03	50.9	8696	14.14	3.067	2.903	1.329	1.247
Two-Freq.	0.003458	12.03	55.3	9212	14.14	1.674	1.586	0.721	0.681
Two-Freq.	0.001717	12.03	57.7	9500	14.14	0.867	0.820	0.375	0.352
Single-Freq.	0.006850	124.10	79.5	3456	14.14	4.759	4.578	2.082	1.962
Single-Freq.	0.003458	124.10	83.8	3852	14.14	3.066	3.046	1.338	1.306
Single-Freq.	0.001717	124.10	86.7	4114	14.14	1.731	1.731	0.752	0.742
Single-Freq.	0.006850	24.63	61.7	7757	14.14	5.982	5.742	2.608	2.462
Single-Freq.	0.003458	24.63	71.0	8622	14.14	3.398	3.282	1.479	1.407
Single-Freq.	0.001717	24.63	77.0	9190	14.14	1.795	1.731	0.776	0.742
Single-Freq.	0.006850	12.03	73.9	11298	14.14	5.521	5.295	2.403	2.270
Single-Freq.	0.003458	12.03	86.3	12565	14.14	3.111	3.046	1.348	1.306
Single-Freq.	0.001717	12.03	94.3	13380	14.14	1.636	1.617	0.701	0.693

Note: Frequency designates the frequency at which the peak voltage at the drain coil occurred, and the value for Rd is the interpolated value at that frequency. V_{IMThi} designates the voltage at the primary, or high impedance side, of the IMT. V_{IMTlo} designates the voltage at the secondary, or low impedance side, of the IMT.

Reproduced with permission of the copyright owner. Further reproduction prohibited without permission.

Comparison of Simplified PSpice Model Simulations to Measurements

The simplified PSpice models of the single-frequency, wideband, and two-frequency coupling systems are shown in Figures B4, B5, and B6, respectively. The measured and simulated values for voltage at the drain coil and at the primary of the IMT are provided in Table B5.

Table B5

Comparison of Simplified PSpice Model Simulations to Voltage Measurements at the Drain Coil and Primary of the Impedance-Matching Transformer (IMT)

System Type	Ccc (μF)	Ld (mH)	Rd (Ω)	Frequency (Hz)	V_{in} (Vpk)	V_{Ld} (Vpk)	Simulated V_{Ld} (Vpk)	V_{IMThi} (Vpk)	Simulated V_{IMThi} (Vpk)
Wideband	0.006850	124.10	53.6	1398	5.66	6.58	7.43	0.041	0.045
Wideband	0.003458	124.10	53.9	1421	5.66	3.43	3.91	0.023	0.024
Wideband	0.001717	124.10	54.1	1435	5.66	1.75	2.00	0.012	0.013
Wideband	0.006850	24.63	23.9	3109	14.14	15.73	17.73	0.483	0.547
Wideband	0.003458	24.63	24.3	3161	14.14	8.39	9.22	0.266	0.295
Wideband	0.001717	24.63	24.5	3196	14.14	4.26	4.62	0.139	0.151
Wideband	0.006850	12.03	25.1	4460	14.14	10.58	9.97	0.694	0.659
Wideband	0.003458	12.03	25.4	4525	14.14	5.46	5.17	0.371	0.353
Wideband	0.001717	12.03	25.6	4566	14.14	2.77	2.57	0.190	0.179
Two-Freq.	0.006850	124.10	71.5	2722	14.14	92.91	90.39	2.141	1.993
Two-Freq.	0.003458	124.10	73.5	2903	14.14	52.61	51.17	1.308	1.266
Two-Freq.	0.001717	124.10	74.7	3013	14.14	28.14	26.90	0.731	0.711
Two-Freq.	0.006850	24.63	46.1	6050	14.14	42.14	40.05	3.362	3.284
Two-Freq.	0.003458	24.63	49.3	6429	14.14	21.95	20.45	1.901	1.832
Two-Freq.	0.001717	24.63	51.1	6653	14.14	11.07	10.15	1.001	0.955
Two-Freq.	0.006850	12.03	50.9	8696	14.14	23.43	21.46	3.067	2.921
Two-Freq.	0.003458	12.03	55.3	9212	14.14	11.81	10.88	1.674	1.599
Two-Freq.	0.001717	12.03	57.7	9500	14.14	5.84	5.41	0.867	0.828
Single-Freq.	0.006850	124.10	79.5	3456	14.14	133.64	137.70	4.759	4.598
Single-Freq.	0.003458	124.10	83.8	3852	14.14	75.52	76.43	3.066	3.063
Single-Freq.	0.001717	124.10	86.7	4114	14.14	39.50	39.00	1.731	1.741
Single-Freq.	0.006850	24.63	61.7	7757	14.14	54.77	50.42	5.982	5.715
Single-Freq.	0.003458	24.63	71.0	8622	14.14	27.29	25.18	3.398	3.270
Single-Freq.	0.001717	24.63	77.0	9190	14.14	13.29	12.27	1.795	1.726
Single-Freq.	0.006850	12.03	73.9	11298	14.14	31.98	29.20	5.521	5.256
Single-Freq.	0.003458	12.03	86.3	12565	14.14	15.84	14.91	3.111	3.029
Single-Freq.	0.001717	12.03	94.3	13380	14.14	7.68	7.39	1.636	1.609

Note: Frequency designates the frequency at which the peak voltage at the drain coil occurred, and the value for Rd is the interpolated value at that frequency. V_{IMThi} designates the voltage at the primary, or high impedance side, of the IMT.

Reproduced with permission of the copyright owner. Further reproduction prohibited without permission.

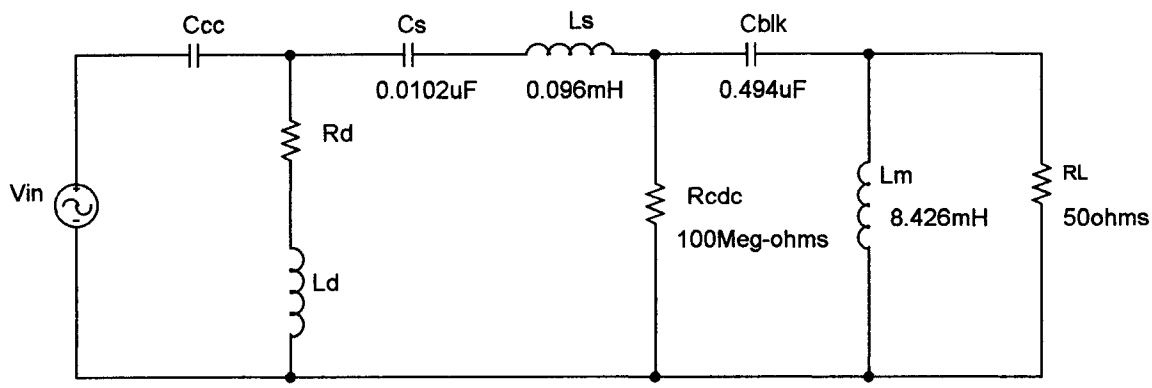

Figure B4. Simplified PSpice model of single-frequency coupling system.

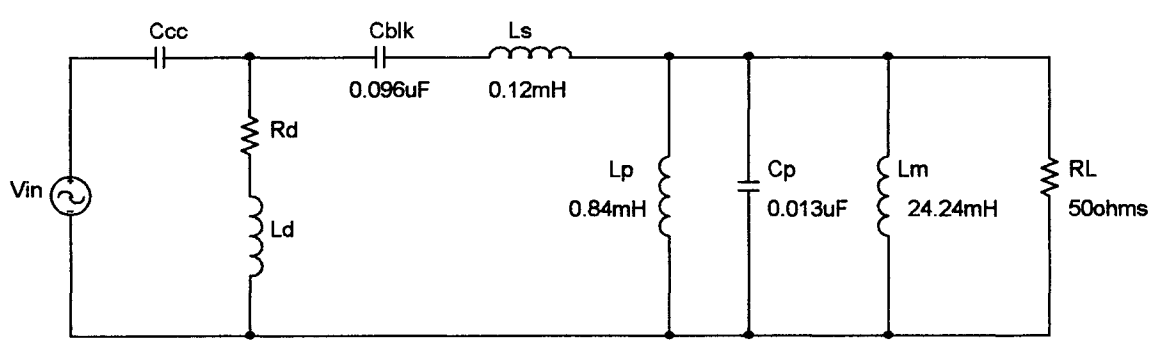

Figure B5. Simplified PSpice model of second-order wideband coupling system.

Reproduced with permission of the copyright owner. Further reproduction prohibited without permission.

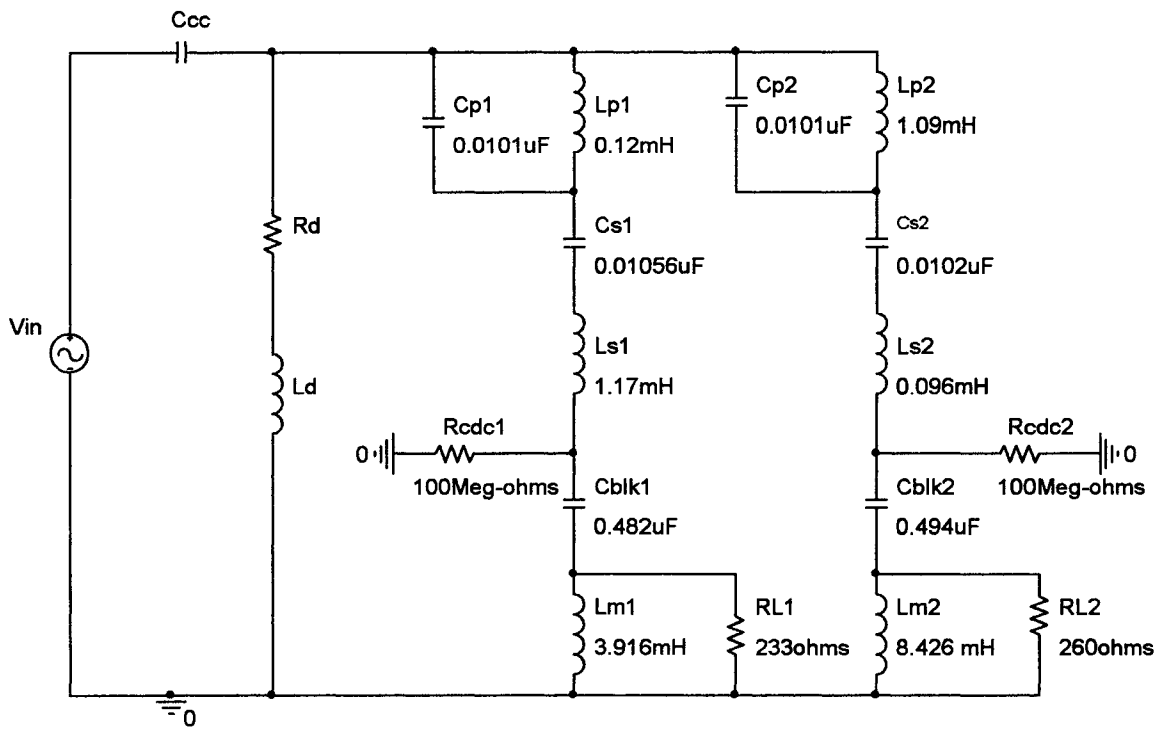

Figure B6. Simplified PSpice model of two-frequency coupling system.

Reproduced with permission of the copyright owner. Further reproduction prohibited without permission.

Matlab Routines Used to Compare the Measured Frequency Responses of the Coupling Systems to the Calculated Frequency Responses using the State-space Models

Matlab Routine for the Single-frequency Coupling System with the Impedance-Matching Transformer (IMT) Terminated into a 2000 Ω Resistance

```
%Routine to calculate the frequency response of a narrowband
%resonant single-frequency system using the general model.
%Frequency response is calculated at the drain coil and
%primary of the IMT and compared to the measured response
%for the system.

clear all
clc

Cblk3 = 1e10;        %no Cblk3 in system
Lp1 = 1e-10;         %shunt the parallel trap unit
Cp1 = 1e10;          %value for Cp1 doesn't matter
Ls1 = 1e-3;
Cs1 = .01e-6;       %high-frequency tuning capacitor enabled
Cblk1 = .5e-6;
Lp2 = 1e10;          %value for Lp2 doesn't matter
Ls2 = 1e10;          %large value for Ls2 open-circuits the second tuning leg
Cp2 = 1e10;          %value for Cp2 doesn't matter
Cs2 = 1e10;          %value for Cs2 doesn't matter
Cblk2 = 1e10;        %value for Cblk2 doesn't matter
Rd = 84;             %interpolated drain coil resistance at the frequency
                     %of peak voltage gain measured for this system
Ld = 125e-3;
Ccc = .003458e-6;
RL1 = 2000*4.6;      %RL was 2000 ohms and IMT tapped on 4.6 impedance ratio
Lm1 = 8.426e-3;      %self-inductance of 4.6 tap of toroidal core IMT
RL2 = 1e10;          %value for RL2 doesn't matter
Lm2 = 1e10;          %value for Lm2 doesn't matter


%General narrowband resonant model system matrix
A=[0 0 0 0 0 0 0 0 1/Ccc 1/Ccc 1/Ccc 0 0 0 0;...
   0 0 0 0 0 0 0 0 0 1/Cblk1 0 0 0 0 0;...
   0 0 0 0 0 0 0 0 0 0 1/Cblk2 0 0 0 0;...
   0 0 0 0 0 0 0 0 0 1/Cblk3 1/Cblk3 0 0 0 0;...
   0 0 0 0 0 0 0 0 0 1/Cs1 0 0 0 0 0;...
   0 0 0 0 0 0 0 0 0 0 1/Cs2 0 0 0 0;...
   0 0 0 0 0 0 0 0 0 1/Cp1 0 -1/Cp1 0 0 0;...
   0 0 0 0 0 0 0 0 0 0 1/Cp2 0 -1/Cp2 0 0;...
   -1/Ld 0 0 0 0 0 0 0 -Rd/Ld 0 0 0 0 0 0;...
   -1/Ls1 -1/Ls1 0 -1/Ls1 -1/Ls1 0 -1/Ls1 0 0 -RL1/Ls1 0 0 0 RL1/Ls1 0;...
   -1/Ls2 0 -1/Ls2 -1/Ls2 0 -1/Ls2 0 -1/Ls2 0 0 -RL2/Ls2 0 0 0 RL2/Ls2;...
   0 0 0 0 0 0 1/Lp1 0 0 0 0 0 0 0 0;...
   0 0 0 0 0 0 0 1/Lp2 0 0 0 0 0 0 0;...
   0 0 0 0 0 0 0 0 0 RL1/Lm1 0 0 0 -RL1/Lm1 0;...
   0 0 0 0 0 0 0 0 0 0 RL2/Lm2 0 0 0 -RL2/Lm2];

%General narrowband resonant model input coupling matrix
B=[0 ;0 ;0 ;0 ;0 ;0 ;0; 0; 1/Ld ;1/Ls1 ;1/Ls2 ;0 ;0; 0; 0];

%Output matrix for calculating voltage at drain coil.
Cdc=[-1 0 0 0 0 0 0 0 0 0 0 0 0 0 0];

%Feed-forward matrix for calculating voltage at drain coil.
```

Reproduced with permission of the copyright owner. Further reproduction prohibited without permission.

```
Ddc=[1];

%Convert to SS model.
drain_coil_sys = ss(A,B,Cdc,Ddc);

%Read data for measured frequency response at drain coil.
[f,gdrain] = textread('singlefreqdraincoilgainwRL2000andCs01.dat', '%f %f');

w = 2*pi*f;   %convert frequencies to rad/s

%Calculate frequency response using frequencies
%where response was measured.
drain_coil_response = freqresp(drain_coil_sys,w);

%Convert to dB
drain_coil_responsedB = 20*log10(abs(drain_coil_response(:)));

h = figure;
figure(h);
plot(f, drain_coil_responsedB(:), 'b');
xlabel('Frequency (Hz)');
ylabel('Voltage Gain at Drain Coil (dB)');

hold on;
figure(h);
plot(f, gdrain, 'r');
hold off;


%Now calculate the gain at the primary of IMT1.
%Output matrix for calculating voltage at IMT1.
Cimt1=[0 0 0 0 0 0 0 0 0 RL1 0 0 0 -RL1 0];  %IMT1 voltage = RL1*(Is1-Im1)

%Feed-forward matrix for calculating voltage at IMT1.
Dimt1=[0];

%Convert to SS model.
IMT1_sys = ss(A,B,Cimt1,Dimt1);

%Read data for measured frequency response at drain coil.
[f,gimt] = textread('singlefreqIMTgainwRL2000andCs01.dat', '%f %f');

w = 2*pi*f;   %convert frequencies to rad/s

%Calculate frequency response using frequencies
%where response was measured.
IMT1_response = freqresp(IMT1_sys,w);

%Convert to dB
IMT1_responsedB = 20*log10(abs(IMT1_response(:)));

h2 = figure;
figure(h2);
plot(f, IMT1_responsedB(:), 'b');
xlabel('Frequency (Hz)');
ylabel('Voltage Gain at Primary of IMT (dB)');

hold on;
figure(h2);
plot(f, gimt, 'r');
hold off;
```

Reproduced with permission of the copyright owner. Further reproduction prohibited without permission.

Matlab Routine for the Single-frequency Coupling System with the Impedance-Matching Transformer (IMT) Terminated into a 50 Ω Resistance

```
%Routine to calculate the frequency response of a narrowband
%resonant single-frequency system using the general model.
%Frequency response is calculated at the drain coil and
%primary of the IMT and compared to the measured response
%for the system.

clear all
clc

Cblk3 = 1e10;        %no Cblk3 in system
Lp1 = 1e-10;         %shunt the parallel trap unit
Cp1 = 1e10;          %value for Cp1 doesn't matter
Ls1 = 1e-3;
Cs1 = .01e-6;       %high-frequency tuning capacitor enabled
Cblk1 = .5e-6;
Lp2 = 1e10;          %value for Lp2 doesn't matter
Ls2 = 1e10;          %large value for Ls2 open-circuits the second tuning leg
Cp2 = 1e10;          %value for Cp2 doesn't matter
Cs2 = 1e10;          %value for Cs2 doesn't matter
Cblk2 = 1e10;        %value for Cblk2 doesn't matter
Rd = 84;             %interpolated drain coil resistance at the frequency
                     %of peak voltage gain measured for this system
Ld = 125e-3;
Ccc = .003458e-6;
RL1 = 50*4.6;        %RL was 50 ohms and IMT tapped on 4.6 impedance ratio
Lm1 = 8.426e-3;      %self-inductance of 4.6 tap of toroidal core IMT
RL2 = 1e10;          %value for RL2 doesn't matter
Lm2 = 1e10;          %value for Lm2 doesn't matter


%General narrowband resonant model system matrix
A=[0 0 0 0 0 0 0 0 1/Ccc 1/Ccc 1/Ccc 0 0 0 0;...
   0 0 0 0 0 0 0 0 0 1/Cblk1 0 0 0 0 0;...
   0 0 0 0 0 0 0 0 0 0 1/Cblk2 0 0 0 0;...
   0 0 0 0 0 0 0 0 0 1/Cblk3 1/Cblk3 0 0 0 0;...
   0 0 0 0 0 0 0 0 0 1/Cs1 0 0 0 0 0;...
   0 0 0 0 0 0 0 0 0 0 1/Cs2 0 0 0 0;...
   0 0 0 0 0 0 0 0 0 1/Cp1 0 -1/Cp1 0 0 0;...
   0 0 0 0 0 0 0 0 0 0 1/Cp2 0 -1/Cp2 0 0;...
   -1/Ld 0 0 0 0 0 0 0 -Rd/Ld 0 0 0 0 0 0;...
   -1/Ls1 -1/Ls1 0 -1/Ls1 -1/Ls1 0 -1/Ls1 0 0 -RL1/Ls1 0 0 0 RL1/Ls1 0;...
   -1/Ls2 0 -1/Ls2 -1/Ls2 0 -1/Ls2 0 -1/Ls2 0 0 -RL2/Ls2 0 0 0 RL2/Ls2;...
   0 0 0 0 0 0 1/Lp1 0 0 0 0 0 0 0 0;...
   0 0 0 0 0 0 0 1/Lp2 0 0 0 0 0 0 0;...
   0 0 0 0 0 0 0 0 0 RL1/Lm1 0 0 0 -RL1/Lm1 0;...
   0 0 0 0 0 0 0 0 0 0 RL2/Lm2 0 0 0 -RL2/Lm2];

%General narrowband resonant model input coupling matrix
B=[0 ;0 ;0 ;0 ;0 ;0 ;0; 0; 1/Ld ;1/Ls1 ;1/Ls2 ;0 ;0; 0; 0];

%Output matrix for calculating voltage at drain coil.
Cdc=[-1 0 0 0 0 0 0 0 0 0 0 0 0 0 0];

%Feed-forward matrix for calculating voltage at drain coil.
Ddc=[1];

%Convert to SS model.
drain_coil_sys = ss(A,B,Cdc,Ddc);
```

Reproduced with permission of the copyright owner. Further reproduction prohibited without permission.

```
%Read data for measured frequency response at drain coil.
[f,gdrain] = textread('singlefreqdraincoilgainwRL50andCs01.dat', '%f %f');

w = 2*pi*f;   %convert frequencies to rad/s

%Calculate frequency response using frequencies
%where response was measured.
drain_coil_response = freqresp(drain_coil_sys,w);

%Convert to dB
drain_coil_responsedB = 20*log10(abs(drain_coil_response(:)));

h = figure;
figure(h);
plot(f, drain_coil_responsedB(:), 'b');
xlabel('Frequency (Hz)');
ylabel('Voltage Gain at Drain Coil (dB)');

hold on;
figure(h);
plot(f, gdrain, 'r');
hold off;


%Now calculate the gain at the primary of IMT1.
%Output matrix for calculating voltage at IMT1.
Cimt1=[0 0 0 0 0 0 0 0 0 RL1 0 0 0 -RL1 0];  %IMT1 voltage = RL1*(Is1-Im1)

%Feed-forward matrix for calculating voltage at IMT1.
Dimt1=[0];

%Convert to SS model.
IMT1_sys = ss(A,B,Cimt1,Dimt1);

%Read data for measured frequency response at drain coil.
[f,gimt] = textread('singlefreqIMTgainwRL50andCs01.dat', '%f %f');

w = 2*pi*f;   %convert frequencies to rad/s

%Calculate frequency response using frequencies
%where response was measured.
IMT1_response = freqresp(IMT1_sys,w);

%Convert to dB
IMT1_responsedB = 20*log10(abs(IMT1_response(:)));

h2 = figure;
figure(h2);
plot(f, IMT1_responsedB(:), 'b');
xlabel('Frequency (Hz)');
ylabel('Voltage Gain at Primary of IMT (dB)');

hold on;
figure(h2);
plot(f, gimt, 'r');
hold off;
```

Reproduced with permission of the copyright owner. Further reproduction prohibited without permission.

Matlab Routine for the Two-frequency Coupling System

```
%Routine to calculate the frequency response of a narrowband
%resonant two-frequency system using the general model.
%Frequency response is calculated at the drain coil and
%primary of the IMT and compared to the measured response
%for the system.

clear all
clc

Cblk3 = 1e10;        %no Cblk3 in system
Lp1 = .25e-3;
Cp1 = .01e-6;
Ls1 = .1e-3;
Cs1 = .01e-6;       %high-frequency tuning capacitor enabled
Cblk1 = .5e-6;
Lp2 = .06e-3;
Cp2 = .01e-6;
Ls2 = .26e-3;
Cs2 = .01e-6;        %high-frequency tuning capacitor enabled
Cblk2 = .5e-6;
Rd = 74;             %interpolated drain coil resistance at the frequency
                     %of peak voltage gain measured for this system
Ld = 125e-3;
Ccc = .003458e-6;
RL1 = 1e6*2.8;       %RL1 was 1 meg-ohm and IMT tapped on 2.8 impedance ratio
Lm1 = 5.094e-3;      %self-inductance of 2.8 tap of toroidal core IMT
RL2 = 1160*1;        %RL2 was 1160 ohms and IMT tapped on 1.0 impedance ratio
Lm2 = 1.795e-3;      %self-inductance of 1.0 tap of toroidal core IMT


%General narrowband resonant model system matrix
A=[0 0 0 0 0 0 0 0 1/Ccc 1/Ccc 1/Ccc 0 0 0 0;...
   0 0 0 0 0 0 0 0 0 1/Cblk1 0 0 0 0 0;...
   0 0 0 0 0 0 0 0 0 0 1/Cblk2 0 0 0 0;...
   0 0 0 0 0 0 0 0 0 1/Cblk3 1/Cblk3 0 0 0 0;...
   0 0 0 0 0 0 0 0 0 1/Cs1 0 0 0 0 0;...
   0 0 0 0 0 0 0 0 0 0 1/Cs2 0 0 0 0;...
   0 0 0 0 0 0 0 0 0 1/Cp1 0 -1/Cp1 0 0 0;...
   0 0 0 0 0 0 0 0 0 0 1/Cp2 0 -1/Cp2 0 0;...
   -1/Ld 0 0 0 0 0 0 0 -Rd/Ld 0 0 0 0 0 0;...
   -1/Ls1 -1/Ls1 0 -1/Ls1 -1/Ls1 0 -1/Ls1 0 0 -RL1/Ls1 0 0 0 RL1/Ls1 0;...
   -1/Ls2 0 -1/Ls2 -1/Ls2 0 -1/Ls2 0 -1/Ls2 0 0 -RL2/Ls2 0 0 0 RL2/Ls2;...
   0 0 0 0 0 0 1/Lp1 0 0 0 0 0 0 0 0;...
   0 0 0 0 0 0 0 1/Lp2 0 0 0 0 0 0 0;...
   0 0 0 0 0 0 0 0 0 RL1/Lm1 0 0 0 -RL1/Lm1 0;...
   0 0 0 0 0 0 0 0 0 0 RL2/Lm2 0 0 0 -RL2/Lm2];

%General narrowband resonant model input coupling matrix
B=[0 ;0 ;0 ;0 ;0 ;0 ;0; 0; 1/Ld ;1/Ls1 ;1/Ls2 ;0 ;0; 0; 0];

%Output matrix for calculating voltage at drain coil.
Cdc=[-1 0 0 0 0 0 0 0 0 0 0 0 0 0 0];

%Feed-forward matrix for calculating voltage at drain coil.
Ddc=[1];

%Convert to SS model.
drain_coil_sys = ss(A,B,Cdc,Ddc);

%Read data for measured frequency response at drain coil.
```

Reproduced with permission of the copyright owner. Further reproduction prohibited without permission.

```
[f,gdrain] = textread('twofreqdraincoilgainwCs01.dat', '%f %f');

w = 2*pi*f;   %convert frequencies to rad/s

%Calculate frequency response using frequencies
%where response was measured.
drain_coil_response = freqresp(drain_coil_sys,w);

%Convert to dB
drain_coil_responsedB = 20*log10(abs(drain_coil_response(:)));

h = figure;
figure(h);
plot(f, drain_coil_responsedB(:), 'b');
xlabel('Frequency (Hz)');
ylabel('Voltage Gain at Drain Coil (dB)');

hold on;
figure(h);
plot(f, gdrain, 'r');
hold off;


%Now calculate the gain at the primary of IMT1.
%Output matrix for calculating voltage at IMT1.
Cimt1=[0 0 0 0 0 0 0 0 0 RL1 0 0 0 -RL1 0];  %IMT1 voltage = RL1*(Is1-Im1)

%Feed-forward matrix for calculating voltage at IMT1.
Dimt1=[0];

%Convert to SS model.
IMT1_sys = ss(A,B,Cimt1,Dimt1);

%Read data for measured frequency response at drain coil.
[f,gimt1] = textread('twofreqCarIMTgainwCs01.dat', '%f %f');

w = 2*pi*f;   %convert frequencies to rad/s

%Calculate frequency response using frequencies
%where response was measured.
IMT1_response = freqresp(IMT1_sys,w);

%Convert to dB
IMT1_responsedB = 20*log10(abs(IMT1_response(:)));

h2 = figure;
figure(h2);
plot(f, IMT1_responsedB(:), 'b');
xlabel('Frequency (Hz)');
ylabel('Voltage Gain at Primary of IMT (dB)');

hold on;
figure(h2);
plot(f, gimt1, 'r');
hold off;


%Now calculate the gain at the primary of IMT2.
%Output matrix for calculating voltage at IMT2.
Cimt2=[0 0 0 0 0 0 0 0 0 0 RL2 0 0 0 -RL2];  %IMT2 voltage = RL2*(Is2-Im2)

%Feed-forward matrix for calculating voltage at IMT2.
Dimt2=[0];
```

Reproduced with permission of the copyright owner. Further reproduction prohibited without permission.

```
%Convert to SS model.
IMT2_sys = ss(A,B,Cimt2,Dimt2);

%Read data for measured frequency response at drain coil.
[f,gimt2] = textread('twofreqRTIMTgainwCs01.dat', '%f %f');

w = 2*pi*f;   %convert frequencies to rad/s

%Calculate frequency response using frequencies
%where response was measured.
IMT2_response = freqresp(IMT2_sys,w);

%Convert to dB
IMT2_responsedB = 20*log10(abs(IMT2_response(:)));

hold on;
figure(h2);
plot(f, IMT2_responsedB(:), ':b');
hold off

hold on;
figure(h2);
plot(f, gimt2, ':r');
hold off;
```

Reproduced with permission of the copyright owner. Further reproduction prohibited without permission.

Matlab Routine for the Second-Order Wideband Coupling System with the Impedance-Matching Transformer (IMT) Terminated into a 2000 Ω Resistance

```
%Routine to calculate the frequency response of a second-order
%wideband band-pass system.
%Frequency response is calculated at the drain coil and
%primary of the IMT and compared to the measured response
%for the system.

clear all
clc

Ccc = .003458e-6;
Cblk = .093e-6;
Ls = .768e-3;
Cp = .0049e-6;
Lp = .179e-3;
Ld = 125e-3;
Rd = 54;          %interpolated drain coil resistance for
                  %measured frequency of peak gain for this system

RL = 2000*5.2;    %RL was 2000 ohms and IMT tapped on 5.2 impedance ratio
Lm = 24.24e-3;    %self-inductance of IMT primary winding on 5.2 impedance ratio


%System matrix for second-order wideband model.
A=[0 0 0 1/Ccc 1/Ccc 0 0;...
   0 0 0 0 1/Cblk 0 0;...
   0 0 -1/(Cp*RL) 0 1/Cp -1/Cp -1/Cp;...
   -1/Ld 0 0 -Rd/Ld 0 0 0;...
   -1/Ls -1/Ls -1/Ls 0 0 0 0;...
   0 0 1/Lp 0 0 0 0;...
   0 0 1/Lm 0 0 0 0];


%Second-order wideband input coupling matrix
B=[0 ;0 ;0 ; 1/Ld ;1/Ls ;0; 0];

%Output matrix for calculating voltage at drain coil.
Cdc=[-1 0 0 0 0 0 0];

%Feed-forward matrix for calculating voltage at drain coil.
Ddc=[1];

%Convert to SS model.
drain_coil_sys = ss(A,B,Cdc,Ddc);

%Read data for measured frequency response at drain coil.
[f,gdrain] = textread('widebanddraincoilgainwRL2000.dat', '%f %f');

w = 2*pi*f;    %convert frequencies to rad/s

%Calculate frequency response using frequencies
%where response was measured.
drain_coil_response = freqresp(drain_coil_sys,w);

%Convert to dB
drain_coil_responsedB = 20*log10(abs(drain_coil_response(:)));

h = figure;
figure(h);
plot(f, drain_coil_responsedB(:), 'b');
```

Reproduced with permission of the copyright owner. Further reproduction prohibited without permission.

```
xlabel('Frequency (Hz)');
ylabel('Voltage Gain at Drain Coil (dB)');

hold on;
figure(h);
plot(f, gdrain, 'r');
hold off;


%Now calculate the gain at the primary of the IMT.
%Output matrix for calculating voltage at IMT.
Cimt1=[0 0 1 0 0 0 0];  %IMT voltage = Vcp

%Feed-forward matrix for calculating voltage at IMT.
Dimt1=[0];

%Convert to SS model.
IMT1_sys = ss(A,B,Cimt1,Dimt1);

%Read data for measured frequency response at drain coil.
[f,gimt] = textread('widebandIMTgainwRL2000.dat', '%f %f');

w = 2*pi*f;   %convert frequencies to rad/s

%Calculate frequency response using frequencies
%where response was measured.
IMT1_response = freqresp(IMT1_sys,w);

%Convert to dB
IMT1_responsedB = 20*log10(abs(IMT1_response(:)));

h2 = figure;
figure(h2);
plot(f, IMT1_responsedB(:), 'b');
xlabel('Frequency (Hz)');
ylabel('Voltage Gain at Primary of IMT (dB)');

hold on;
figure(h2);
plot(f, gimt, 'r');
hold off;
```

Reproduced with permission of the copyright owner. Further reproduction prohibited without permission.

Matlab Routine for the Second-Order Wideband Coupling System with the Impedance-Matching Transformer (IMT) Terminated into a 50 Ω Resistance

```
%Routine to calculate the frequency response of a second-order
%wideband band-pass system.
%Frequency response is calculated at the drain coil and
%primary of the IMT and compared to the measured response
%for the system.

clear all
clc

Ccc = .003458e-6;
Cblk = .093e-6;
Ls = .768e-3;
Cp = .0049e-6;
Lp = .179e-3;
Ld = 125e-3;
Rd = 54;          %interpolated drain coil resistance for
                  %measured frequency of peak gain for this system

RL = 50*5.2;      %RL was 50 ohms and IMT tapped on 5.2 impedance ratio
Lm = 24.24e-3;    %self-inductance of IMT primary winding on 5.2 impedance ratio


%System matrix for second-order wideband model.
A=[0 0 0 1/Ccc 1/Ccc 0 0;...
   0 0 0 0 1/Cblk 0 0;...
   0 0 -1/(Cp*RL) 0 1/Cp -1/Cp -1/Cp;...
   -1/Ld 0 0 -Rd/Ld 0 0 0;...
   -1/Ls -1/Ls -1/Ls 0 0 0 0;...
   0 0 1/Lp 0 0 0 0;...
   0 0 1/Lm 0 0 0 0];


%Second-order wideband input coupling matrix
B=[0 ;0 ;0 ; 1/Ld ;1/Ls ;0; 0];

%Output matrix for calculating voltage at drain coil.
Cdc=[-1 0 0 0 0 0 0];

%Feed-forward matrix for calculating voltage at drain coil.
Ddc=[1];

%Convert to SS model.
drain_coil_sys = ss(A,B,Cdc,Ddc);

%Read data for measured frequency response at drain coil.
[f,gdrain] = textread('widebanddraincoilgainwRL50.dat', '%f %f');

w = 2*pi*f;   %convert frequencies to rad/s

%Calculate frequency response using frequencies
%where response was measured.
drain_coil_response = freqresp(drain_coil_sys,w);

%Convert to dB
drain_coil_responsedB = 20*log10(abs(drain_coil_response(:)));

h = figure;
figure(h);
plot(f, drain_coil_responsedB(:), 'b');
```

Reproduced with permission of the copyright owner. Further reproduction prohibited without permission.

```
xlabel('Frequency (Hz)');
ylabel('Voltage Gain at Drain Coil (dB)');

hold on;
figure(h);
plot(f, gdrain, 'r');
hold off;


%Now calculate the gain at the primary of the IMT.
%Output matrix for calculating voltage at IMT.
Cimt1=[0 0 1 0 0 0 0];  %IMT voltage = Vcp

%Feed-forward matrix for calculating voltage at IMT.
Dimt1=[0];

%Convert to SS model.
IMT1_sys = ss(A,B,Cimt1,Dimt1);

%Read data for measured frequency response at drain coil.
[f,gimt] = textread('widebandIMTgainwRL50.dat', '%f %f');

w = 2*pi*f;   %convert frequencies to rad/s

%Calculate frequency response using frequencies
%where response was measured.
IMT1_response = freqresp(IMT1_sys,w);

%Convert to dB
IMT1_responsedB = 20*log10(abs(IMT1_response(:)));

h2 = figure;
figure(h2);
plot(f, IMT1_responsedB(:), 'b');
xlabel('Frequency (Hz)');
ylabel('Voltage Gain at Primary of IMT (dB)');

hold on;
figure(h2);
plot(f, gimt, 'r');
hold off;
```

Reproduced with permission of the copyright owner. Further reproduction prohibited without permission.

GRADUATE SCHOOL
UNIVERSITY OF ALABAMA AT BIRMINGHAM
DISSERTATION APPROVAL FORM
DOCTOR OF PHILOSOPHY

Name of Candidate Gregory A. Franklin

Graduate Program Computer Engineering

Title of Dissertation Analysis and Mitigation of High Frequency Harmonic Interference in High Voltage Power Line Carrier Coupling Systems

I certify that I have read this document and examined the student regarding its content. In my opinion, this dissertation conforms to acceptable standards of scholarly presentation and is adequate in scope and quality, and the attainments of this student are such that he may be recommended for the degree of Doctor of Philosophy.

Dissertation Committee:

Name		**Signature**
Gregg L. Vaughn	, **Chair**	
Dale W. Callahan		
Henry J. Holley		
Shih-Min Hsu		
Jeffrey H. Kulick		

Director of Graduate Program

Dean, UAB Graduate School

Date 12/22/05

Reproduced with permission of the copyright owner. Further reproduction prohibited without permission.